Characterization of High Porosity Drainage Layer Materials for M-E Pavement Design

Yinning Zhang

Dissertation submitted to the faculty of the Virginia Polytechnic Institute and State University in partial fulfillment of the requirements for the degree of

Doctor of Philosophy

In

Civil Engineering

Linbing Wang

Montasir Abbas

Joseph E. Dove

Cristian Druta

December 2nd, 2014

Blacksburg, Virginia

Keywords: drainage layer, air void content, permeability, dynamic modulus, M-E pavement design

Characterization of High Porosity Drainage Layer Materials for M-E Pavement Design

Yinning Zhang

ABSTRACT

The objective of this study is to characterize the properties of typically adopted drainage layer materials in VA, OK, and ID. A series of laboratory tests have been conducted to quantify the volumetric properties, permeability and mechanical properties of the laboratory-compacted asphalt treated and cement treated permeable base specimens. The modified test protocols to determine the dynamic modulus of the drainage layer materials have been provided, which can be followed to determine the dynamic modulus of the drainage layers as level 1 input in Mechanistic-Empirical (M-E) pavement design. The measured dynamic moduli have been used to calibrate the original NCHRP 1-37A model to facilitate its application on drainage layer materials for prediction of the dynamic modulus as level 2 input. The compressive strength of the cement treated permeable base mixture of different air void contents has also been quantified in laboratory. Numerical simulations are conducted to investigate the location effects and the contribution of the drainage layer as a structural component within pavement. The optimal air void content of the drainage layer is recommended for Virginia, Oklahoma and Idaho based on the laboratory-determined permeability and the predicted pavement performances during 20-year service life.

DEDICATION

I would like to dedicate this dissertation to my family and friends. It is with their love, understanding and support that I could accomplish what I set out to do.

ACKNOWLEGEMENTS

Firstly I would like to express sincere gratitude to my advisor Professor Linbing Wang for the encouragement, support, and guidance during my doctoral period. I would also like to express my gratitude to my committee members, Dr. Montasir Abbas, Dr. Joseph E. Dove and Dr. Cristian Druta for their suggestions and support to my dissertation. I would like to thank the faculty members, staff, and all my friends at Virginia Tech for making Virginia Tech a memorable place for me.

Research presented here was conducted as part of the Transportation Pooled Fund study TPF-5(229) program. The author would also like to acknowledge with much the following state department of transportation for providing technical and financial support to this study.

- Virginia Department of Transportation
- Wisconsin Department of Transportation
- Oklahoma department of Transportation
- Idaho Transportation Department

TABLE OF CONTENTS

LIST OF FIGURES

LIST OF TABLES

LIST OF ABBREVIATIONS

AASHTO	American Association of State Highway and Transportation Officials
ACPA	American Concrete Pavement Association
AMRL	AASHTO Materials Reference Laboratory
ANOVA	Analysis of variance
ASTM	American Society for Testing and Materials
ATPB	Asphalt Treated Permeable Base
Caltrans	California Department of Transportation
CTPB	Cement Treated Permeable Base
CV	Coefficient of Variance
DEM	Discrete Element Method
DF	Degree of Freedom
DOT	Department of Transportation
FEM	Finite Element Method
FHWA	Federal Highway Administration
G_{mm}	Theoretical Maximum Specific Gravity
G_{sb}	Bulk Specific Gravity
HMA	Hot Mixed Asphalt
INDOT	Indiana Department of Transportation
ITD	Idaho Transportation Department
LMLC	Lab Mixed-Lab Compacted
Lower CL	Lower Confidence Limits
LVDT	Linear variable differential transducer
MEPDG	Mechanistic-Empirical Pavement Design Guide
NCHRP	National Cooperative Highway Research Program
ODOT	Oklahoma Department of Transportation
OGBB	Open Graded Bituminous Base
OGDL	Open-Graded Drainage Layer
OGPCCB	Open Graded Portland Cement Concrete Base
PCC	Portland Cement Concrete

PG	Performance Grade
PMLC	Plant Mixed-Lab Compacted
SGC	Superpave Gyratory Compactor
SHRP	Strategic Highway Research Program
SSD	Saturated Surface Dry
Upper CL	Upper Confidence Limits
VDOT	Virginia Department of Transportation
VTM	Voids in Total Mixture
WisDOT	Wisconsin Department of Transportation

CHAPTER 1. INTRODUCTION

MOTIVATION FOR RESEARCH

Moisture related problems have long been recognized as a primary cause of pavement failure. Water enters into the pavement structure through various ways which may increase the risk of moisture damages. The subsurface drainage systems, especially the systems incorporated with drainage layers, have been widely adopted to minimize the moisture damage and prevent moisture related deterioration by effectively draining excessive water out. An increase in using the drainage layers can date back to the 1980s and 1990s in the U.S. [1] After that, although some states claimed that the drainage layers have been adopted much less than before, there are still many states keep using drainage layers in newly constructed pavements today, and there are also numerous drainage layers which have been constructed years ago but still in service today.

The drainage layers are typically consisting of treated or untreated open-graded aggregates with high porosity. The large air void content and the special gradations have led to very different properties of the drainage layers, compared with regular dense-graded asphalt or cement concrete. As a result, the conventional test methods to characterize the regular materials may not be applicable on the drainage layer materials in several aspects as stated in the following sections.

Volumetrically, unlike the dense graded mixtures, the absence of fine aggregates leads to more internal air pockets inside the ATPB mixture as well as more air voids connected to the surface. This is benefit to permeability but results in difficulties in determining the volumetric properties of the laboratory compacted or field cored drainage layer specimens by the conventional procedures such as Saturated Surface Dry (SSD) method. However, as important parameters to Hot Mix Asphalt (HMA) mix design and pavement design, accurately determined volumetric properties such as bulk specific gravity and air void content will contribute to more reliable performance prediction [4]. Application of suitable techniques to achieve reliable volumetric properties is significant.

Mechanically, the more than thirty-year experience of the drainage layer applications in the U.S. has revealed that including a drainage layer reduces pavement deterioration [2-4] by removing moisture from the pavement system rather than providing strength by itself. In fact, consisting of open-graded aggregates and limited fines, the drainage layer at high air void content is less stiff as other asphalt mixtures. The backcalculated or laboratory determined modulus of the Asphalt Treated Permeable Base (ATPB) drainage layer typically ranges from 400 MPa to 2,000 MPa, which is much lower than that of regular asphalt concrete, as documented in many reports[5-9]. The stiffness of conventional asphalt concrete can be 5.5 to 7 times larger than the stiffness of ATPB even in a dry state [6]. There are also studies reporting that the heavy traffic loading causes stripping and modulus reduction of saturated ATPB drainage layer, finally leading to the failure of pavement in the form of rutting and fatigue cracking [4, 6]. All these studies have indicated that the ATPB drainage layer is possibly to be a weak load bearing layer and its mechanical properties may dominate the performance of the pavement. Therefore it is necessary to investigate the mechanical properties of typical drainage layer materials and to consider the structural performance of the drainage layer in M-E pavement design. However, the current available test methods to determine the dynamic modulus of traditional asphalt concrete, the AASHTO TP 342-11 which is originally designed for regular

asphalt concrete, is approved to be not suitable for ATPB materials not only in testing temperatures but also in stress levels. Customized or modified test methods are needed for characterizing the mechanical properties of drainage layer materials. In addition, there are two typical locations for the drainage layer in pavement structure, which are either above the base course, or below the base course as a part of subbase. Being a relatively weak load bearing part in pavement, the stress and strain within the drainage layer at different locations could be totally different under traffic loading and should be checked to avoid structural failures. However, few studies have focused on the location effects of the drainage layer as a structural component so far.

In pavement design consideration, the current M-E pavement design procedure uses three-level hierarchal material inputs: directly using the laboratory data, predicting the inputs from empirical correlations, or adopting default values. The structural contribution of the drainage layer to a pavement structure is not considered in the 1993 AASHTO pavement design guide. Some states follow this approach and do not give the drainage layer a structural layer coefficient although others do. In the Mechanistic-Empirical Pavement Design Guide (MEPDG), while each different layer can be evaluated individually, there is no procedure specifically developed to characterize the fundamental properties of the drainage layers, which are usually composed of asphalt/cement treated or granular materials with high porosities ranging from 20% to 35%. With such high level porosities, it is rather difficult to prepare laboratory specimens to evaluate the modulus and the strength of these materials. Besides the necessary of modification in current dynamic modulus test for level 1 input, the commonly used NCHRP 1-37A model, which is developed to predict the dynamic modulus of asphalt mixture in level 2 M-E pavement design, also need to be calibrated for the ATPB materials. In addition, the selection of the air void content is a tradeoff between permeability and stability. Increase in air void content may improve the permeability performance but impair the mechanical properties. In this regard, there should be a range of optimal air void content, among which both required permeability and good structural performance can be achieved.

All the previously stated problems have illustrated the very significant needs in developing more convenient methods or modifying existing methods to characterize the typical drainage layer materials at high porosity, to consider the structural contribution of the drainage layer and evaluate its location effects, and to develop approaches to investigate the ranges of the optimal air void content for the ATPB drainage layers.

OBJECTIVE AND SCOPE

Objectives

The objectives of this study are to develop methods for characterizing the volumetric, permeability and mechanical properties such as modulus and strength of pavement drainage layers for the Mechanistic-Empirical pavement design, to perform analysis of the stability and structural contribution of the drainage layer in the pavement structure, to evaluate the location effect of the drainage layer, and to recommend the optimal air void content for the drainage layers to satisfy both required effective drainage and structural performances.

Scope of the study

Acquire material and design information

The representative drainage-layer materials and the typical pavement structure designs of selected states, including Virginia, Oklahoma and Idaho, are acquired and presented in this dissertation. This information is used for analyzing the structure contribution and location effect of the drainage layer, as well as specifying the optimal porosity for effective drainage and structural performance of the drainage layer in pavement.

Develop testing methods or modify/adapt existing methods to characterize the modulus and strength of ATPB and Cement Treated Permeable Base (CTPB) materials at high porosities

In this study, the typical drainage-layer materials obtained from each participating state are tested using a series of standard laboratory testing methods or modified approaches. Based on a comprehensive literature review of the major databases in the area of pavement materials evaluation, the following set of testing methods have been adopted in this study. Volumetrically, the dimensional method, Parafilm method and CoreLok vacuum sealing method are adopted and compared with each other to determine the air void content of different mixtures. The permeability of ATPB specimens with different air void content is determined through both constant head method and flexible wall falling head method. Mechanically, for ATPB materials, the modified dynamic modulus test is used as the baseline method for measuring directly the modulus of the asphalt-treated materials. For CTPB materials, the laboratory uniaxial test is used as the baseline testing method for the cement-treated materials. The *ASTM C39 Compressive Strength of Cylindrical Concrete Specimens* is followed to determine the strength of the cement-treated materials.

All the laboratory-determined dynamic moduli of the typical ATPB drainage layer materials adopted by the participating states have been used to calibrate the NCHRP 1-37A model. Utilizing the laboratory-determined dynamic modulus of the specific ATPB mixture adopted by each state, three calibrated local models with customized gradation parameters as used in local quality control are provided. In addition, a calibrated general model which can be used to predict dynamic modulus of ATPB mixtures with different gradations, asphalt types, asphalt contents and air void contents is also provided, by calibrating the original NCHRP 1-37A model using the laboratory-determined dynamic modulus data of all the three kinds of ATPB mixtures in this study.

Perform pavement analysis to evaluate how the drainage layers will perform in a typical pavement structure under typical traffic loading

Finite element method is used to investigate the structural contribution and the location effect of the drainage layer. Since a minimum porosity is necessary to ensure the effective seepage/drainage of the drainage layer, the porosity is usually a major factor affecting the modulus and strength properties of the drainage layer materials. The influence of the air void content of drainage layer is investigated through FEM simulation on a typical drained pavement structure. In addition, other factors such as the influence of the traffic loading on the responses of drained pavement have also been investigated.

Formulate recommendations of drainage layer material properties and the optimal air void content of the drainage layer

The optimum/default values, calibrated empirical correlations, and modified testing procedures to directly or indirectly determine the volumetric, permeability and mechanical properties for the drainage layer are recommended. Recommendations of the drainage layer's optimal air void content ranges, which are determined by the integrated results from permeability test, dynamic modulus test and the M-E pavement design procedures have also been provided for the better performance of drainage layers.

OVERVIEW OF DOCUMENT

This dissertation has included the findings from a series of laboratory tests and numerical simulations to characterize the typical drainage layer materials and evaluate the performance of pavement with a drainage layer incorporated, which is divided into six chapters and two appendices. Chapter 2 presents the synthesized information about typical materials, the thickness and locations for drainage layers, and the testing methods to determine permeability and mechanical properties of asphalt mixtures, based on a literature review of current available documents. Chapter 3 provides the information of the materials collected for laboratory testing in this study, including aggregate gradation, asphalt type, asphalt content, laydown temperature and so forth. Chapter 4 has presented the laboratory tests in details which have been conducted in this study to characterize the high porosity drainage layer materials. Due to the specificity caused by high porosity of the drainage layer, some conventional test methods are no longer applicable for the ATPB or CTPB materials, therefore customized test methods have been developed. The selected or customized test methods to investigate primarily the volumetric properties, permeability and dynamic modulus of drainage layer materials are all specified in detail as presented in chapter 4. In chapter 5, the results of the series of laboratory tests have been presented and analyzed. Statistical analysis to determine the most appropriate methods for ATPB material to determine volumetric properties, the relationship between permeability and air void content of different ATPB mixtures, the dynamic modulus master curves, the moisture susceptibility of the ATPB mixtures, and the calibrated NCHRP 1-37A model have all been illustrated in chapter 5. The chapter 6 focuses on the FEM simulation of the location effect and structural contribution of the drainage layer. The optimal air void content obtained based on laboratory determined permeability-air voids relationship and M-E pavement analysis is also included in chapter 6. Chapter 7 concludes all the findings and provides recommendations for drainage layer applications. Appendix A and B have listed the examples of dynamic modulus master curves for each mixture, and the Prony series applied in FEM simulations.

CHAPTER 2. LITERATURE REVIEW

Moisture related problems have long been recognized as primary causes of pavement failures. Water enters into the pavement structure through surface infiltration such as joints and cracks, from higher ground, rising ground water, capillary action and vapor movement [10]. It is extremely hard to completely prevent moisture from entering the pavement section in real situation. However, the presence of water in pavement structure is undesirable because it would adversely affect the short-term and long-term performance of both the flexible and PCC pavement in several forms. In flexible pavements, the moisture induced problems come from the deterioration of the base, subbase and subgrade in saturated or partly saturated conditions. In rigid pavements, entrapped water causes erosion of subgrade and creates voids below the concrete slab. Several primary pavement failures related with entrapped water have been recognized as follows [11, 12]. The moisture induced deteriorations and damages of pavements especially under heavy traffic loading have become one of the most concerns for engineers.

- Reducing the load bearing capacity by increasing the pore water pressure;
- Resulting in swelling in subgrade of expansive soil;
- Frost heave and reduction in strength during melting;
- Causing the erosion problem under heavy traffic loading and further causing faulting and slab cracking within PCC pavement;
- Fines immigration into the base and subbase, which reduces the permeability;
- Moisture caused stripping in asphalt treated permeable base (ATPB) under wheel loading.

The moisture sources are usually prevented from entering the pavement structure or accumulating in the subgrade through the surface drainage and subsurface drainage approaches. It is more cost effective and less risky to prevent water/moisture entry and accumulation using surface drainage than to remove water/moisture using subsurface drainage. Theoretically, the best way for reducing the detrimental effects of moisture is to prevent moisture from entering the pavement system. However, in practice this is too hard to be achieved. From this standpoint, the subsurface drainage approaches have been necessary for achieving a robust pavement system which is subjected to moisture access. Nowadays, to reduce the moisture induced premature deterioration for both flexible and rigid pavements, over 30 states have incorporated the drainage layer as a part of pavement structure, constructed as daylighted or working together with the edge drain system to prevent or minimize moisture damage [13].

For pavements subjected to water-related problems, a subsurface drainage system typically consisting of three basic elements is used. The three basic elements of the subsurface drainage system include:

1. A permeable base (typically 2-4 inches in thickness) to provide for rapid removal of water which enters the pavement structure. Depending on structural requirements, the materials used to construct the permeable base could be open-graded granular material with limited fines, or cement/asphalt-treated aggregate with a required value of permeability.
2. A method of conveying the removed water away from the pavement structure; which could simply consist of a base sloped towards a drainage ditch or more complexly a pipe and edgedrain collector system.

3. A filter layer such as using a geotextile, graded aggregate layer or HMA to prevent the migration of fines into the permeable base from the subgrade, subbase or shoulder base material. Excess fines in the permeable base will clog its drainage routes and affect the effectiveness. Depending on the subgrade and pavement structure, a filter layer may not be used.

Additional components of a subsurface drainage system include: an outlet consisting of short pipes that carry water from the pipe edgedrains collectors to the side ditches, and side ditches that carry water collected from the outlet away from the pavement. There are various subsurface drainage systems available to meet different design requirements. Commonly used systems are: permeable base system with pipe edgedrains collector, daylighted permeable base system, nonerodible base with pipe edgedrains collector, nonerodible base with pipe edgedrains and porous concrete shoulder, and daylighted dense-graded aggregate base.

To characterize the drainage layer materials and evaluate the performance of drainage layers, a comprehensive literature review has been done to collect information about the current status of drainage layers, including the typical drainage layer thickness, locations, the strength and modulus of drainage layers, current available test methods to determine the volumetric, permeability and mechanical properties of asphalt mixtures, and common drainage layer failures and problems encountered in practice. The following next few sections will focus on these aspects for drainage layers based on the literature review of the major databases.

Typical materials used for the drainage layer

Except serving the important function of removing water out from pavement, the drainage layer also works as a load bearing layer within the pavement structure. It should also satisfy stability requirement to resist the loadings during construction and in service period. The selection of material for drainage layer is a tradeoff between permeability and stability, stiffness and strength. Omitting the fines in gradation can increase the permeability but will affect the stability and other mechanical properties of the drainage layer. Therefore, to balance between the requirement of permeability and mechanical properties, part of the fines in dense gradation are removed or the stabilized open graded aggregates are adopted, which result in two types of typical drainage layer materials: unstabilized and stabilized. Unstabilized drainage layer includes some fine aggregates to improve the interlock between the particles while the stabilized drainage layer relies on the stabilizer to provide cementing between particles. The typical stabilizing material include asphalt and Portland cement. Asphalt treated permeable base (ATPB) and cement treated permeable base (CTPB) are the two commonly used stabilized drainage layers by many states in the U.S.

Gradation for unstabilized aggregate

The recommended gradation usually differs for the unstabilized and the stabilized drainage layers. Very limited fines are allowed in unstabilized aggregate to keep stability under construction and traffic loadings. Generally, the crushed stone is required in unstabilized drainage layer for the sake of stability during construction operation. The gradations of the unstabilized drainage layer are determined in accordance with two criteria: (1) sufficient permeability capacity and (2) enough stability and strength. The Norwegian Road Research Laboratory found that the percent passing No.200 sieve should not exceed 9% for the gravel base

drainage layer to achieve acceptable permeability capacity and shear strength [14]. An Illinois cooperative highway research grogram suggested that sieves smaller than 2mm (No.10) should be minimized for the permeable base material. The U.S. Army Corps of Engineers recommended the Rapid draining material (RDM) and open graded material (OGM) for the drainage layer in airfield pavement [15]. The American Concrete Pavement Association (ACPA) suggested more intermediate aggregates be added to the No.57 or No.67 gradation for the unstabilized drainage layer [14]. Today many states have their own requirements on the gradation of unstabilized drainage layer materials in the local specifications.

Gradation for Stabilized Aggregate

For the stabilized drainage layer, ASSHTO No.57 and No.67 gradations are commonly used. Several SHA's use the AASHTO No. 57 gradation for their stabilized permeable bases and the Wisconsin Department of Transportation (DOT) has reported success of using the AASHTO No. 67 gradation in stabilized bases [10]. Florida DOT has reported that the typical ATPB was single coarse aggregate No.57 or No.67 according to the statewide evaluation [16]. In some states a combination of these two gradations is adopted for the drainage layer to reach better performance. The amount of material passing the No.200 sieve is limited to 0 to 2 percent to reduce the amount of fines by some states [10]. Many studies have been focused on improving the gradations of stabilized aggregate. Virginia DOT utilized a 50-50 blend of No.68 and No.8 aggregate with thick asphalt films in a flexible pavement and received good results in both constructability and durability [1].

Content of the stabilizer

For stabilizer, typically 2% to 3% (by weight) of asphalt is applied to ATPB and 2 to 3 bags (112 to 167 kg/m^3) of Portland cement are applied to CTPB per cubic yard [13]. It is reported that many highway agencies utilize lightly stabilized open-graded materials with asphalt content in the range of 2-3% and cement content of 100-150 pounds per cubic yard for the drainage layers [17]. The ACPA recommended the 2.0% to 2.5% of asphalt binder (by weight) and 90 to 165 kg/m^3 (150-280 lb/yd^3) of cement used for stabilized aggregate [14].

Drainage layer thickness

To ensure the structural performance as well as the permeability capacity of the pavement, the thickness of each layer is determined firstly by satisfying the structural requirement to support traffic loading, then the drainage capacity is checked to see whether the thickness is appropriate from the drainage point of view [11]. Typically a minimum of 4 inches of drainage layer is recommended [10].

For ATPB, the FHWA has recommended the thickness to be 4 inches to 6 inches in an implementation package for drainage blankets early in 1972. Mathis suggested 4 inches of ATPB as drainage layer [18]. Forsyth indicated the range of ATPB used is from 3 to 6 inches and the most common thickness of ATPB is 4 inches [19]. California specifies 3 inches of ATPB for drainage layer and Oregon uses 3 to 4 inches ATPB in several designs [20]. According to an evaluation of asphalt treated permeable base conducted by the Florida DOT, the condition of the ATPB layers in several concrete pavement throughout the state are typically 4 to 5 inches [16]. For CTPB, the typical thickness ranges from 3 to 6 inches, with the most commonly value of 4

inches. The thickness of untreated permeable base used in Oregon typically ranges from 6 to 15 inches. The minimum requirement of 6 inches could ensure the permeability of the drainage layer. In addition, the untreated drainage layer of 6-inch thickness is easy to compact [20].

Drainage layer locations

In order to effectively remove the water which has infiltrated into the pavement, the drainage layer should be located at a depth to allow the time for drainage within required limit. It is recommended that for the highest-class highways the time for draining 50% of the free water should be within 1 hour, and for most interstate highways the limit is 2 hours [10]. As a result, drainage layer should be located at a depth where the drainage pathway is short enough for effective draining according to different pavement classes. At the same time, for the sake of stability, it should not be placed too near the surface, neither. Typically the drainage layer is located below the base course or act as a part of the base course.

The typical locations of drainage layer in the pavement structure are shown in Figure 1 and Figure 2 [21]. Figure 1 shows the base works as drainage layer. Therefore the drainage layer should satisfy both the permeability and the strength requirements. The disadvantages of base as drainage layer are inadequate stability and inconvenience for the drainage of water in subbase and lower structure. Figure 2 shows the drainage layer below subbase or as part of subbase. The disadvantage of this location is that the water pathway from drainage layer to infiltration surface is relatively longer therefore it would take more time for drainage. The permeability of the base and subbase materials should be greater than the infiltration rate to eliminate water trapping in the structure on top of the drainage layer.

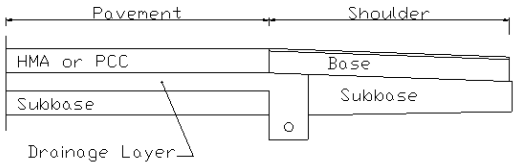

Figure 1. Base as drainage layer [21]

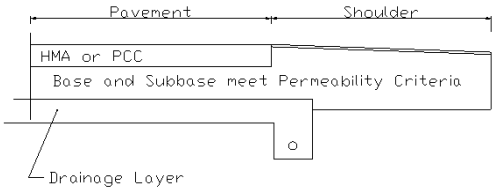

Figure 2. Drainage layer below subbase or as part of subbase [21]

Modulus and strength of drainage layer

The resilient modulus of the ATPB materials with very high air void contents ranging from 34.2% to 35.7% were investigated by the University of California, Berkley and the

Caltrans. The resilient modulus was obtained under different stress levels with the sum of the principal stresses (SPS) of 200kpa, 500kpa and 1000kpa through laboratory testing on the ATPB specimens [6]. The as-compact resilient modulus of ATPB used for the pavement design based on the Caltrans method and the elastic layer theory is 1172 MPa [7]. The ranges of the resilient moduli of the ATPB mixtures are from the minimum of 689 MPa to the maximum of 1034 MPa, and the modulus of 1034 MPa for the ATPB was used to model the pavement fatigue life [21]. Amara Loulizi et al. assigned the modulus of 1034 MPa for the open-graded drainage layer (OGDL) in their study to calculate the vertical stress responses within the pavement [8]. The resilient modulus was recommended to be 110,500 psi, or 762MPa for the ATPB according to Vermont Agency of Transportation Pavement Design Committee [9].

Compared with the conventional dense-graded asphalt concrete, the modulus of ATPB is much lower. The stiffness of ATPB materials were reported to be on the order of 1×10^6 kPa in the dry state while decreasing to a half in the wet state. The stiffness of conventional asphalt concrete can be 5.5 to 7 times than the stiffness of ATPB even in dry state [6]. Based on the back calculated effective pavement thickness, it is found that the pavement incorporated with permeable asphalt treated aggregate base would have smaller strength than pavement with regular dense-graded asphalt treated base in SPS-1 flexible pavement [22].

For CTPB materials, the typical strength of the CTPB materials ranges from 500 psi to more than 1,000 psi, at 7-day or 14-day ages based on both laboratory and field tests [23]. Therefore, the drainage layer can be considered as a weak load bearing layer in the pavement structure and its strength should be checked and incorporated into the pavement structural analysis for further study.

Stress state within drainage layer

The stress within the drainage layer varies with different pavement structures and temperatures. The practical stress levels inside the drainage layers are typically lower than that in the surface layers. Amara Loulizi et.al conducted field measurement of the compressive vertical stress under the asphalt surface and above the Open Graded Drainage Layer (OGDL). It shows that the vertical stresses under SM-9.5A surface layer vary with the temperature and range from less than 50 KPa to more than 200 KPa when the structure is subjected to 80-psi tire pressure [8]. It is reported that the vertical stress above the drainage layer is about 100 KPa when the temperature is 20℃. Imad L. Al-Qadi et.al measured the vertical stress under HMA surface layer for single load of 25.8KN on a pavement with 3-in asphalt stabilized open graded drainage layer locating below the base course. The vertical stress varies with temperature and ranges from less than 50KPa to more than 250KPa from 0℃ to 40℃. The vertical stress at 20℃ is about 80KPa, which shows consistency with former results [24].

Permeability test on asphalt mixtures

There are generally two kinds of testing method to determine the hydraulic conductivity of HMA mixtures in laboratory, which are constant head method and falling head method respectively. The ASTM D5084 *Standard Test Methods for Measurement of Hydraulic Conductivity of Saturated Porous Materials Using a Flexible Wall Permeameter* is the standard test protocols of the falling head method. According to this method, materials with hydraulic conductivities greater than 1×10^{-5} m/s may be determined by Test Method D 2434, which is a

constant head method. However, the ASTM D2434 may not be suitable for laboratory-compacted ATPB and CTPB specimens, or road cores, since it requires compacting specimens in the permeability testing container right before the test is being conducted. Many states have specific local testing methods to determine the permeability of asphalt concrete specimens in laboratory. Virginia validates the constant head method to determine the hydraulic conductivity of asphalt mixture with high permeability, as described in VTM-84. Oklahoma applies a flexible wall permeameter for laboratory permeability testing of regular asphalt mixtures as described in Oklahoma testing method OHD L-44. However, since the asphalt treated open graded aggregates are much porous than regular HMA mixtures, the inlet cylinder tube should be larger to ensure the time during the falling water head is not too short and is easy to be recorded. To investigate the permeability of unbonded aggregate base, Naji N. Khoury et al. used a device that was fabricated at the University of Oklahoma Broce Laboratory [25]. The device used an inlet tube with larger diameter and the inlet tube is longer than the one provided by the typical flexible wall permeameter.

Dynamic modulus test on asphalt mixtures

As one of the viscoelastic materials, the relationship between stress and strain of HMA is determined by complex dynamic modulus E*, which is a complex number to relate the stress to strain for the viscoelastic materials subject to continuous sinusoidal loading. The dynamic modulus is defined as the absolute value of the complex modulus. To determine the dynamic modulus of HMA materials in laboratory, typically five different test temperatures and six different loading frequencies are applied, to investigate the time and temperature dependency of the asphalt mixtures. The AASHTO T342-11 standard is the current available test protocols for determining the dynamic modulus of regular dense-graded asphalt mixtures [26]. There is currently no specific test protocols designed for ATPB mixtures. Under some circumstances, reduced test temperatures and loading frequencies can also be used to describe the dynamic modulus of asphalt mixtures and to construct the master curves. The dynamic modulus at least at three temperatures and three frequencies determined in laboratory testing are allowed in Mechanistic-Empirical pavement level 1 design. In order to construct master curve for the asphalt mixture, seven frequencies are required [27].

Drainage layer failures and problems

During the service life, the treated permeable materials of drainage layer may experience material and structural failures due to the combination effects of traffic loading and the environment. The California Department of Transportation (Caltrans) and the Indiana Department of Transportation (INDOT) both reported the material failures including fines injection from the beneath base course into the ATPB, and the stripping of asphalt coatings within the drainage layer. In addition to these material failures, the structural capacity of the stabilized permeable base may deteriorate when exposure to moisture or poor environmental conditions. Once the drainage layer loses its structural capacity, the pavement structure will be affected and damages are caused. Illinois monitored the effectiveness of drainage layer in nine pavements during late 1980's and early 1990's, finding two of them deteriorated quickly in forms of superficial distresses, severe lane to shoulder settlement and high deflections [28].

To prevent the material and structural failures in drainage layers, effective measurements should be applied. The majority of the material failures in the drainage layer is related with the intrusion of fines from other layers into the drainage layer, causing clogging of drainage paths. To prevent fine intrusions, dense-graded filter layer is applied to separate the drainage layer with other layers. However, there is currently few research focuses on the structural performance of the drainage layers. Within this context, research is needed to develop more convenient methods or modify existing methods to characterize the modulus and strength of these materials at high porosity, to perform analysis of the structural contribution and location effect of the drainage layer in the pavement structure, and to specify the optimal air void content for the effective drainage layers.

CHAPTER 3. MATERIAL COLLECTION FROM PARTICIPATING STATES

There are different kinds of materials which have been widely adopted for drainage layers in the U.S. Typically the materials used for drainage layers can be grouped into two categories: treated and untreated. Even among the treated materials, not only the stabilizing agent can be different in types and contents, the gradations of aggregates may also vary. In addition, there are also different laboratory tests to characterize the properties of treated and untreated materials. Each state has their own experience in drainage layer materials and applications. Therefore it is necessary to investigate what are the typical drainage layer materials and the typical pavement structure incorporated with drainage layer that are adopted in each participating state to facilitate experimental planning and further study. An online survey has been performed by the participating state DOTs to collect adequate information about the drainage layers.

Once enough information about the typically adopted materials for drainage layer has been obtained through the survey, technicians from each state DOTs were contacted to help acquire enough materials for laboratory testing. If there was an on-going project producing drainage layer materials, technicians from each DOT were asked to collect materials directly from the site and mail them to the asphalt laboratory where the tests are going to be performed. For states that have no on-going project, material collection was planned and waiting for the next available project. For states which have no project producing drainage layer materials within the term of this study, the virgin aggregates, asphalt binder and additives were collected to produce asphalt mixture in laboratory. To produce the asphalt treated permeable base mixture in laboratory, the temperature, asphalt content and additive content were strictly followed with the requirements provided by state specifications. The collected materials were then stored under appropriate environment and tested within a few months of storage to avoid environmental-induced deteriorations. Consequently, all the materials collected and tested are considered to be representative of the typical drainage layer materials adopted by the participating states.

ATPB materials

With the help of stuffs at VDOT, ODOT and ITD, different kinds of materials were collected for laboratory testing to characterize the volumetric properties, permeability and mechanical properties of the drainage layers in the three states. For Virginia, ATPB mixtures and unbound aggregates were collected from the asphalt plant in Lynchburg, VA in July, 2011. For Oklahoma, ATPB mixtures and virgin aggregates for CTPB were collected and mailed to the asphalt laboratory in April, 2012. The virgin aggregates, asphalt binder and anti-stripping additives were collected from Idaho in April, 2012. Because no ATPB mixtures were produced or would be produced during the period of this study in Idaho, the ATPB specimens for Idaho were mixed and compacted in the asphalt laboratory. Table 1 shows the parameters of the materials collected from the participating states.

Table 1. Drainage layer materials collected from Virginia, Oklahoma and Idaho

Asphalt treated materials		Total % passing		
	sieves	Virginia (ATPB-VA)	Oklahoma (OGBB-OK)	Idaho (ATPB-ID)
	1 1/2''		100	
	1''	100	95	
	3/4''	92		
	1/2''	73	47	50
	3/8''			35
	#4		3	4
	#8	4	2	1
	#200	1	1.4	
		Asphalt type		
		Virginia	Oklahoma	Idaho
		PG(70-22)	PG(64-22)	PG(64-28)
		Asphalt content		
		Virginia	Oklahoma	Idaho
		4.3%	2.5%	3.0%
		Laydown temperature		
		Virginia	Oklahoma	Idaho
		280°F	240°F	280°F
Cement treated materials		Total % passing	Cement content	Water to cement ratio
	sieves	Oklahoma (OGPCCB-OK)	Oklahoma (OGPCCB-OK)	Oklahoma (OGPCCB-OK)
	1 1/2''	100	270lb/yd^3	0.4
	1''	95		
	1/2''	47		
	#4	3		
	#8	2		
	#200	1.4		

These collected materials were stored in the monitored storage room of the asphalt lab before they were used in laboratory testing. The temperature was maintained at about 25°C in the storage room. All the plant-produced asphalt mixtures were used to compact cylindrical specimens within a few months of storage to avoid aging problem during storage. Figure 3 to Figure 10 have shown the ATPB mixtures and the virgin materials collected from Virginia, Oklahoma and Idaho for the series of laboratory testing.

Figure 3. ATPB-VA materials

Figure 4. Unbound aggregates from VA

Figure 5. OGPCCB-OK materials

Figure 6. Unbound aggregates from OK

Figure 7. ATPB-ID 1/2'' aggregates

Figure 8. ATPB-ID 3/8'' aggregates

Figure 9. ATPB-ID No.4 aggregates

Figure 10. ATPB-ID No.8 aggregates

CTPB materials

With the help of ODOT, two barrels of mixed open graded aggregates from the producer in Oklahoma have been collected. Theses aggregates were from the batches which were used for paving drainage layer in Oklahoma. These aggregates were then stored in the Thomas M. Murray Structure's Lab in Blacksburg, VA under room temperature before being used to fabricate CTPB specimens.

CHAPTER 4. LABORATORY TEST

A series of laboratory tests have been conducted to investigate the volumetric properties, permeability, dynamic modulus and compressive strength of the typical ATPB and CTPB materials adopted for drainage layers in Virginia, Oklahoma and Idaho. All the tests have followed the AASHTO, ASTM standard or the local specification of each state.

SPECIMEN PREPARATION

The ATPB mixtures collected from Virginia and Oklahoma were used directly to compact specimens in lab. These specimens are Plant Mixed-Lab Compacted (PMLC) specimens. However, due to the limited production of ATPB materials in Idaho during the period of this study, the materials collected from ITD were all virgin materials which need to be mixed in the lab to produce the ATPB mixture. Therefore all the Idaho's specimens are Lab Mixed-Lab Compacted (LMLC) specimens. Due to the different conditions (temperature, way of mixing, etc.) during production, the Idaho's ATPB specimens may exhibit some differences with the specimens for Virginia and Oklahoma in mechanistic properties, putting aside the influences of aggregate gradation, asphalt binder type and content.

Mixing ATPB in lab using typical materials from Idaho

The original materials collected from ITD include virgin aggregates, asphalt binder and additives which are typical materials used to produce ATPB in Idaho. The ATPB mixtures were produced using the drum mixer in lab as shown in Figure 11. The gradation in accordance with Idaho's specifications was adopted as in Table 1 in Chapter 3. The amount of aggregates of each sieve size was calculated firstly, then aggregates of different sizes with the desired amount were thoroughly mixed together. After this step, the aggregates and a jar of asphalt binder were heated separately in oven until that they all reached 280°F (monitored by thermometer). The aggregates were placed into the bucket and the bucket with aggregates was placed onto the electronic balance with resolution of 0.1 gram. The asphalt binder PG 64-28 and the approved additive Superbond® of calculated mass were slowly added into the bucket. After that, the bucket was fixed onto the mixer frame and the materials were mixed thoroughly. Blazer torch was used to heat the materials and maintain the required temperature during mixing. Figure 12 shows the process of adding aggregates of different sizes together for ATPB-ID production in the asphalt lab. Figure 13 shows the laboratory-produced ATPB-ID mixture.

Figure 11. ATPB production for Idaho using drum mixer

Figure 12. Adding aggregates of different sizes to produce ATPB-ID mixture

Figure 13. The LMLC ATPV-ID mixture

Compacting asphalt treated open-graded specimen

The gyratory compactor has been used to compact ATPB-VA, OGBB-OK and ATPB-ID specimens into 6 inches diameter and about 7 inches height with the air void contents ranging from 18% to 32%. These specimens were then cored and trimmed into appropriate dimensions to facilitate a series of further tests. The AASHTO standard T312 *Standard Method of Test for Preparing and Determining the Density of Hot-Mix Asphalt (HMA) Specimens by Means of the Superpave Gyratory Compactor* was followed to prepare the specimens by gyratory compactor in a height controlled mode [29]. To obtain specimens with different target air void contents, trial specimens were compacted to investigate the typical amount of mixture that is needed to obtain desired air void contents of the specimens. By adjusting the amount of ATPB materials placed into the cylindrical mold and compacted into the cylinders of the same volumes, different air void contents can be achieved. However, the air void contents of specimens after coring and trimming would be different from the original specimens prepared by the gyratory compactor. Therefore, to achieve desired air void content of specimens after coring and trimming, trial and error method was used. Figure 14 and Figure 15 show the Superpave Gyratory Compactor (SGC) and the as-compacted ATPB specimen. Figure 16 exhibits an example of the compaction curve on ATPB-VA specimen.

The temperatures at which the mixtures were compacted into specimens were chosen to be the laydown temperatures at field construction as shown in Table 1 in Chapter 3. Therefore, it is expected that all the PMLC and LMLC specimens can represent the real in-field properties of the newly-constructed drainage layer, and the data obtained from the series of laboratory tests can be applied for pavement design purposes.

Figure 14. Using the Superpave Gyratory Compactor (SGC) to compact specimens

Figure 15. The as-compacted ATPB specimen

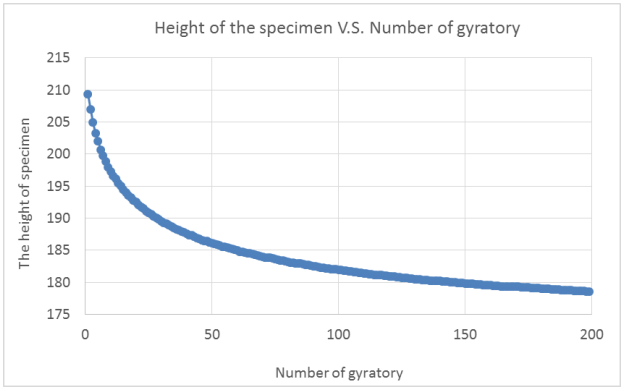

Figure 16. Height of the specimen versus the number of gyratory using SGC

Preparing cement treated open-graded specimens

To investigate the mechanical properties of the cement treated open-graded aggregates which have been incorporated into base or subbase courses as the drainage layers, specimens of 4 inch diameter and 8 inch height were fabricated for compressive strength test. The air void content of these specimens range from 27% to 35%.

The first step to produce the cement treated open-graded mixtures is to remix the unbound aggregates thoroughly to eliminate segregation of fines during the hauling of materials. The aggregates were poured out from the barrels and remixed on clean and flat floor free from cracks as shown in Figure 17. To reduce the size of the aggregate sample into a desired one for CTPB fabrication, and to maintain the original properties and conditions of the aggregates, the aggregate quartering method has been adopted. Firstly, these aggregates were piled in a cone with a shovel. Then the cone was flattened from the top and spread into a circular layer with even thickness. The aggregate layer was then divided into four quarters by two lines at right angles. Two diagonal quarters were discarded and the left two quarters were mixed thoroughly

and used to fabricate CTPB materials. Figure 18 shows the aggregate quartering method adopted in this study to sampling aggregates with desired size for producing the CTPB mixture.

Figure 17. Mixing the unbound aggregates in laboratory

Figure 18. Sampling the aggregates by quartering method

The traditional cement concrete producing method, ASTM standard C192/C192M *Standard Practice for Making and Curing Concrete Test Specimens in the Laboratory* was followed to fabricate the cement treated specimens [30]. Based on typical mix design, cement content used for CTPB in field is about 120kg/m^3 and the water cement ratio is 0.43. In this study, the production of the CTPB materials followed the Oklahoma's specification OHD L-53 as the open-graded Portland cement concrete base construction requirements. The mix design is present as in Table 2.

Table 2. Mix design of the open-graded Portland cement concrete base

Cement content	w/c ratio	Fly ash
270lb/yd^3	0.40	N/A

The unbound aggregates collected from the ODOT are No. 57 aggregates which were used in this study to compact the cement stabilized mixture OGPCCB-OK. The gradations are presented in Table 3.

Table 3. Gradation of the cement stabilized aggregates for Oklahoma

Sieve size	Percent passing
1-1/2''	100
1''	95
1/2''	47
No.4	3
No.8	2
No.200	1.4

The steps for fabricating the OGPCCB-OK specimens are described as follows. The thoroughly-mixed aggregates, water and Portland cement were weighted to get desired amount according to the mix design. The aggregates and part of the water were added into concrete mixer with the mixer running for a few minutes. Then the Portland cement was added into the mixer for mixing. The rest of the water and cement were added and mixed for three minutes,

followed by a three-minute rest time. After that, the mixer is started again for a final two-minute mixing and the mixture was used to fabricate specimens. All the specimens were made into 4 inches diameter and 8 inches height cylinders according to ASTM C192/ C192M. Three lifts of the mixture were placed into the plastic mold and each lift of the mixture was tamped before the next lift was placed during the compaction. Different air void contents were achieved by placing different amount of mixture into the mold and applying different numbers of rodding to get the specimen compacted to desired density. Trial and error method was used to obtain desired air void content. Figure 19 and 20 show the OGPCCB-OK mixture produced in laboratory and the molded specimens after compaction.

Figure 19. The laboratory-produced OGPCCB-OK mixture

Figure 20. The molded OGPCCB-OK specimens

The compacted specimens were stored under room temperature and fine spray of water was applied onto the surface of the specimens as long as the cement paste was set. Water curing was applied every two hours during a period of 16 hours for these specimens to simulate the situation in field construction as described in Oklahoma specification. During the storage, polypropylene sheets are applied to cover the specimens in molds. At 7 days after fabrication, six of the specimens were tested for the compressive strength and the rest of the specimens were not tested until they reach 14-day age, 21-day age or 28-day age. Table 4 lists all the OGPCCB-OK specimens fabricated for the compressive strength test at different ages.

Table 4. Number of OGPCCB-OK specimens of different air void contents for permeability and mechanical testing

Age	Specimens for compressive strength test	Specimens for permeability test
	Number of specimen with air void content from 27% to 35%	Number of specimen with air void content from 27% to 38%
7-day age	6	8
14-day age	6	
21-day age	6	
28-day age	6	

DETERMINING VOLUMETRIC PROPERTIES

Determining the bulk specific gravity of the aggregate (G_{sb})

The bulk specific gravity is a measurement of the density of the aggregates compared to the density of pure water at 23 ℃. The mass and volume considered in the bulk specific gravity G_{sb} are the oven-dried aggregate mass and overall aggregate volume including the permeable voids, respectively. The G_{sb} of aggregates, as the required parameter to predict the effective asphalt binder content, and to further predict the dynamic modulus of ATPB mixtures through empirical correlations, has been determined following the AASHTO standard T85, *Standard Method of Test for Specific Gravity and Absorption of Course Aggregate* [31]. The unbound aggregates collected from Lynchburg, VA, which were also the aggregates used to produce the ATPB-VA mixtures have been tested to determine the G_{sb} of ATPB-VA mixtures as shown in Figure 21 to Figure 23. Figure 24 to 25 present the unbound aggregates collected from Oklahoma, which were also the aggregates used to produce OGBB-OK and OGPCCB-OK mixtures. Figure 26 and Figure 27 show the aggregates used for ATPB-ID mixtures.

Figure 21. Saturated state of the unbound aggregates from VA

Figure 22. Dry the aggregates in oven

Figure 23. The dried unbound aggregates from VA

Figure 24. The saturated unbound aggregates from OK

Figure 25. The Saturated Surface Dry (SSD) state of the unbound aggregates from OK

Figure 26. The saturated unbound aggregates from ID

Figure 27. The Saturated Surface Dry (SSD) state of the unbound aggregates from ID

According to AASHTO T85, the bulk specific gravity of the aggregate is calculated by Equation 1.

$$G_{sb} = \frac{A}{B-C} \quad (1)$$

Where,

A= Mass of oven dry sample in air, g;

B= Mass of SSD sample in air, g;

C= Mass of SSD sample in water, g.

Determining theoretical maximum specific gravity (G_{mm})

The theoretical maximum specific gravity refers to the specific gravity of the mixtures with no air voids in it, which is also the maximum specific gravity can be reached in theory. With given bulk specific gravity, it can be used to calculate the air void contents of the specimens.

The theoretical maximum specific gravities of the ATPB-VA, OGBB-OK and ATPB-ID mixtures were determined following AASHTO T209 *Theoretical Maximum Specific Gravity and Density of Hot Mix Asphalt Paving Mixtures* [32]. Before the G_{mm} was determined, the mixture was heated in oven for 2 hours to facilitate further handling. The aggregates were then separated carefully by hand to eliminate clumps of fine particles. Figure 28 has shown the separated asphalt treated aggregates. Water replacement method, by weighing the specimen in air and under water, was used to determine the volume of solid aggregates. Before weighing the coated aggregates in water, a vacuum of 3.7 ±0.3 kPa (27.5 ±2.5 mm Hg) residual pressure was applied on the mixture for 15 ±2 minutes to remove air by agitating the water and mixture in container at 2-minute intervals. The apparatus used to determine the G_{mm} are shown in Figure 29 to Figure 31. The theoretical maximum specific gravity was calculated by dividing the weight of the dry mixture by the total volume of the mixture obtained from the water replacement method.

Figure 28. Separation of coated aggregates

Figure 29. Aggregates in bowl for evacuation

Figure 30. Vacuum the aggregates in water in a bowl

Figure 31. The system to determine the weight in air and in water bath

For each mixture the maximum theoretical specific gravity was tested twice and the average was used to calculate the air void content of different ATPB specimens. The maximum theoretical specific gravities of the ATPB-VA, OGBB-OK and ATPB-ID mixtures are determined to be 2.474, 2.524 and 2.525, respectively. The formula to calculate the G_{mm} is presented in Equation 2.

$$G_{mm} = \frac{A}{A-C} \quad (2)$$

Where,

G_{mm}= Theoretical maximum specific gravity of asphalt mixture;

A = Mass of dry sample in air, g;

C = Mass of sample in water bath at 25 ℃ (77 ℉), g.

To determine the air void contents of the OGPCCB-OK specimens, the theoretical maximum specific gravity of the OGPCCB-OK mixture was determined through the same test method which has been applied on ATPB materials, except that the cement treated materials need not to be heated to get separate particles.

Determining the Bulk Specific Gravity and Air Void Content of specimens

As aforementioned, unlike traditional dense-graded asphalt concrete, the materials used for drainage layer are usually much more porous, increasing the difficulties in determining air void content by traditional test method such as Saturated Surface Dry (SSD) method. However, as important parameters to Hot Mix Asphalt (HMA) mix design and pavement design, accurately determined volumetric properties such as bulk specific gravity and air void content will contribute to more reliable performance prediction. It is necessary to determine which test method is better to determine the air void content of drainage layer materials. Among those available test methods, the paraffin method is time consuming and the specimens are not reusable after the test, therefore is not adopted in this study. The dimensional method, parafilm method and vacuum sealing method has been adopted to determine the bulk specific gravity of the ATPB drainage layer materials. The air void content of each specimen was then calculated from the bulk specific gravity and theoretical maximum specific gravity determined through laboratory tests. The difference of the air void content between the specimens before and after coring and cutting were investigated to better predict the weight of mixture needed for compacting specimens into desired air void content. A comparison among the three methods has been conducted and suggestions are made for choosing the appropriate test method to determine the air void content of the drainage layer materials. Finally, based on the findings obtained from the comparison among the three test methods on ATPB-VA and ATPB-OK specimens, the vacuum sealing method was applied to quantify the air void contents of ATPB-ID and OGPCCB-OK specimens.

Dimensional method

The diameter and height of each specimen were measured by caliper for three times at 120 degree along the circumference. The weight of dry specimen in air was divided by the volume calculated from the average dimensions to get the bulk specific gravity by Equation 3. Although this method worked properly for some specimens, it had disadvantages. The major problem of this method lies in determining the volume of each specimen accurately especially for large-air-void specimens. With stabilized open-graded aggregates, the absence of fine aggregates in the drainage layer leads to more internal pockets of air in the mixture as well as air voids connected to the surface compared with dense graded mixtures. As a result, the surface of the specimen is quite rough, increasing the errors by using the dimensional method to determine the volume and air void content of specimens.

$$\text{Bulk Specific Gravity} = \frac{A}{\frac{1}{4}\pi d^2 h \rho_w} \quad (3)$$

Where,

A = the mass of the dry specimen in air, g;

d = the average diameter measured from the specimen, cm;

h = the average height measured from the specimen, cm;

ρ_w = the density of water at 4 ℃.

Parafilm method and CoreLok vacuum sealing method

As stated before, the traditional SSD method cannot work properly for the specimens of drainage layer materials. When getting the saturated specimen out from the water tank, the water drains out before the weight of saturated specimen could be determined. It is also hard to dry the specimen's surface because water inside would be pull out through the voids connected to the surface. These difficulties were both encountered in the trial testing of this study and reported by many other studies [33, 34]. As a result, the parafim method and the CoreLok vacuum sealing method were applied on these porous specimens to determine the air void content. The basic principle lies behind these two methods is similar, which is sealing the specimens and determine the volume of specimens by water replacement method, then calculate the bulk specific gravity and the air void content. To determine the volume of each specimen by water replacement, the weight of the wrapped specimen both in air and in water are measured. The parafilm method utilizes a waxy film to stretch it over the surface of specimens preventing water infiltrating into the specimen while the CoreLok vacuum sealing method applies plastic bags and also vacuums the sealed specimen before determining the weight in water. The bulk specific gravity of the specimen is calculated through dividing the weight of dry specimen in air by the specimen's volume using Equation 4.

$$Bulk\ Specific\ Gravity = \frac{A}{D-E-\left(\frac{D-A}{F}\right)} \quad (4)$$

Where,

A = mass of the dry specimen in air, g;

D = mass of the specimen wrapped with parafilm in air, g;

E = mass of the specimen wrapped with parafilm in water, g;

F = specific gravity of the parafilm at 25±1℃.

According to the manufacturer the specific gravity of the parafilm at 25±1℃ is 0.922, which was used to calculate the air void content for each specimen.

The air void content, known as one of the important volumetric parameters influencing the performance of asphalt mixtures, is defined as the percentage of the air voids between the asphalt coated aggregates to the total volume of the compacted asphalt mixture, which is also expressed by Voids in Total Mixture (VTM). It can be calculated by Equation 5.

$$VTM = \left(1 - \frac{G_{mb}}{G_{mm}}\right) \times 100 \quad (5)$$

Where,

VTM = Voids in total mixture;

G_{mb} = Bulk specific gravity;

G_{mm} = Maximum theoretical specific gravity.

Figure 32 and Figure 33 shows the specimen in sealed plastic bag by the Parafilm method and the vacuum sealing method. It can be seen that the vacuumed sealing bag attached more tightly to the surfaces of the specimen compared with the Parafilm method. Figure 34 to Figure

35 show the apparatus used to seal and vacuum the specimens, and the system to determine the weight and volume of each specimen.

Figure 32. Wrapped specimen in Parafilm

Figure 33. Sealed and vacuumed specimen

Figure 34. CoreLok System to seal and vacuum the specimens

Figure 35. Water displacement measurement of sealed specimen

The bulk specific gravity and the air void content of the OGPCCB-OK specimens were determined by the vacuum sealing method. Figure 36 and Figure 37 present the cured OGPCCB-OK specimen after demoulding and the specimen wrapped by the vacuum sealing method respectively.

Figure 36. The OGPCCB-OK specimen

Figure 37. The OGPCCB-OK specimen wrapped by vacuum sealing method

PERMEABILITY TEST

The main purpose of adopting the drainage layer is to get water drained out from the pavement effectively to avoid moisture accumulation in pavement structure, and to avoid further moisture-induced problems. Therefore the permeability of drainage layer is an essential property that should satisfy the effective draining requirements. To investigate the hydraulic conductivity of the typical treated open-graded materials used for drainage layers, laboratory permeability test has been conducted on PMLC ATPB-VA, PMLC OGBB-OK, LMLC OGPCCB-OK, and LMLC ATPB-ID specimens. Since some states have their specific testing method to determine the hydraulic conductivity of asphalt mixtures, the state specifications or the ASTM standard were followed to test the local materials. In this study, constant head method was applied on ATPB-VA specimens while the others were tested by the falling head method. For the cement treated specimens (LMLC OGPCCB-OK) of typically larger air void content than the ATPB specimens, constant head method has been applied primarily due to its convenience in testing specimens with large air void content and high permeability, and also because its requirements in specimen dimensions are in consistent with that of the compressive strength test. By adopting the constant head method, it is more time and cost effective to avoid casting new specimens to satisfy specific dimensions for the falling head method but also obtain paired permeability and strength data.

It should be noted that currently there is no nationwide standard for determining the permeability of laboratory compacted specimens made with open graded or gap graded asphalt or cement mixtures. The existing flexible wall falling head permeameters are more effective for dense graded asphalt mixtures. Therefore modifications of the current available permeability test method are necessary for the ATPB or CTPB materials. The local specifications, VTM-84 test method, which is constant head test for open graded drainage layer material has been used for Virginia's permeability testing [35]. Oklahoma typically facilitate the flexible wall falling head method to determine the hydraulic conductivity of laboratory compacted specimens. However, to apply the falling head method on open-graded asphalt treated specimens, customized inlet tube has been used to obtain better results. Except the inlet tube size, the Oklahoma testing standard OHD L-44 has been followed to determine the permeability of OGBB mixture with air void content from 18% to 29% [36]. There is no local specification to determine the permeability of ATPB specimens in Idaho, therefore the ASTM D5084 *Standard Test Methods for Measurement of Hydraulic Conductivity of Saturated Porous Materials Using a Flexible Wall Permeameter* has been followed to test ATPB-ID specimens [37].

The dimensions of the specimen adopted in the constant head or the falling head permeameter method are different. In the constant head method, specimens are cylinders of 4'' diameter while the in the falling head method, cylindrical disk specimen of 6'' diameter are typically used. Currently no standard test protocols are available to quantify the permeability of the cement-treated open-graded mixtures. Considering the most commonly used cement concrete specimens are of 4'' diameter, and the advantages of the constant head method on specimens of high permeability, the same test procedures as adopted for testing ATPB-VA specimens was followed on OGPCCB-OK specimens. Table 5 lists the permeability test methods that has been applied on the different mixtures characterized in this study.

Table 5. Permeability test methods on different mixtures

Material	ATPB-VA	OGBB-OK	OGPCCB-OK	ATPB-ID
Type of test	Constant head permeability test	Flexible wall falling head method	Constant head permeability test	Flexible wall falling head method
Specification	VTM-84	OHD L-44	VTM-84	ASTM D5084

Constant head method for ATPB-VA, OGPCCB-OK specimens

The ATPB-VA specimens were tested by the constant head method VTM-84 to determine the permeability. Before applying a water head above the specimen, the specimen was wrapped tightly with rubber membrane and was hold by a cylinder plastic mold which comfort tightly to the wrapped specimen. This will prevent water flowing along the space between the mold and specimen during the permeability test and affecting the results. Then the specimen was placed on a suspension device which was submerged in a tray full of water. By keeping a constant water head above the specimen in the plastic mold and measuring the amount of water running out of the tray during a certain period of time, the permeability can be calculated by the following equation:

$$k = \frac{Q \times L}{H \times A \times t} \tag{6}$$

Where,

Q = Amount of water collected;

t = Time to collect water;

A = Cross sectional area of the sample;

L = Length of sample;

H = Head Elevation;

The schematic of apparatus for the constant head method as described in VTM-84 is present in Figure 38. The water accumulated in the tray at the bottom of the frame is used to calculate the permeability. The shortcoming of this test method is that there may be a space between the rubber membrane and the specimen which provides a path to water. As a result, the water collected does not represent the water running through the specimen itself during a certain time period. Close attention has been placed on this problem during performing the test in this study. The advantage of the constant head method is that it is suitable for specimens with large permeability because there is no efforts to record the rapidly falling water head during the testing, compared with the falling head method. Figure 39 presents the set-up of constant-head permeability test in laboratory.

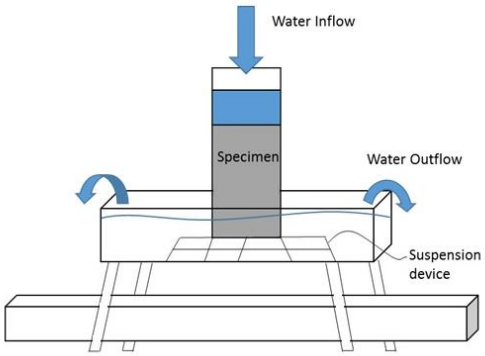

Figure 38. Schematic of apparatus for constant-head permeability test

Figure 39.Apparatus for constant-head permeability test

With no specified standard method designed for the cement treated open-graded mixtures, this constant head method has also been adopted to determine the permeability of the OGPCCB-OK specimens.

Flexible wall falling head method for OGBB-OK, ATPB-ID specimens

The flexible wall falling head permeameter has been used to determine the permeability of the PMLC mixture OGBB-OK and the LMLC mixture ATPB-ID with different air void contents. According to former studies, the degree of saturation may significantly influence the hydraulic conductivity of the asphalt concrete. To eliminate the impact of degree of saturation and focus on the influence of air void content on the permeability, all the specimens have been saturated before the testing. The AASHTO T283 *Standard Method of Test for Resistance of Compacted Asphalt Mixtures to Moisture-Induced Damage* was followed to saturate the specimens by applying a vacuum of 20 inch Hg for 10 minutes [38]. The specimen was then placed into permeameter and a vacuum of 10 to 15 psi was applied to the specimen in mold to get the rubber membrane comfort tightly to the surface of specimen, preventing water leaking through the space between specimen and membrane. By recording the time elapsed during water head dropping from the initial position to the final position, the hydraulic conductivity can be calculated by Equation (7).

$$k = \frac{aL}{At} \ln\left(\frac{h1}{h2}\right) C \tag{7}$$

Where,

k = coefficient of permeability;

a = inside cross-sectional area of the graduated cylinder;

L = average thickness of the test specimen;

A = average cross-sectional area of the test specimen;

t = elapsed time between h1 and h2;

h1 = initial head across the test specimen;

h2 = final head across the test specimen;

C = temperature correction for viscosity of water;

ln = natural logarithm.

As stated before, the permeameter with 500 c.c. capability of water head will not work properly on the treated open graded specimens. It takes only 2 to 3 seconds to get the water head falling to zero and makes it hard to record the time of water head dropping. In order to obtain a longer falling head time, the customized permeameter with a larger inlet tube which is capable of 2000 c.c. water as the water head has been adopted. At the bottom of inlet tube there's a part with the same diameter as the original inlet tube to make it easier to fix into the lid of permeameter. The customized inlet tube is shown in the Figure 40. Firgure 41 to Figure 42 show the setup of the apparatus for the flexible wall falling head method.

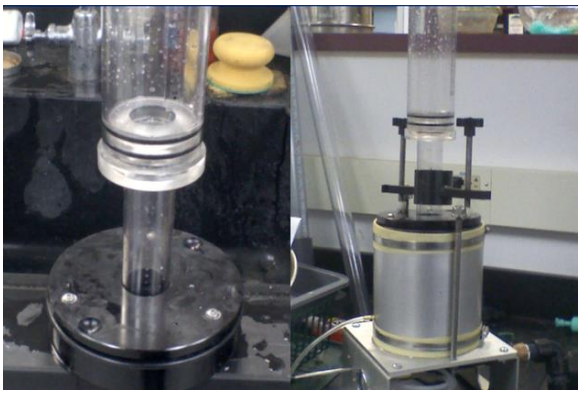

Figure 40. Customized large inlet tube with small diameter connection part

Figure 41. Setup for specimen saturation

Figure 42. The customized permeameter to determine the hydraulic conductivity of ATPB specimens

Except the modified inlet tube and water head used, the Oklahoma specification OHD L-44, which is a falling head permeameter method, was followed to test OGBB-OK specimens. The ASTM D5084 has been followed as the test protocols for ATPB-ID specimens. Before the permeability test was conducted, all the specimens were prepared following the AASHTO T283 to be fully saturated. For each specimen, the permeability has been tested for two times following the standard protocols, and an average has been used as the final permeability. In the situation when the permeability determined from the two measures are not consistent with each other, the possible causes such as broken rubber membrane or low pressure are investigated firstly, and then the test is re-performed.

DYNAMIC MODULUS TEST

Complex Modulus and Dynamic Modulus

As one of the linear-viscoelastic materials, the relationship between stress and strain of HMA is determined by complex dynamic modulus E*, which is a complex number to relates the stress to strain of viscoelastic materials subject to continuous sinusoidal loading. The complex dynamic modulus is defined as the ratio of the magnitude of the stress at any time and frequency to the magnitude of the strain corresponding to the stress as described in Equation 8.

$$E^* = \frac{\sigma}{\varepsilon} = \frac{\sigma_0 \sin(\omega t)}{\varepsilon_0 \sin(\omega t - \phi)} = \frac{\sigma_0 e^{i\omega t}}{\epsilon_0 e^{i(\omega t - \phi)}} = E' + iE'' \quad (8)$$

Where:

σ_0= the maximum peak stress;

ε_0= the maximum peak strain;

ω= angular velocity;

ϕ= phase angle;

t= time;

$E' = \frac{\sigma_0 \cos(\phi)}{\varepsilon_0}$, storage modulus;

$E'' = \frac{\sigma_0 \sin(\phi)}{\varepsilon_0}$, loss modulus.

E' and E'' correspond to the real part and the imaginary part of the complex modulus respectively. The real part represents the energy that has been stored during elastic deformation of viscoelastic materials while the imaginary part describes the energy converted into heat or the loss of energy during the deformation.

The dynamic modulus is defined as the absolute value of the complex modulus as the ratio of the peak stress and the peak strain under a certain loading frequency and temperature. The following equation can be used to calculate the dynamic modulus.

$$|E^*| = \frac{\sigma_0}{\varepsilon_0} \tag{9}$$

In the 2002 MEPDG, the dynamic modulus becomes an important input parameter for pavement design. It is recommended that the dynamic modulus of the paving materials obtained from laboratory testing should be used for level 1 input. Even in level 2 and level 3 designs, the dynamic modulus is still an important parameter predicted through empirical correlations with other easily obtained properties, or the default values are adopted. However, due to varied mechanical properties between the dense-graded asphalt concrete and the asphalt treated open-graded mixtures, the current available dynamic modulus test method may not be applicable on the ATPB specimens therefore the customized test method is necessary.

Modified Dynamic Modulus Test

Compared with traditional dense-graded asphalt concrete, differences in gradations, compaction temperatures and air void contents all contribute to the differences in mechanical properties of the drainage layer materials. Current available test method to determine the dynamic modulus of asphalt concrete, the ASSHTO T342-11 *Standard Method of Test for Determining Dynamic Modulus of Hot-Mix Asphalt Concrete Mixtures*, is originally designed for the traditional dense-graded asphalt concrete rather than the ATPB mixtures [26]. Generally, the reasons for modifying the conventional dynamic modulus test to facilitate its application on ATPB materials include:

- The temperature inside the ATPB drainage layer is different from that within the surface layer because it is not directly in contact with air. In addition, the high test temperature as recommended for regular asphalt mixtures is possibly destructive to ATPB specimens during conditioning even before the test can be conducted. During the test, high temperature will also trigger large permanent deformation of the specimen. Therefore different testing temperatures associated with the realistic temperatures inside the drainage layer in field should be investigated and adopted.

- Conventionally recommended loading magnitudes (stress levels) are too large for the drainage layer materials to keep the strains within 50-150 micro-strains during the

dynamic modulus test. According to the research conducted by Nam H Tran and Kevin D Hall, it was found that keeping the strain level within low ranges gave consistent results of dynamic modulus for linear-viscoelastic materials. The difference between the dynamic modulus obtained under 50-100 microstrain and 100-150 microstrain can reach up to 55% [39]. Therefore it is hard to achieve consistent dynamic modulus test results under the conventional loadings.

- The conditioning time of the dynamic modulus test varies with each environmental chamber and there is no experience on the conditioning time of the modified testing temperatures on ATPB specimens.

As a result, the AASHTO T342-11 has been modified especially in terms of the stress level, test temperature and the conditioning time to facilitate its application on ATPB mixtures.

Determining the stress levels of the modified dynamic modulus test

In this study, although the difference between the dynamic modulus under each strain level is not as high as 55% as mentioned in literature [39], it is still necessary to keep the strain under 150 microstrain as much as possible to maintain the material within linear-elastic domain and get reliable results. Figure 43 shows the largely deformed ATPB specimen under the traditional stress levels recommended in AASHTO T342-11 standard, indicating that the conventional stress levels are far too large for the ATPB specimens. In this regard, the applied stress level was selected independently rather than complying with the stress level ranges suggested by the AASHTO T342-11 standard, to keep the strain of ATPB specimens within 50 to 150 micro strains as much as possible. Totally about 30 dummy ATPB specimens with different air void contents have been used to determine the proper stress levels by observing the strains under different stress levels. Under some circumstances, it is hard to keep the strains under 150 micro-strain especially when the ATPB specimen is of 30% VTM and loaded under 37.8℃ at low frequency. At the same time, keeping reducing the stress level is either unpractical due to the limits of the instrument resolution. Taking all of these into consideration, the upper limit of the strains to determine the stress levels has been increased to 200 micro-strains. It has also been approved during the modified dynamic modulus test that consistent dynamic modulus data can be achieved for ATPB specimens when the strain levels are kept below 200 micro-strains. The frequencies, stress magnitudes and number of cycles applied during the dynamic modulus in this study are listed in Table 6. Figure 44 shows the load-time and strain-time relationship of the ATPB-VA specimen with 28% VTM at 0.5 Hz loading frequency under 29.4℃. The average peak-peak strain is 142.97 micro-strain. This specimen deformed too much under 37.8℃ so no valid data under 37.8℃ was adopted from the test. It can be found that the strains have been controlled to under 150 micro strains for this specimen with the proposed stress levels.

Table 6. Frequency, pressure and cycles applied at different temperatures for modified dynamic modulus test

Temperature ℃ (℉)	Frequency	Pressure (kPa)	Cycles	Recommended Pressure by AASHTO T 342-11 (kPa)
4.4 (40)	25	500	200	700-1400
	10	500	200	
	5	400	100	
	1	400	20	
	0.5	300	15	
	0.1	300	15	
12.7(54.9)	25	300	200	N/A
	10	300	200	
	5	250	100	
	1	250	20	
	0.5	200	15	
	0.1	200	15	
21.1 (70)	25	200	200	350-700
	10	200	200	
	5	150	100	
	1	150	20	
	0.5	100	15	
	0.1	100	15	
29.4(84.9)	25	100	200	N/A
	10	100	200	
	5	75	100	
	1	75	20	
	0.5	50	15	
	0.1	50	15	
37.8 (100)	25	50	200	140-250
	10	50	200	
	5	30	100	
	1	30	20	
	0.5	15	15	
	0.1	15	15	

Figure 43. Largely deformed specimen under traditional stress levels

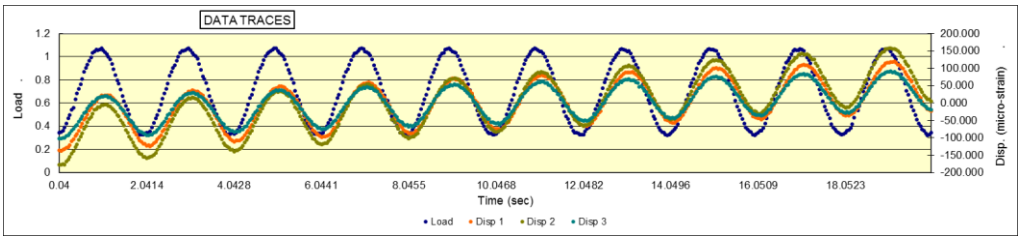

Figure 44. Load-time and Strain-time relationship obtained from the modified dynamic modulus test (ATPB-VA, 28%VTM)

Determining the test temperatures of the modified dynamic modulus test

Additionally, the temperatures at which the dynamic modulus is determined are also modified. Unlike the surface courses, the drainage layer is typically located at the top of the base course or on the top of the subbase. The energy exchange between the external world and the drainage layer is not as much as the surface layer which exposes to the environment directly. The temperatures within the drainage layer are different from that of the surface layer. Former studies showed that the temperatures near the location where the drainage layer settled are 30 ℃ to 35 ℃ in July in Los Angles [40]. In addition, the absolute values of the thermal gradients from the pavement surface to quarter-depth are much larger than that from quarter-depth to mid-depth. From the mid-depth to the bottom of the pavement the thermal gradients are not significant at all. In Virginia, the temperatures within pavement structure at different depths have also verified that the temperatures within drainage layer are much lower than that in the surface layer, according to the field-determined temperature within smart road located in Blacksburg, Virginia in April and October, 2000 [41]. The highest temperatures at depth of 0.188m and 0.413m, which can be seen as the typical depths for the drainage layer located above and below the base course, is 25 ℃. The measured temperature inside the typical locations of the drainage layer is much lower than the temperature measured on the pavement surface.

To further investigate the temperature distribution inside the drainage layer in the three states, the climate data of Lynchburg (VA), Oklahoma City (OK) and Boise (ID) have been used to predict the pavement temperature by the Enhanced Integrated Climate Model (EICM). According to the calculated temperature distribution, the highest mean temperatures inside the drainage layer which is located above the base occur in July are all below 34℃ in the three states, as illustrated in Figure 45. When the drainage layer is located below the base course, lower temperatures are obtained. Figure 46 shows the quintile temperatures in associated with 10%, 30%, 50%, 70% and 90% accumulated frequencies in July, indicating that there is a 90% probability that the temperatures inside the drainage layer are below 43.8℃, 44.5℃ and 44.8℃ in July in Lynchburg, Oklahoma City and Boise, respectively. However, testing at these elevated temperatures could increase the potential for permanently deforming the ATPB specimen. Therefore, the highest temperature in the proposed modified dynamic modulus test was selected to be 37.8℃.

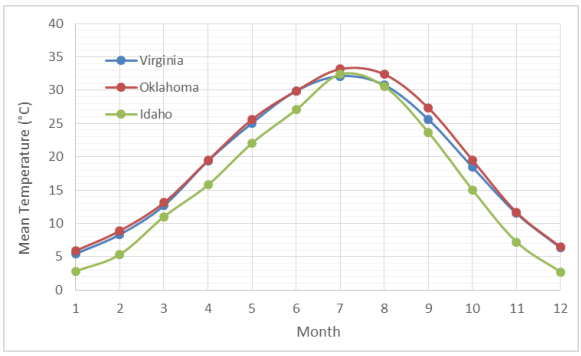

Figure 45. Mean temperature inside the drainage layer located above base calculated by EICM in MEPDG

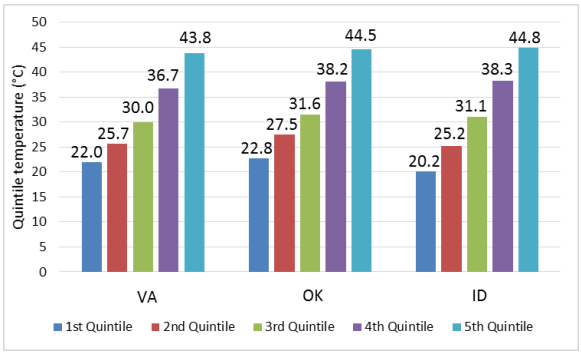

Figure 46. Quintile temperatures inside the drainage layer in July calculated by EICM in MEPDG

According to the results from former studies and the temperatures predicted by ECIM in this study, the temperatures inside the drainage layer are statistically at low possibility to reach up to 54.4℃ even in summer, which is the highest temperature in the dynamic modulus test standard for the dense-graded asphalt concrete. The low thermal gradients in the drainage layer also allow similar temperatures with little changes throughout the drainage layer. The comparatively low and less fluctuated temperatures in drainage layer make some of the recommended temperatures in AASHTO T342-11 not necessary for characterizing the drainage layer materials. In this case, based on the real temperatures generated in the drainage layer, modified test temperatures and the equilibrium time are recommended for characterizing the drainage layer materials. The 54.4℃ is removed and two more temperatures of 12.7℃ and 29.4℃ are inserted between other conventional temperatures provided by the AASHTO T342. Finally, the temperatures for the modified dynamic modulus test were set to be within 4.4℃ to 37.8℃. In addition to the standard temperatures of 4.4℃, 21.1℃ and 37.8℃, the interpolated temperatures of 12.7℃ and 29.4℃ were also adopted.

Determining the conditioning time for each test temperature

The conditioning time for specimens to reach an equilibrium temperature of 4.4 ℃, 21.1 ℃, 37.8 ℃ and 54.4 ℃ are recommended by AASHTO T342-11. However, due to different efficiency of the environmental chamber, the time needed to condition the specimens varies. Therefore the conditioning time suggested by the ASSHTO standard should be used with caution

and the real time needed should be determined for each equipment. In addition, the temperatures at which the dynamic modulus is determined for the drainage layer materials have been modified based on the real temperatures existing in the drainage layer as previously stated. Part of the test temperatures are different from what is recommended by AASHTO standard with no experience on the appropriate conditioning time. To determine the conditioning time needed within the environment chamber for specimens to reach the equilibrium temperature of 4.4 ℃, 12.7 ℃, 21.1 ℃, 29.4 ℃ and 37.8 ℃, a thermometer was placed on the top of dummy specimens inside the chamber to monitor the temperature changing with time during conditioning to reach modified test temperatures. The changing temperature of the specimen inside the chamber with the time released from the beginning of conditioning is shown in Figure 47 to Figure 54.

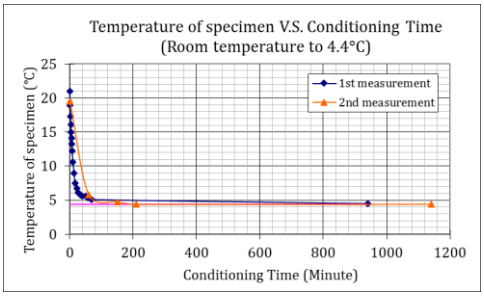

Figure 47. Chart. Temperature change of specimen in the environmental chamber from room temperature to 4.4 ℃

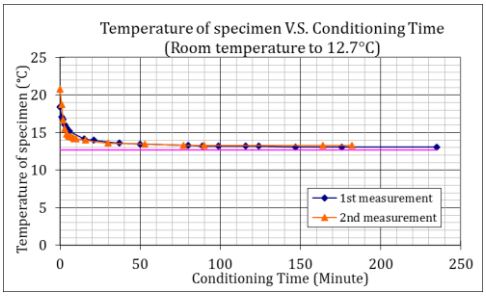

Figure 48. Chart. Temperature change of specimen in the environmental chamber from room temperature to 12.7 ℃

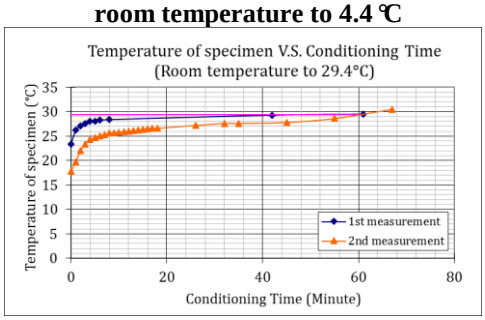

Figure 49. Chart. Temperature change of specimen in the environmental chamber from room temperature to 29.4 ℃

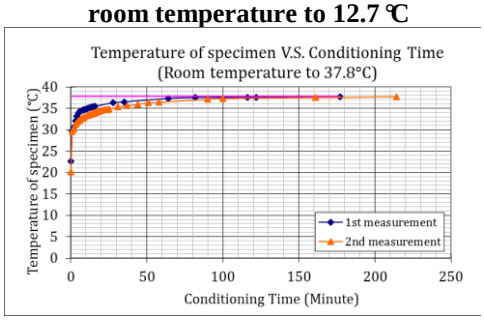

Figure 50. Chart. Temperature change of specimen in the environmental chamber from room temperature to 37.8 ℃

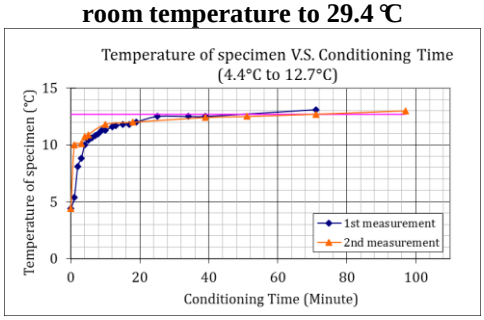

Figure 51. Chart. Temperature change of specimen in the environmental chamber from 4.4 ℃ to 12.7 ℃

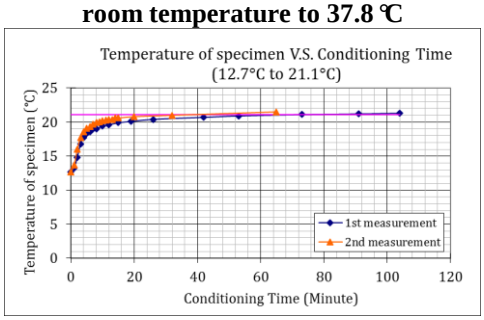

Figure 52. Chart. Temperature change of specimen in the environmental chamber from 12.7 ℃ to 21.1 ℃

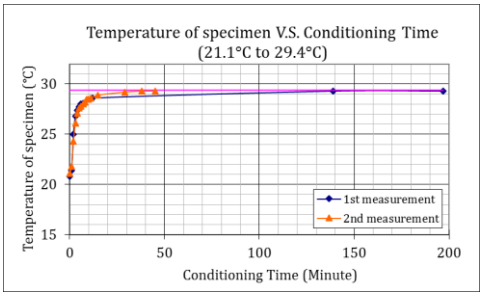

Figure 53. Chart. Temperature change of specimen in the environmental chamber from 21.1 ℃ to 29.4 ℃

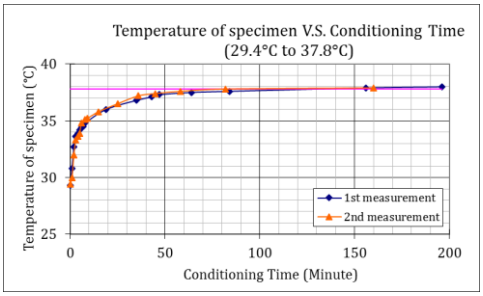

Figure 54. Chart. Temperature change of specimen in the environmental chamber from 29.4 ℃ to 37.8 ℃

Based on the measured relationship between the temperature of specimens inside the environmental chamber and the conditioning time, the required conditioning time to reach the equilibrium temperatures are determined and listed in Table 7. Both the required time to condition the specimens from room temperature and from the previous temperature are provided. All the conditioning time is determined based on the temperature monitoring results to ensure the equilibrium temperature is reached throughout the whole specimen. In the modified conditioning temperatures, similar conditioning time has been obtained for 4.4℃, 21.1℃ and 37.8℃ as in AASHTO T 342-11 standard. It should be noted that application of this required condition time with other environmental chamber should be with caution due to different conditioning efficiency. However, the conditioning time for ATPB materials is generally shorter than that for regular surface mixtures as recommended by AASHTO standard possibly due to the high air voids throughout the specimens.

Table 7. Time to condition the specimens at each temperature

Temperature ℃ (°F)	Time to condition the specimens from room temperature	Time to condition the specimens from last temperature
4.4 (40)	Overnight	
12.7(54.9)	3 hours	2 hours
21.1 (70)	1 hour	1.5 hours
29.4(84.9)	1.5 hours	1 hour
37.8 (100)	2 hours	1 hour

The dynamic moduli of the PMLC ATPB-VA, OGBB-OK and the LMLC ATPB-ID specimens were determined following the proposed modified dynamic modulus test as stated in this chapter using the Interlaken Compact Soil & Asphalt Test System in this study.

Specimen preparation

The diameter, height and mass of each specimen were determined before the dynamic modulus test. All the specimens were cut into 6 inches height with tolerant difference of 1/8 inches. The end surface will not depart from the plane perpendicular to the axis for more than one degree. Small aluminum studs were attached to the specimens on the side face for connecting the strain gauge. A steel jig was used to attach those studs equally spaced on the

specimens using epoxy glue. Difficulties were encountered during attaching studs onto the specimens because of the voids on the specimen surfaces. As a result, some studs were not attached properly and became loose under cyclic loading. To reduce the failure in test due to loosen studs, every specimen has been carefully observed to determine the optimal positions at 120 °interval along the circumference to stick the studs. The stress-strain results in loosen-studs case were not included for data analysis. Before the test was conducted, all the specimens to be tested were conditioned to reach the equilibrium temperature by the condition time as listed in Table 7. When specimens were conditioned to equilibrium temperature, they were placed onto steel disks under the load cell and three sets of linear variable differential transducers (LVDT) with a gauge length of 102mm (4 inches) were mounted on aluminum studs attached to the specimens for strain measurement. Figure 55 is the apparatus used to prepare specimens with aluminum studs and Figure 56 shows the prepared specimen.

Figure 55. Apparatus for attaching aluminum studs on specimens

Figure 56. Specimen with aluminum studs

Modified dynamic modulus test facilities

The Interlaken Compact Soil & Asphalt Test System controlled by Unitest software was used to conduct the modified dynamic modulus test. The same equipment and setup for testing traditional dense-graded asphalt concrete are used as shown in Figure 57 and Figure 58.

Figure 57. Apparatus for conducting the modified dynamic modulus test

Figure 58. Inside the environmental chamber

Compressive strength test

At the age of 7 days, 14 days 21 days and 28 days, four groups of specimens were tested for the compressive strength by using the Forney Testing Equipment. Specimens were firstly capped with bonded gypsum to level the ends and provide uniform distribution of loading. Then they were mounted under the load cell and loaded to failure. The maximum force shown on the panel during the compressive loading was recorded. The compressive strength of each specimen was calculated through dividing the maximum force by the cross sectional area of the specimen. The capped specimen and the setup for the compressive strength test are shown in Figure 59 and Figure 60. The compressive strength test was performed following ASTM C192/C192M standard.

Figure 59. The capped OGPCCB-OK specimen

Figure 60. The compressive strength test on OGPCCB-OK specimen

CHAPTER 5. LABORATORY TEST RESULTS

Based on the series of laboratory tests performed on totally about 150 specimens including asphalt and cement treated open graded drainage layer materials adopted by Virginia, Oklahoma and Idaho, data analysis has been conducted and the results have been presented in this chapter. Not only the volumetric properties, but also the permeability and the mechanical properties obtained from laboratory tests are provided. Finally, the recommended test methods to determine the bulk specific gravity and air void content of the treated open-graded materials, the relationship between permeability and air void content, and the mechanical properties of different kinds of treated open graded drainage layer materials are presented.

VOLUMETRIC PROPERTIES

The volumetric properties are basic material properties influencing both the permeability and the mechanical performance. Therefore, the selection of proper test method to determine the volumetric properties of the treated open-graded drainage layer materials with large air void content is the prerequisite for further study. The volumetric properties of the drainage layer materials presented here include the bulk specific gravity of the aggregate, theoretical maximum specific gravity, the bulk specific gravity and the air void content of the specimens which are representative of the drainage layer materials.

Bulk specific gravity of the aggregate

To obtain the effective binder content (V_{beff}) of ATPB-VA, OGBB-OK and ATPB-ID mixtures, the bulk specific gravity of the aggregate (G_{sb}) has been determined by following AASHTO standard T85. According to AASHTO T85, the bulk specific gravity of the aggregate adopted in ATPB-VA, OGBB-OK and ATPB-ID mixtures have been determined as shown in Table 8.

Table 8. The bulk specific gravity of the aggregates for ATPB-VA, OGBB-OK and ATPB-ID mixtures

Types of aggregate	Aggregates in ATPB-VA	Aggregates in OGBB-OK	Aggregates in ATPB-ID
G_{sb}	2.578	2.680	2.569

Theoretical maximum specific gravity

The maximum specific gravity of ATPB-VA, OGBB-OK, OGPCCB-OK and ATPB-ID mixtures were determined following the AASHTO T209 standard. The theoretical maximum specific gravities of different mixtures were calculated through equation as shown in Figure 35 in chapter 4 and the results are listed in Table 9.

Table 9. Theoretical maximum specific gravity of different mixtures

	ATPB-VA	OGBB-OK	OGPCCB-OK	ATPB-ID
G_{mm}	2.474	2.524	2.687	2.525

Bulk specific gravity and air void content

The dimensional method, parafilm method and CoreLok vacuum sealing method were performed on ATPB-VA and OGBB-OK specimens to determine which method is the most suitable one for testing the bulk specific gravity and air void content of the drainage layer materials with high air void content. Then the test methods adopted for ATPB-ID and OGPCCB-OK specimens were selected based on the conclusions of the comparison among the three methods. The air void contents obtained by proper test methods were used for further study.

Air void content before and after coring and cutting

The as-compacted cylindrical specimens are of 6'' diameter and about 7'' height, which are not of the standard dimensions required for further testing, such as the dynamic modulus test and the permeability test. The dynamic modulus test requires specimens to be of 4'' diameter and 6'' height while the falling head permeability test requires the specimens to be of 6'' diameter and 3'' thickness. As a result, the as-compacted specimens will be handled by coring and cutting to change them into desired dimensions before further testing. In this study, all the specimens have cored side surface but a few of them are with as-compacted ends due to difficulty in getting completely undamaged specimens after coring and cutting with such high air void content.

Due to the way of compaction by the gyratory compactor, specimens usually have different air void contents before and after coring and cutting. The way of rotating during compaction possibly leads to larger air void content on the peripheral of the specimen [42]. In order to obtain desired air void content after coring and cutting, this discrepancy should be considered ahead during specimen compaction phase. The relationship between the difference of air void content before and after coring and cutting by dimensional and parafilm method are plotted in Figure 61 and Figure 62 respectively. Due to the requirements in specimen dimensions of the CoreLok vacuum sealing method, the specimens before coring and cutting are too large to be tested, thus no comparison has been presented here on the vacuum sealing method. However, the comparisons from dimensional method and Parafilm method have exhibited that the specimens before coring and cutting usually have larger air void contents than the cored and trimmed specimens. The difference typically ranges from 1.5% to 3.5% and can reach up to 4% for the compacted asphalt treated open graded mixtures with air void content from 18% to 35%. For specimens with higher air void content the difference before and after coring and cutting has a deceasing tendency. In addition, the Parafilm method obtains smaller before-after differences in air void content with less variation on the same group of specimens, compared with the Dimensional method, as shown in Figure 61 and Figure 62.

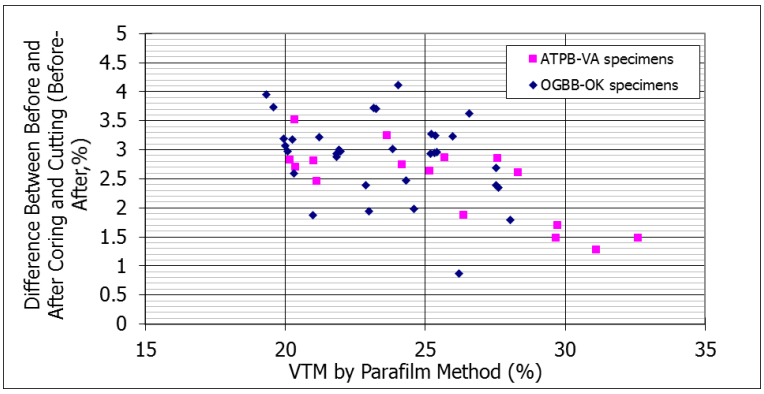

Figure 61. Relationship between the air void content before and after coring and cutting by dimensional method

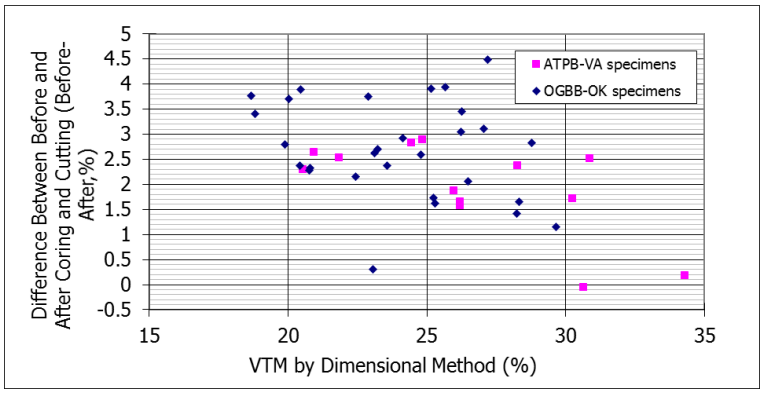

Figure 62. Relationship between the air void content before and after coring and cutting by Parafilm method

Air void content (VTM) determined from different methods

The air void content obtained from dimensional method and parafilm method on ATPB-VA and OGBB-OK specimens indicates that the dimensional method usually yields higher VTM than the parafilm method for the most asphalt treated open graded specimens, with most of the points falling below the equality line. Figure 63 has presented the comparison between the dimensional and parafilm method. During the tests it is also found that as long as the parafilm comport tightly to the specimen surfaces, the parafilm method could get more consistent specific gravity and consequently VTM than the dimensional method especially for high-air-void specimens. For asphalt treated open graded specimens with air void content up to 30%, the as-compact surfaces are rough and the specimen cannot be seen as true cylinders when aggregates lost on the edges. In this case the dimensional method which relies on the measured diameter and thickness to calculate the volume might be unreliable while the parafilm method utilizing water replacement method could get good estimations.

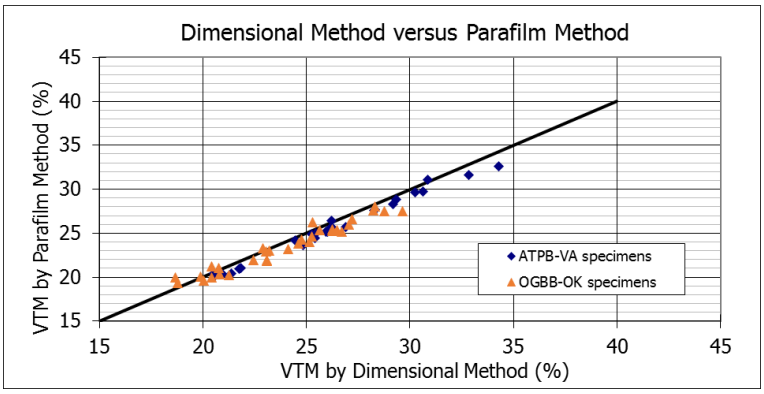

Figure 63. Relationship of the air void content obtained from dimensional and Parafilm method

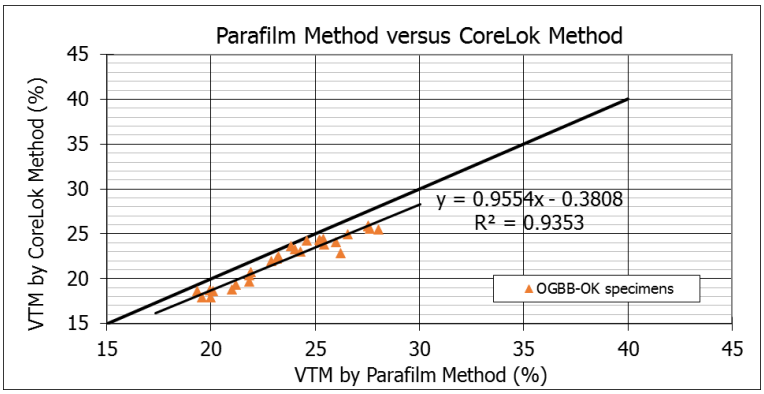

Figure 64. Relationship of the air void content obtained from Parafilm and CoreLok method

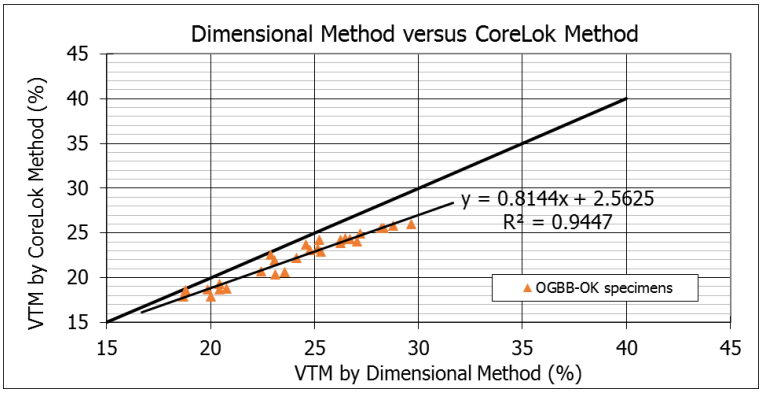

Figure 65. Relationship of the air void content obtained from dimensional and Parafilm method

A linear regression prediction between the VTM obtained from Parafilm method and CoreLok vacuum sealing method has been conducted on 38 OGBB-OK specimens and the relationship is shown in Figure 64. All the data points are below the equality line, indicating that the air void contents obtained from the CoreLok vacuum sealing method are all lower than the results of Parafilm method. With the slope of the predicted relationship less than 1, the predicted air void content deviates further from the equality line at larger air void contents. It is also found that with increasing air void content the differences between these two methods will increase. Therefore selection of proper test method is essential for determining the air void content of asphalt-treated-permeable specimens. Similar findings can be obtained from the comparison

between Dimensional method and CoreLok method as shown in Figure 65. The CoreLok vacuum sealing method is shown to be more suitable than the parafilm method for specimens prepared with drainage layer materials in this study. This is because the vacuum procedure will get the plastic bag lying more tightly to the specimen surface than the parafilm method and consequently the volume obtained is closer to the true volume.

According to a previous study by Xie et al., there is a system error for the CoreLok method when testing specimens with low air void content, and this error should be checked for each equipment [43]. The system error can be confirmed by testing a steel cylinder which can be seemed as material with no air void content by the CoreLok sealing method. A steel cylinder with 4 in. diameter and 4.5 in. thickness was tested by the CoreLok method. It is found that the air void content is 0.612%, indicating the system error for the equipment used in this study is 0.612%. However, considering the specimens used in this study are of air void content larger than 20%, no correction is applied on the testing data.

Based on the statistical analyses of the air void content determined by the three methods on all the specimens, the coefficient of variance (CV) of the vacuum sealing method is the smallest while dimension method has the largest CV as present in Table 10. The Coefficient of Repeatability (CR) of the three methods were also determined by repeated pairs of measurements on the same specimen operated by the same technician. The CR of the Dimensional method, Parafilm method and CoreLok vacuum sealing method are determined to be 0.02458, 0.0049 and 0.00479 based on the measurements on five ATPB specimens by each method, indicating that the differences of 2.458%, 0.490% and 0.479% in air void content would be exceeded by 5% of measurements by each method. With both the smallest CV and CR, the vacuum sealing method is considered to be the most repeatable procedure with less variation than the other methods for the ATPB materials used in this study.

Table 10. Statistical analyses of the air void content determined by the three methods

	Mean	Std Dev	Coefficient of Variance (CV)
Dimensional Method	23.205	3.188	13.740
Parafilm Method	23.343	2.912	12.477
CoreLok Vacuum Sealing Method	21.465	2.575	11.996

The ANOVA analyses was also conducted to confirm whether there is significant difference between the air void content obtained from the three methods. The F-test indicates that there is no significant difference of the variance between the three methods in determining the air void content, with the P value of 0.0647 larger than 0.05. However, the P value for T-test of the air void content obtained from the Parafilm method and the CoreLok vacuum sealing method is 0.0357 at 95% confidence level, showing that there is a significant difference of the mean between these two methods. The results of the ANOVA analyses are present in Figure 66 and Table 11.

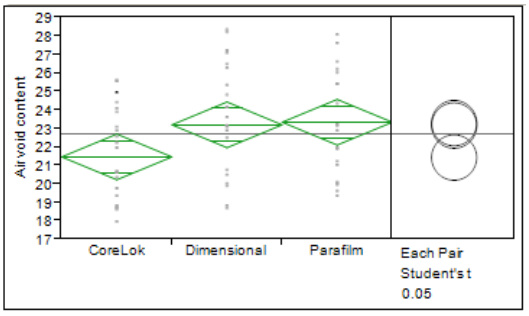

Figure 66. ANOVA analyses on the significant difference between the three methods in determining air void content

Table 11. Analysis of variance

Source		DF	Sum of squares	Mean squares	F ratio	Prob>F
Methods		2	48.21675	24.1084	2.8612	0.0647
Error		63	530.84348	8.4261		
C. Total		65	579.06023			
Level		Difference	Std Err Dif	Lower CL	Upper CL	p-Value
Parafilm	CoreLok	1.878363	0.8752188	0.12938	3.627348	0.0357*
Dimensional	CoreLok	1.740006	0.8752188	-0.00898	3.488991	0.0512
Parafilm	Dimensional	0.138357	0.8752188	-1.61063	1.887342	0.8749

The results show that for the specimens with high air void content larger than 20% as representative of the drainage layer, the testing method adopted to determine the air void content can influence the results significantly. Therefore each method has its own applications and should only be adopted within certain VTM ranges to obtain good results and improve time and cost efficiency. The ANOVA analysis reveals that for specimens of larger than 21% VTM, significant difference exists among the three methods or within each pair of two methods based on 95% confidence. Therefore the influences of the applied methods on testing results cannot be ignored on specimens of VTM larger than 21% especially when accurate result is required. With decreasing in the air void content from 25% to 20%, the differences among the three methods or between each two of the methods become less significant, with no significant difference observed on specimens with 20% or less air void content. When the VTM is increasing to larger than 24%, the difference between parafilm method and vacuum sealing method becomes significant. Therefore, in laboratory test, dimensional method can be used for specimens of less than 21% VTM and Parafilm method is good to test specimens of less than 24% VTM, for the sake of cost efficiency. The CoreLok method should be applied for specimens of VTM larger than 24%. To determine which method should be applied at the first place, an estimation of the air void content by the dimensional method can be used. However, in practice, there might be large variations between the real and target air void content, or the batch of specimens have wide ranges of air void contents. In this case, it is more important to conform to a consistent test method, and the CoreLok vacuum sealing method is preferable. The recommended steps to determine the choice of test method for drainage layer materials are shown below. Firstly, the rough ranges of the air void content should be estimated. If the air void contents are with small

variation all below 24%, the Parafilm method can be adopted. This situation is more common in laboratory test on laboratory-compacted specimens. Once there is specimen with air void content exceeding 24%, the vacuum sealing method should be applied on all specimens to facilitate comparison. In this study, the VTM used in further data analysis were determined by appropriate test methods as recommended here.

PERMEABILITY PROPERTIES

Following the local and national modified or standard permeability test protocols, the correlations between the permeability and VTM have presented different forms. The constant head method has achieved concave permeability-VTM curve on ATPB-VA specimens while the flexible wall falling head method has obtained slightly convex permeability-VTM relationships on OGBB-OK and ATPB-ID specimens, with the largest R^2. The VTM of ATPB-VA specimens were obtained by Parafilm method rather than the vacuum sealing method due to the equipment problems encountered, but still good relationship was achieved. Considering quite amount of the laboratory compacted specimens are with VTM larger than 24%, the VTMs from vacuum sealing method have been used for OGBB-OK and ATPB-ID specimens to achieve reliable results. The relationship between the permeability and VTM of ATPB-VA, OGBB-OK and ATPB-ID mixtures are shown in Figure 67 to Figure 69.

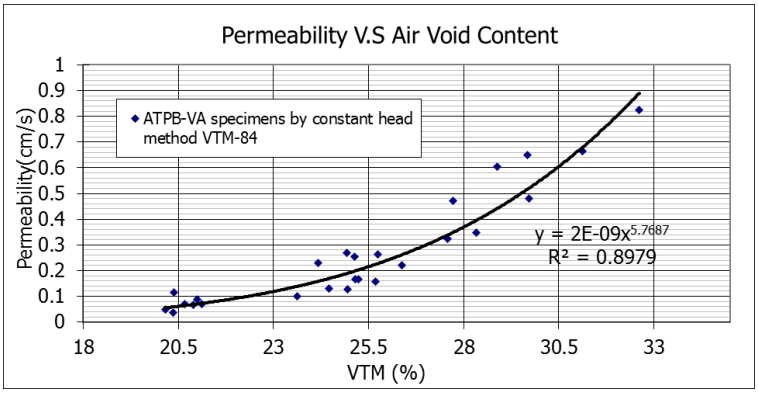

Figure 67. The relationship between the air void content and permeability for ATPB-VA specimens

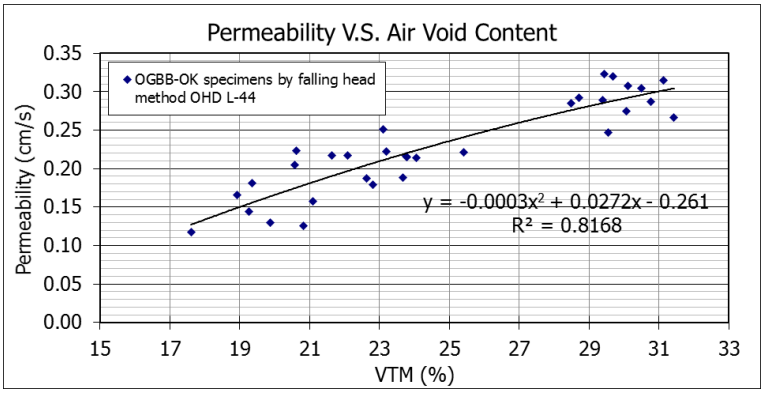

Figure 68. The relationship between the air void content and permeability for OGBB-OK specimens

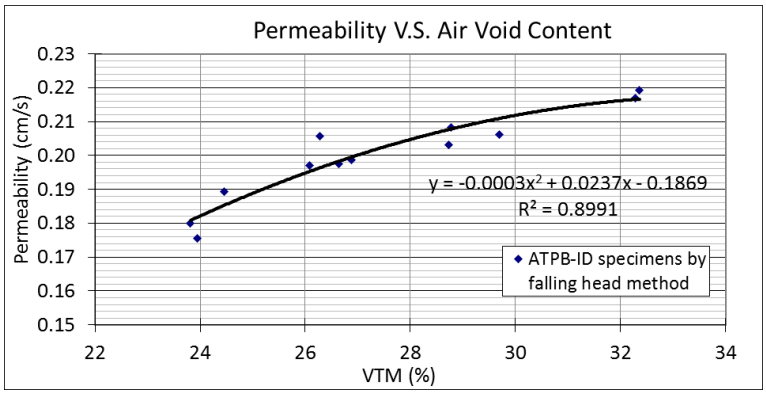

Figure 69. The relationship between the air void content and permeability for ATPB-ID specimens

The permeability of the PMLC ATPB-VA specimens by constant head method VTM-84 has larger increasing rate of permeability when the VTM increases as shown in Figure 67, compared with other mixtures tested by falling head method. The permeability under room temperature ranges from 0.0382cm/s to 0.826cm/s for specimens at air void contents from 20.39%m to 32.61%. The empirical relationship with the largest R^2 between the permeability and the air void content by the Parafilm method on ATPB-VA mixture is presented in Equation 10.

$$\text{Permeability} = 2 \times 10^{-9} VTM^{5.7687} \quad (10)$$

$$R^2=0.8979$$

The relationship between permeability and air void content of the OGBB-OK mixture is very different from that of the ATPB-VA mixture as shown in Figure 68. The reasons for this inconsistency include different test methods adopted and the properties of mixtures due to different gradations, asphalt types and asphalt contents. In fact, the constant head method was also conducted on the Oklahoma's specimens to check the influences caused by different testing methods. A comparison between the permeability obtained from constant head method and the modified flexible wall falling head method on the specimens of same air void content shows that the former method typically obtains larger permeability results than the latter one, indicating that the influences of the test method do exist and should be considered when the permeability obtained from different methods are used for comparison. The permeability of the OGBB-OK specimens ranges from 0.117cm/s to 0.319cm/s at air void contents from 17.62% to 31.43%, which is consistent with former studies [25]. The empirical relationship of the largest R^2 value is shown in Equation 11.

$$\text{Permeability} = -0.0003 \times VTM^2 + 0.0272 \times VTM - 0.261 \quad (11)$$

$$R^2=0.8168$$

The permeability of ATPB-ID specimens obtained from flexible wall falling head method was shown in Figure 69. Although 16 specimens were made for the permeability test, only the results from 12 specimens were useful and were adopted for data analysis. Some of the specimens collapsed during preparation, or the trimmed specimen cannot satisfy the dimensional requirements and therefore have been discarded. No permeability result was obtained from these

under-qualified specimens. The effective testing data is plotted in Figure 69. Compared with the permeability of typical asphalt treated specimens for Virginia and Oklahoma, the permeability of Idaho's ATPB specimens is of small variance as the air void content changes. The different gradations of aggregates used in ATPB-ID mixture is possibly the reason for this variation. Equation 12 shows the empirical relationship between VTM and permeability with the largest R^2 for the ATPB-ID specimens.

$$\text{Permeability} = -0.0003 \times VTM^2 + 0.0237 \times VTM - 0.1869 \qquad (12)$$

$$R^2=0.8991$$

Since there is no standard test method to determine the permeability of cement treated open graded materials, the constant head method has been applied on OGPCCB-OK specimens. The specimens after the constant head permeability test can be reused in the compressive strength test and obtain paired VTM-permeability and VTM-strength results. Therefore, the OGPCCB-OK specimens were compacted to 4'' diameter and 8'' height for the constant head method to determine the permeability of specimens with different air void contents. The VTM and permeability of OGPCCB-OK specimens are listed in Table 12. The relationship between VTM and permeability is shown in Figure 70.

Table 12. Permeability determined using constant method for OGPCCB-OK specimens

Specimen #	VTM (%)	Permeability (m/s)	Permeability (ft/day)
S19	29.686	0.038935	11036.83
S20	30.378	0.037709	10689.03
S21	31.950	0.046710	13240.76
S22	29.184	0.033820	9586.70
S24	29.351	0.035994	10203.12
S27	26.876	0.022828	6470.79
S30	31.739	0.050761	14388.86

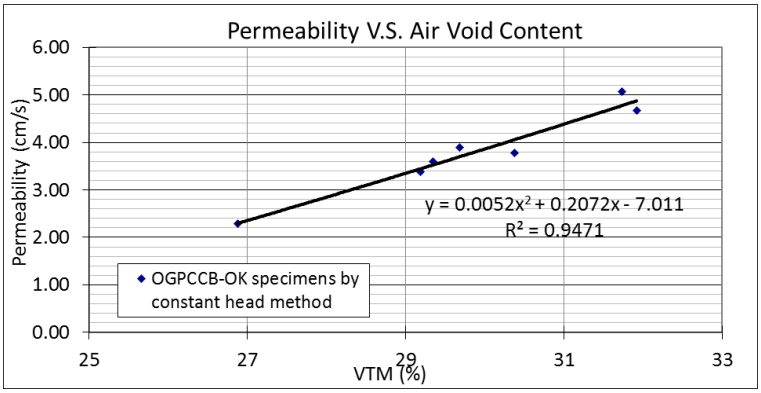

Figure 70. The relationship between air void content and permeability for OGPCCB-OK specimens

In this study, since the lowest VTM which can be achieved by hand punning for the OGPCCB-OK specimens is 27%, the permeability test was performed only on the specimens

with a limited ranges of porosity. Based on the test results, the permeability of OGPCCB-OK specimens ranges from 2.0 cm/s to 5.1 cm/s with the VTM from 27% to 32%. It should be noted that the permeability of the OGPCCB-OK specimens by constant head method is much higher than that of the asphalt treated drainage layer materials no matter determined by constant head or falling head method. Except the effects of gradation, air void content, binder content and so forth, the rough specimen surface may also attribute to this phenomenon. The rough surfaces of the OGPCCB-OK specimens have increased the interspace between the side surface of the specimen and the rigid mold which is used to hold the specimen and keep the constant water head above the specimen. As a result, when the constant head permeability test was conducted, water flew through the interspace and increase the permeability. For asphalt treated specimens with cored side surface, the space between mold and specimen is so small that little water can get through. This is considered to be the major reason for the large permeability of OGPCCB-OK specimens obtained in this study. The empirical relationship between the permeability and VTM for OGPCCB-OK specimens is shown in Equation 13.

$$\text{Permeability} = -0.0004 \times VTM^2 + 0.027 \times VTM - 0.4263 \quad (13)$$

$$R^2=0.9675$$

DYNAMIC MODULUS OF ASPHALT TREATED DRAINAGE LAYER MATERIALS (MEPDG LEVEL 1 INPUT)

Totally about one hundred ATPB-VA, OGBB-OK and ATPB-ID specimens have been tested to determine the dynamic modulus of asphalt treated drainage layer materials with different air void contents. The proposed modified dynamic modulus test has been adopted to test all the specimens. The laboratory-determined dynamic moduli have been compared with the dynamic moduli of traditional asphalt concrete, utilized to construct empirical correlations to predict the dynamic modulus through more easily obtained material properties, and used as references to suggest for default dynamic modulus of drainage layer materials. The provided empirical correlations can be incorporated into level 2 and level 3 M-E pavement design procedures to consider the structural performance of the drainage layer.

Modified Dynamic Modulus and Phase Angle Results

During the modified dynamic modulus test, three specimens of air void content within 1% variation from the average were considered as a group with the same VTM level. Each group of specimens were tested from the lowest to the highest temperature. At each temperature, the axial load was applied from the highest to the lowest frequency until the planned loading cycles were reached. Totally five temperatures and six loading frequencies as previously stated in the modified dynamic modulus test were used. The average dynamic modulus of each group has been utilized to construct master curves. The ATPB-VA specimens with the VTM levels of 20%, 21%, 24%, 25%, 26% and 28%, OGBB-OK specimens with the VTM levels of 18%, 19%, 20%, 22%,23%, 24%, 25% and 26%, and ATPB-ID specimens with the VTM levels of 22%, 24%, 26% and 28% have been tested for dynamic modulus and used to construct master curves. In

following figures showing dynamic modulus and phase angle properties, every point actually represents the average of triplicated specimens.

Figure 71 shows an example of the relationship between axial stress and strain under cyclic axial loading on ATPB-VA specimen A3. The three curves have presented the data obtained from three LDVTs mounted on the side surface of specimen at 120 degree interval. Figure 72 and Figure 73 show the normalized load and displacement. The other modified dynamic modulus data of every specimen and each group are included in Appendix A.

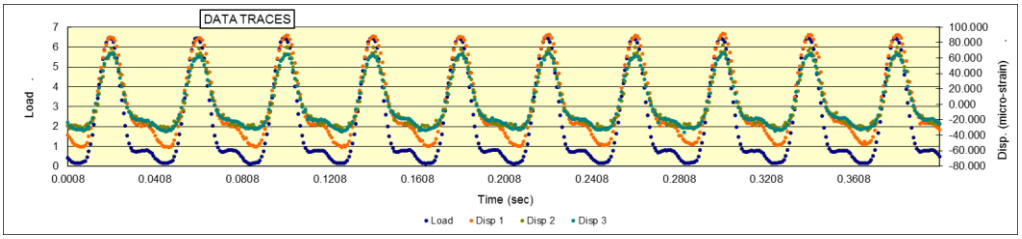

Figure 71. Load and displacement versus time during the modified dynamic modulus test on ATPB-VA specimen A3

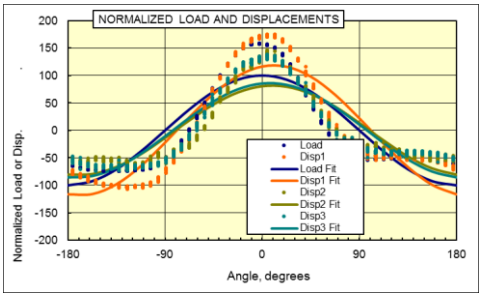

Figure 72. Normalized load and displacement of the ATPB-VA specimen A3 representative of 20% air void content

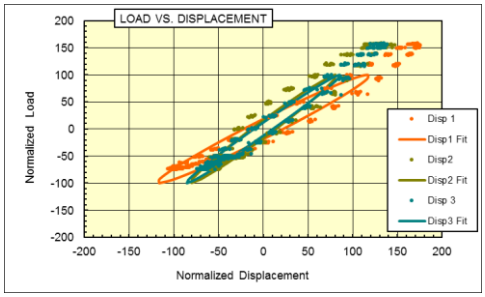

Figure 73. Normalized load and normalized displacement of the ATPB-VA specimen A3 representative of 20% air void content

It should be noted that during the testing, several ATPB-ID specimens collapsed and the moduli of most specimens of 28% air void content above 29.4 ℃ were hardly obtained due to large strains during the testing, even though the loadings have been reduced down to the minimum. As a result, the master curve of ATPB-ID specimens with 28% air void content was constructed based on the dynamic modulus obtained under three temperatures, which are 4.4 ℃, 12.7 ℃ and 21.1 ℃.

Construct the dynamic modulus master curves

As a viscoelastic material, the stiffness of the asphalt mixture is not only related with the temperature but also the rate of loading. By shifting the dynamic moduli under different temperatures into one smooth curve at a reference temperature (usually 21.1°C), the relationship between the dynamic modulus, temperature and time of loading can be expressed by one single master curve. The master curve of dynamic modulus describes the time dependency of the material while the shifting factors at each temperature describe the temperature dependency.

According to former researches the master curves are constructed based on the principle of time-temperature superposition. The dynamic moduli obtained from tests at various

temperatures are shifted with respect to time until the curves merge into a smooth sigmoidal function [44, 45]. Therefore the modulus master curve can be modeled into a sigmoidal function including four parameters as shown in Equation 14.

$$\log|E^*| = \delta + \frac{\alpha}{1+e^{\beta+\gamma(\log t_r)}} \quad (14)$$

Where,

t_r is reduced time of loading at reference temperature,

α, β, γ, δ are all fitting coefficients.

The reduced time of loading at reference temperature is also related to the shift factor as:

$$\mathrm{a}(T) = \frac{t}{t_r} \quad (15)$$

In which $\mathrm{a}(T)$ is the shift factor as a function of temperature.

The method which has been adopted to construct the master curve is presented as follows. Firstly, the relationship between the logarithm of the shift factor and the temperature is expressed as a second order polynomial as shown in Equation 16.

$$\log a(T_i) = aT_i^2 + bT_i + c \quad (16)$$

Then by simultaneously solving for the four coefficients of the sigmoidal function (α, β, γ and δ) as described in Equation 14 and the three coefficients of the second order polynomial (a, b, and c) as described in Equation 16, the master curve can be constructed. In this study, a Microsoft Excel worksheet has been made to conduct the nonlinear optimization for simultaneously solving these seven parameters. By minimize the sum of squared residuals between the laboratory test results and the modulus calculated from the sigmoidal function, the parameters of the sigmoidal function were determined and the master curve was constructed.

The master curves of dynamic modulus for ATPB-VA mixtures with different air void contents are shown from Figure 74 to Figure 79. At each air void content the master curve is constructed by the average dynamic modulus over triplicates. The modified dynamic modulus master curves for OGBB-OK and ATPB-ID specimens with different air void contents are presented in Appendix A.

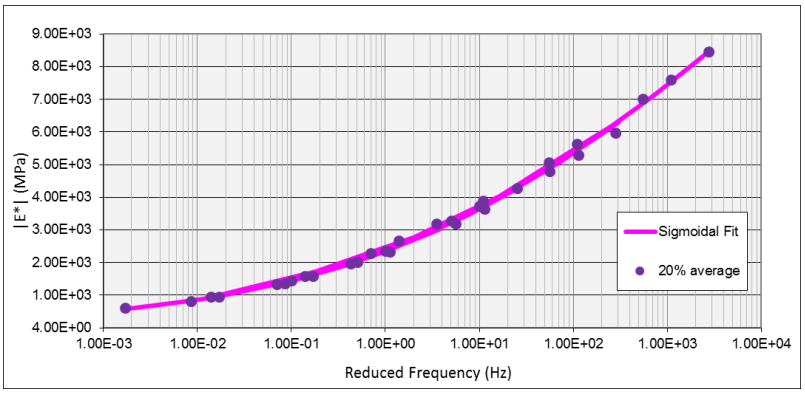

Figure 74. Dynamic modulus master curve of ATPB-VA 20% average VTM specimen

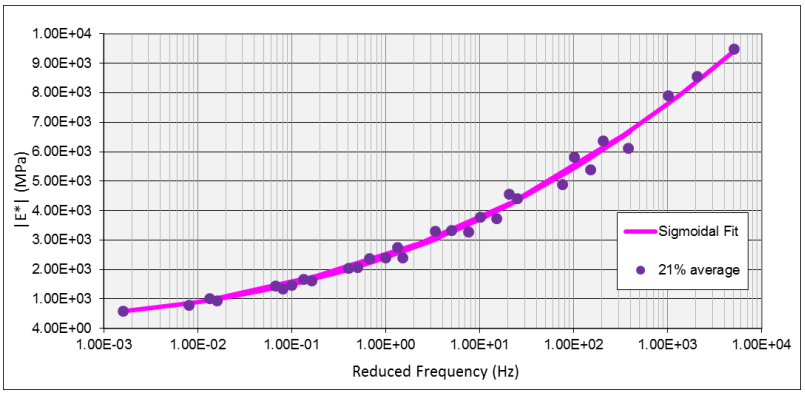

Figure 75. Dynamic modulus master curve of ATPB-VA 21% average VTM specimen

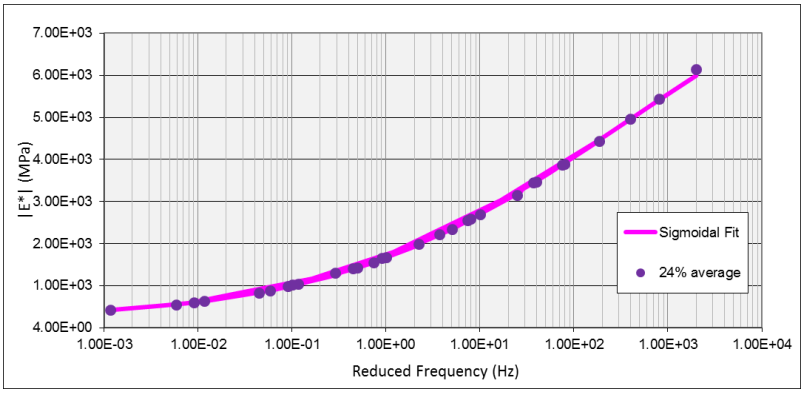

Figure 76. Dynamic modulus master curve of ATPB-VA 24% average VTM specimen

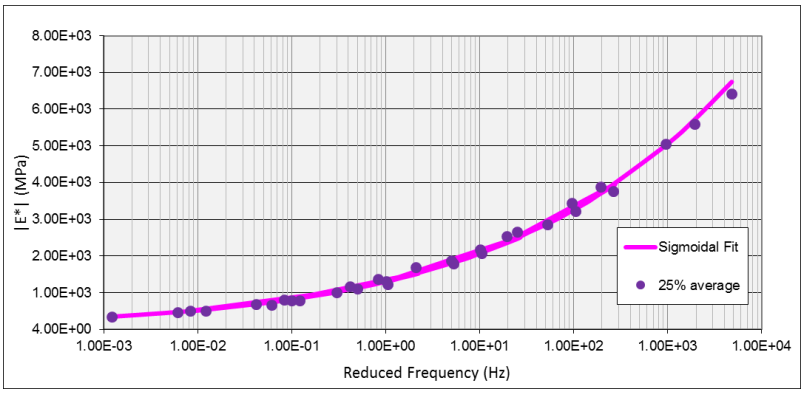

Figure 77. Dynamic modulus master curve of ATPB-VA 25% average VTM specimen

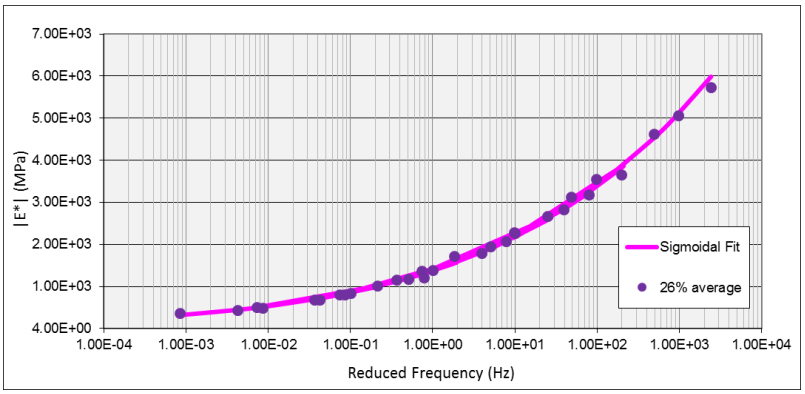

Figure 78. Dynamic modulus master curve of ATPB-VA 26% average VTM specimen

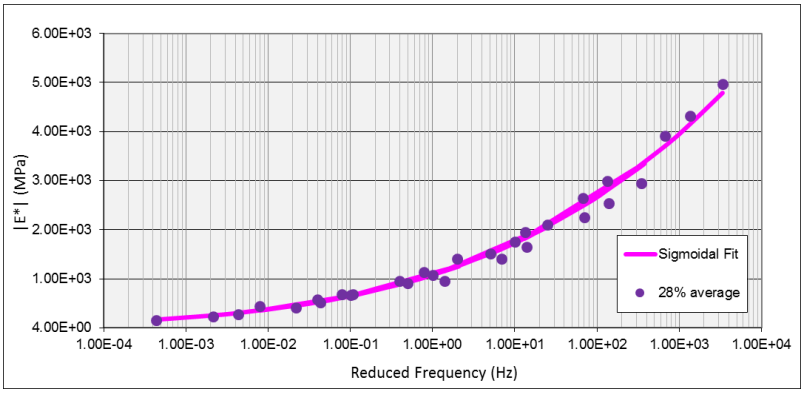

Figure 79. Dynamic modulus master curve of ATPB-VA 28% average VTM specimen

All the master curves were constructed by nonlinear optimization in Microsoft Excel worksheet to model the laboratory testing results into sigmoidal function. It has been noticed that after modification on temperatures and loading magnitudes in proposed modified dynamic modulus test, consistent dynamic modulus results of the high porosity drainage layer materials have been achieved.

In order to investigate the influence of the air void content on the dynamic modulus results, all the testing results from ATPB-VA specimens with different air void contents were plotted in Figure 80. Generally the dynamic modulus decreased with the increase in air void

content, as can be seen from the plotting. When the reduced frequency is getting larger, the differences between the dynamic modulus caused by change in VTM is also increasing. With 8% discrepancy in VTM the difference of dynamic modulus can reach up to 5,000 MPa. Figure 81 shows the time-temperature shift factor of ATPB-VA specimens with different air void contents.

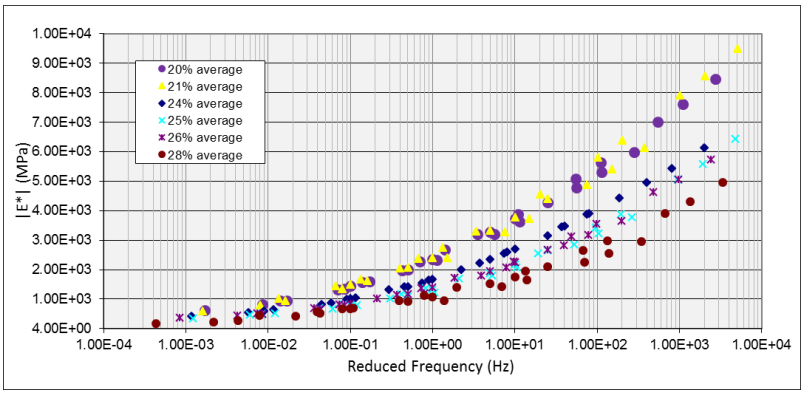

Figure 80. Dynamic modulus master curve of ATPB-VA specimens with different air void contents

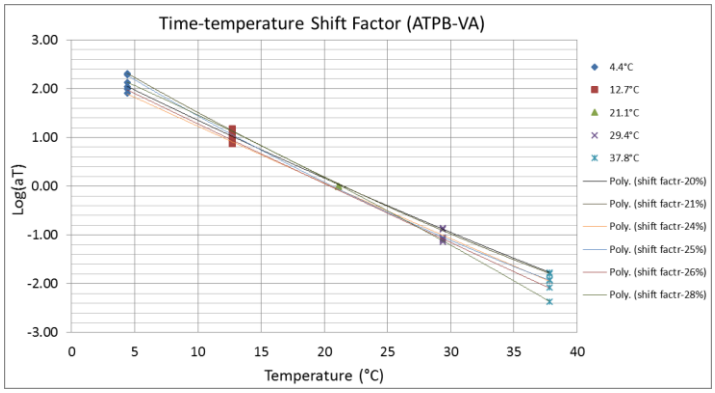

Figure 81. Time-temperature shift factor of ATPB-VA specimens with different air void contents

The dynamic moduli of OGBB-OK and ATPB-ID specimens were determined following the modified dynamic modulus test procedures as proposed in Chapter 4 in this study. Master curves and shift factors of these two mixtures with different VTM are shown in Figure 82 to Figure 85.

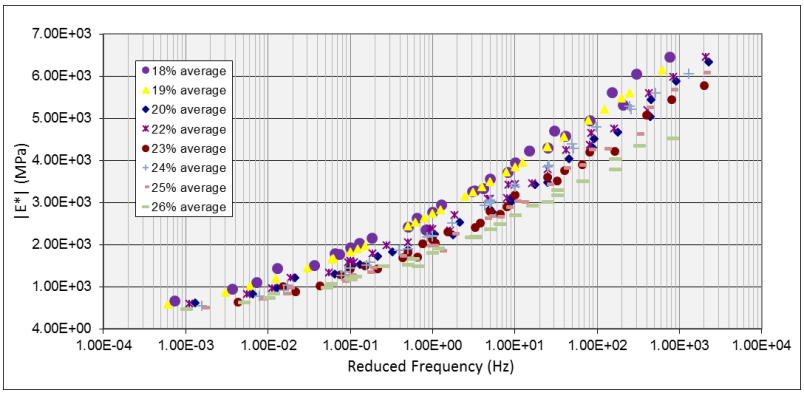

Figure 82. The master curves for OGBB-OK mixtures with different air void contents

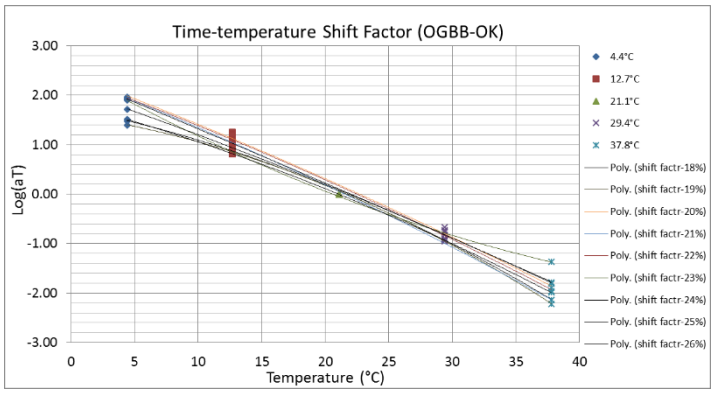

Figure 83. Time-temperature shift factor of OGBB-OK specimens with different air void contents

Figure 82 shows that typically the dynamic modulus decreases with increase in air void content on OGBB-OK specimens, which exhibits the same trend as the ATPB-VA specimens. The difference between the dynamic modulus due to air void content is larger when the reduced frequency increases, although the differences between OGBB-OK specimens are not as significant as the ATPB-VA specimens. The difference of specimens with 8% variance in VTM can cause up to 2,000 MPa difference in dynamic modulus of the OGBB-OK specimens adopted in this study. Figure 83 shows the time-temperature shift factor of OGBB-OK specimens with different air void contents.

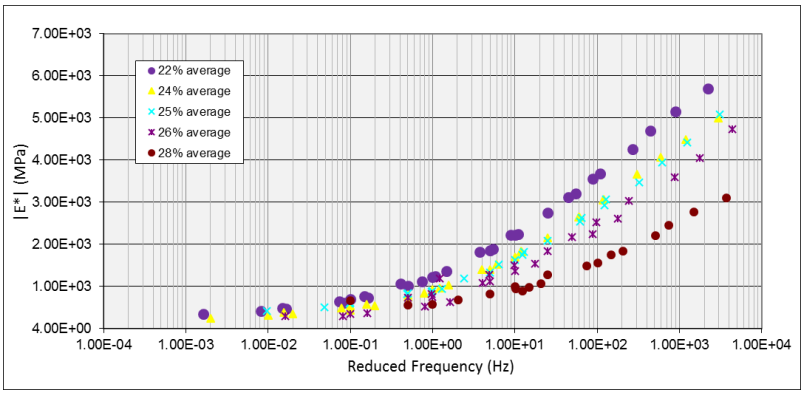

Figure 84. The master curves for ATPB-ID mixtures with different air void contents

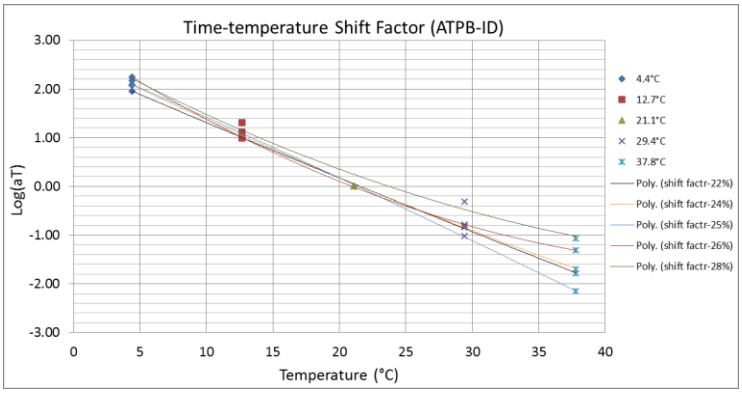

Figure 85. Time-temperature shift factor of ATPB-ID specimens with different air void contents

Figure 84 shows the master curves of ATPB-ID specimens. The same trend can be observed as ATPB-VA and OGBB-OK specimens. A comparison among the three mixtures has indicated that with the increasing in air void content, generally the mixture has a decreasing dynamic modulus. The difference in dynamic modulus which is induced by the increase in air void content is more significant in ATPB-VA and ATPB-ID mixtures rather than the OGBB-OK mixtures. In addition, compared with the dynamic modulus of regular asphalt concrete, which can reach up to 25,000MPa at 4.4℃, the dynamic modulus of the drainage layer materials is much lower [46]. The laboratory-determined dynamic modulus of ATPB specimens have indicated that the ATPB drainage layer is possibly a weak load bearing layer within pavement structure. Therefore incorporating the drainage layer into M-E Design procedure as a structural layer is necessary and of vital importance.

Comparison between the laboratory-determined dynamic modulus and typical modulus values provided by the MEPDG

In MEPDG the typical modulus of traditional asphalt concrete at 68℉ and 0.1Hz is 300,000-1,500,000 psi (2,000-10,000MPa) with the mean of 500,000 psi (3,500MPa). However, as shown in Table 13, the laboratory-determined dynamic modulus of the ATPB-VA specimens at the same temperature and frequency is 671MPa to 1447MPa, which is much lower than the typical modulus adopted in MEPDG. The laboratory-determined dynamic modulus data of OGBB-OK and ATPB-ID specimens with different air void contents are also much lower than the typical modulus of traditional asphalt concrete in MEPDG. To reasonably consider the structural performance of drainage layers, it is necessary to construct a new series of prediction models or default modulus value for the drainage layer materials in M-E pavement design.

Table 13. The dynamic modulus of ATPB-VA specimens with different air void contents

Temperature (℃)	Frequency (Hz)	Dynamic modulus (MPa)					
		20%	21%	24%	25%	26%	28%
4.4	25	8468.706	9504.015	6143.557	6431.133	5733.412	4972.584
	10	7612.289	8566.412	5442.765	5597.803	5074.623	4322.767
	5	7021.732	7924.056	4969.488	5066.662	4624.979	3911.208
	1	5631.580	6392.053	3900.710	3886.882	3557.483	2994.014
	0.5	5079.706	5818.95	3476.811	3442.135	3140.724	2649.219
	0.1	3893.660	4562.901	2602.250	2547.241	2281.573	1947.919
12.7	25	5987.189	6130.247	4435.714	3775.460	3656.005	2952.221
	10	5309.411	5409.160	3875.090	3235.746	3190.896	2548.123
	5	4798.407	4896.800	3457.819	2857.588	2833.777	2250.966
	1	3635.805	3730.787	2563.286	2084.472	2081.430	1647.225
	0.5	3198.813	3289.797	2228.809	1795.744	1796.053	1416.371
	0.1	2326.720	2405.510	1562.327	1230.105	1212.897	958.6597
21.1	25	4285.141	4410.776	3159.143	2667.431	2677.692	2100.202
	10	3730.375	3783.761	2696.169	2183.735	2264.236	1762.647
	5	3283.707	3332.196	2355.260	1881.605	1962.015	1524.546
	1	2362.498	2416.202	1686.497	1321.910	1394.245	1087.244
	0.5	2012.362	2071.027	1432.312	1114.078	1174.744	921.0182
	0.1	1447.453	1491.524	1031.253	791.790	841.205	671.543

Table 13. (Continued)

Temperature (℃)	Frequency (Hz)	Dynamic modulus (MPa)					
		20%	21%	24%	25%	26%	28%
29.4	25	3200.628	3303.324	1996.000	1697.976	1718.295	1409.839
	10	2673.110	2752.110	1663.091	1382.885	1378.151	1136.652
	5	2291.545	2379.970	1421.683	1173.786	1154.882	962.6527
	1	1588.128	1690.118	992.2281	820.222	818.867	685.291
	0.5	1340.173	1442.587	838.0825	692.401	695.398	586.281
	0.1	951.721	1034.984	608.5079	504.121	515.594	451.067
37.8	25	1972.075	2048.396	1317.002	1018.862	1023.184	693.413
	10	1598.813	1621.786	1040.927	801.887	808.913	516.359
	5	1353.654	1362.077	881.294	676.848	683.266	414.403
	1	951.9185	954.172	641.908	519.735	501.139	287.677
	0.5	815.972	812.429	559.205	465.484	439.853	236.525
	0.1	614.224	605.179	436.814	359.117	375.598	163.617

CALIBRATED NCHRP 1-37A MODEL TO PREDICT DYNAMIC MODULUS OF ASPHALT TREATED DRAINAGE LAYER MATERIALS (MEPDG LEVEL 2 INPUT)

In MEPDG, the level 1 design require the laboratory-determined properties be used directly as inputs. The dynamic modulus determined by the modified dynamic modulus test on ATPB-VA, OGBB-OK and ATPB-ID specimens as stated previously can be used as the level 1 inputs in MEPDG to incorporate the drainage layer into structural design. The MEPDG level 2 designs utilize regression models to predict the dynamic modulus from more commonly available mixture parameters, such as the aggregate gradations, asphalt binder properties and volumetric properties of the mixture. The "NCHRP 1-37A" model is one of the models that incorporated in MEPDG to predict dynamic modulus E* as shown in Equation 17 [47].

$$\log E^* = -1.249937 + 0.029232\rho_{200} - 0.001767(\rho_{200})^2 - 0.002841\rho_4 - 0.058097V_a - 0.082208\frac{V_{beff}}{V_{beff}+V_a} + \frac{3.871977-0.0021\rho_4+0.003958\rho_{3/8}-0.000017(\rho_{3/8})^2+0.005470\rho_{3/4}}{1+e^{(-0.603313-0.313351\log(f)-0.393532\log(\eta))}} \quad (17)$$

Where,

E^* = dynamic modulus of mix, 10^5psi;

η = viscosity of binder, 10^6 poise;

f = loading frequency, Hz;

ρ_{200} = % passing #200 sieve;

ρ_4 = accumulative % retained on #4 sieve;

$\rho_{3/8}$ = accumulative % retained on 3/8 in. sieve;

$\rho_{3/4}$ = accumulative % retained on 3/4 in. sieve;

V_a = air voids, % by volume;

V_{beff} = effective binder content, % by volume.

This model has been used to predict the dynamic modulus of the typical ATPB-VA, OGBB-OK and ATPB-ID mixtures in this study to verify its applicability on the ATPB drainage layer materials. The predicted dynamic modulus of the ATPB drainage layer materials using the NCHRP 1-37A model was then compared with laboratory-measured dynamic modulus. Firstly, the parameters required in the equation as shown in Equation 17 are determined for each mixture as follows.

Determining the effective binder content

To investigate whether the NCHRP 1-37A model can be applied on drainage layer materials, and to construct the calibrated NCHRP 1-37A model to predict the dynamic modulus of ATPB-VA, OGBB-OK and ATPB-ID mixtures, the parameters of aggregate and asphalt binder as required in Equation 17 are determined. The effective binder content V_{beff} refers to the portion of Voids in the Mineral Aggregate (VMA) which is filled with asphalt binder, expressed as a percent of the total volume of the specimen. The effective binder content V_{beff} can be calculated by Equation 18 [48].

$$V_{beff} = G_{mb}\left[\frac{Pb}{Gb} - (100 - Pb)\frac{(G_{se} - G_{sb})}{G_{se} \cdot G_{sb}}\right] \quad (18)$$

Where,

G_{mb} = bulk specific gravity of the mix;

Pb = binder content by weight;

Gb = specific gravity of the binder at 60 ℉;

G_{se} = effective specific gravity of the aggregate;

$G_{se} = \frac{100 - Pb}{\frac{100}{G_{mm}} - \frac{Pb}{Gb}}$;

G_{sb} = bulk specific gravity of the aggregate.

The effective binder content V_{beff} was calculated for ATPB-VA, OGBB-OK and ATPB-ID specimens with different air void contents by Equation 18. All the parameters needed to calculate the effective asphalt content are presented in Table 14 to Table 16. The bulk specific gravity of the mix, the effective specific gravity and bulk specific gravity of the aggregate were determined in laboratory for each mixture. The binder content of each mixture provided by the manufacturers has been used. The typical specific gravity of the binder at 60 ℉ provided in literature has been adopted [49]. Table 14 to Table 16 has also listed the effective binder contents of ATPB-VA, OGBB-OK and ATPB-ID mixtures with different air void contents determined from Equation 18.

Table 14. Determining the effective binder content for ATPB-VA specimens

ATPB-VA 20%										
P_b	G_b	G_{mm}	G_{se}	G_{sb}	G_{mb}			V_{beff}		
					A1*	A2	A3	A1	A2	A3
4.3	1.011	2.474	2.646	2.578	1.975	1.970	1.970	6.515	6.497	6.498
ATPB-VA 21%										
P_b	G_b	G_{mm}	G_{se}	G_{sb}	G_{mb}			V_{beff}		
					A5	A6	A1-1	A5	A6	A1-1
4.3	1.011	2.474	2.646	2.578	1.954	1.951	1.957	6.447	6.437	6.455
ATPB-VA 24%										
P_b	G_b	G_{mm}	G_{se}	G_{sb}	G_{mb}			V_{beff}		
					B2	B3	B2-2	B2	B3	B2-2
4.3	1.011	2.474	2.646	2.578	1.889	1.876	1.869	6.232	6.187	6.164
ATPB-VA 25%										
P_b	G_b	G_{mm}	G_{se}	G_{sb}	G_{mb}			V_{beff}		
					B4	B1-1	B1-2	B4	B1-1	B1-2
4.3	1.011	2.474	2.646	2.578	1.851	1.857	1.850	6.107	6.127	6.101
ATPB-VA 26%										
P_b	G_b	G_{mm}	G_{se}	G_{sb}	G_{mb}			V_{beff}		
					B1	B5	B6	B1	B5	B6
4.3	1.011	2.474	2.646	2.578	1.837	1.821	1.839	6.060	6.008	6.065
ATPB-VA 28%										
P_b	G_b	G_{mm}	G_{se}	G_{sb}	G_{mb}			V_{beff}		
					C3	C4	C1-1	C3	C4	C1-1
4.3	1.011	2.474	2.646	2.578	1.773	1.792	1.788	5.849	5.910	5.899

*Note: A1, A2, A3, etc. are specimen numbers.

Table 15. Determining the effective binder content for OGBB-OK specimens

OGBB-OK 18%										
P_b	G_b	G_{mm}	G_{se}	G_{sb}	G_{mb}			V_{beff}		
					E1*	E3	E6	E1	E3	E6
2.5	1.030	2.524	2.621	2.680	2.055	2.072	2.071	6.663	6.719	6.718
OGBB-OK 19%										
P_b	G_b	G_{mm}	G_{se}	G_{sb}	G_{mb}			V_{beff}		
					E2	E4	E5	E2	E4	E5
2.5	1.030	2.524	2.621	2.680	2.050	2.051	2.053	6.649	6.652	6.658
OGBB-OK 20%										
P_b	G_b	G_{mm}	G_{se}	G_{sb}	G_{mb}			V_{beff}		
					E7	E8	F3	E7	E8	F3
2.5	1.030	2.524	2.621	2.680	2.013	2.011	2.027	6.528	6.523	6.573
OGBB-OK 19%										
P_b	G_b	G_{mm}	G_{se}	G_{sb}	G_{mb}			V_{beff}		
					E2	E4	E5	E2	E4	E5
2.5	1.030	2.524	2.621	2.680	2.050	2.051	2.053	6.649	6.652	6.658
OGBB-OK 20%										
P_b	G_b	G_{mm}	G_{se}	G_{sb}	G_{mb}			V_{beff}		
					E7	E8	F3	E7	E8	F3
2.5	1.030	2.524	2.621	2.680	2.013	2.011	2.027	6.528	6.523	6.573

Table 15. (Continued)

OGBB-OK 22%										
P_b	G_b	G_{mm}	G_{se}	G_{sb}	G_{mb}			V_{beff}		
					F1	F7	G3	F1	F7	G3
2.5	1.030	2.524	2.621	2.680	1.970	1.969	1.964	6.389	6.387	6.369
OGBB-OK 23%										
P_b	G_b	G_{mm}	G_{se}	G_{sb}	G_{mb}			V_{beff}		
					G1	G2	G7	G1	G2	G7
2.5	1.030	2.524	2.621	2.680	1.955	1.946	1.936	6.342	6.312	6.280
OGBB-OK 24%										
P_b	G_b	G_{mm}	G_{se}	G_{sb}	G_{mb}			V_{beff}		
					H1	H3	H5	H1	H3	H5
2.5	1.030	2.524	2.621	2.680	1.908	1.917	1.912	6.187	6.217	6.200
OGBB-OK 25%										
P_b	G_b	G_{mm}	G_{se}	G_{sb}	G_{mb}			V_{beff}		
					H4	H7	I3	H4	H7	I3
2.5	1.030	2.524	2.621	2.680	1.885	1.899	1.894	6.113	6.158	6.143
OGBB-OK 26%										
P_b	G_b	G_{mm}	G_{se}	G_{sb}	G_{mb}			V_{beff}		
					I2	I4	I5	I2	I4	I5
2.5	1.030	2.524	2.621	2.680	1.880	1.869	1.872	6.097	6.061	6.071

*Note: E1, E2, E3, etc. are specimen numbers.

Table 16. Determining the effective binder content for ATPB-ID specimens

ATPB-ID 22%										
P_b	G_b	G_{mm}	G_{se}	G_{sb}	G_{mb}			V_{beff}		
					Q1*	Q2	Q3	Q1	Q2	Q3
3.0	1.030	2.525	2.644	2.569	1.959903	1.949	1.915	3.624	3.604	3.541
ATPB-ID 24%										
P_b	G_b	G_{mm}	G_{se}	G_{sb}	G_{mb}			V_{beff}		
					R1	R4	R5	R1	R4	R5
3.0	1.030	2.525	2.644	2.569	1.914	1.917	1.926	3.540	3.545	3.561
ATPB-ID 25%										
P_b	G_b	G_{mm}	G_{se}	G_{sb}	G_{mb}			V_{beff}		
					S1	S2	S3	S1	S2	S3
3.0	1.030	2.525	2.644	2.569	1.896	1.896	1.894	3.506	3.507	3.502
ATPB-ID 26%										
P_b	G_b	G_{mm}	G_{se}	G_{sb}	G_{mb}			V_{beff}		
					T1	T2	T3	T1	T2	T3
3.0	1.030	2.525	2.644	2.569	1.876	1.851	1.839	3.469	3.423	3.401
ATPB-ID 28%										
P_b	G_b	G_{mm}	G_{se}	G_{sb}	G_{mb}			V_{beff}		
					U2	U4	U5	U2	U4	U5
3.0	1.030	2.525	2.644	2.569	1.827	1.827	1.812	3.377	3.378	3.350

*Note: Q1, Q2, Q3, etc. are specimen numbers.

Determining the viscosity of the asphalt binder

The viscosity of each type of binder was determined by the "A-VTS relationship" as shown in the following equation [50]. The regression parameters A and VTS were obtained through typical A and VTS values for different purchase specification grades from NCHRP 1-37A project.

$$\log\log(\eta) = \begin{cases} A + VTS\log(T_R) & T_R > T_{critical} \\ 2.7 \times 10^{12} & T_R \leq T_{critical} \end{cases} \quad (19)$$

Where,

η = Viscosity of the binder (cP);

A, VTS = Regression parameters;

T_R = Temperature of interest in Rankine;

$T_{critical}$ =Temperature in Rankine at which the viscosity is equal to 2.7×10^{12}cP.

The asphalt binder used to cement aggregates for ATPB-VA, OGBB-OK and ATPB-ID mixtures are Superpave PG 70-22, PG64-22 and PG64-28 respectively. According to the relationship between asphalt binder grade and viscosity parameters provided by NCHRP 1-37A, typical A and VTS for each binder are listed in Table 17.

Table 17. Regression parameters for the viscosity of asphalt binder

Mixture	A	VTS
ATPB-VA	10.2990	-3.4260
OGBB-OK	10.3120	-3.4400
ATPB-ID	10.9800	-3.6800

As long as the regression parameters A and VTS have been determined, the critical temperature $T_{critical}$ of each asphalt binder is calculated as in Equation 20 to Equation 22.

ATPB-VA: $$\log\log(2.7 \times 10^{12}) = 10.2990 - 3.4260 \times \log(T_{critical}) \quad (20)$$

$$T_{critical} = 486.021°R$$

OGBB-OK: $$\log\log(2.7 \times 10^{12}) = 10.9800 - 3.6800 \times \log(T_{critical}) \quad (21)$$

$$T_{critical} = 485.593°R$$

ATPB-ID: $$\log\log(2.7 \times 10^{12}) = 10.3120 - 3.4400 \times \log(T_{critical}) \quad (22)$$

$$T_{critical} = 478.080°R$$

According to whether the test temperature is below or above the critical temperature, the viscosity of each asphalt binder can be calculated by Equation 19. The viscosity of binder at different temperatures associated with the modified dynamic modulus test is listed in Table 18 to Table 20.

Table 18. Viscosity of binder PG 70-22 (ATPB-VA) at different temperatures

T_R (℃)	T_R (℟)	η (cP)
4.4	499.590> $T_{critical}$	2.05238×10^{11}
12.7	514.530> $T_{critical}$	1.68278×10^{10}
21.1	529.650> $T_{critical}$	1.81995×10^{9}
29.4	544.590> $T_{critical}$	2.62010×10^{8}
37.8	559.710> $T_{critical}$	4.61749×10^{7}

Table 19. Viscosity of binder PG64-22 (OGBB-OK) at different temperatures

T_R (℃)	T_R (℟)	η (cP)
4.4	499.590> $T_{critical}$	1.57396×10^{11}
12.7	514.530> $T_{critical}$	1.11265×10^{10}
21.1	529.650> $T_{critical}$	1.07320×10^{9}
29.4	544.590> $T_{critical}$	1.41902×10^{8}
37.8	559.710> $T_{critical}$	2.34683×10^{7}

Table 20. Viscosity of binder PG 64-28 (ATPB-ID) at different temperatures

T_R (℃)	T_R (℟)	η (cP)
4.4	499.590> $T_{critical}$	4.84014×10^{10}
12.7	514.530> $T_{critical}$	4.51738×10^{9}
21.1	529.650> $T_{critical}$	5.48688×10^{8}
29.4	544.590> $T_{critical}$	8.74633×10^{7}
37.8	559.710> $T_{critical}$	1.68972×10^{7}

Since all the inputs for the NCHRP 1-37A model have been determined, the dynamic modulus of the asphalt treated drainage layer mixtures can be predicted by Equation 17. The predicted E* has been compared with the laboratory determined dynamic modulus to see whether this model can be directly applied on the asphalt treated drainage layer mixtures. It is found that the predicted dynamic modulus of these mixtures is much lower than the measured values if no calibration was applied on the NCHRP 1-37A model, indicating that the NCHRP 1-37A model cannot be used directly to predict the asphalt treated drainage layer mixtures. Extremely the predicted dynamic modulus is approaching zero in some cases, which is obviously incorrect. Figure 86 shows an example of the comparison between the laboratory-determined and the predicted dynamic modulus by the NCHRP 1-37A model, showing largely underestimated dynamic modulus by NCHRP 1-37A prediction. Under this circumstance, calibrated prediction models based on the "NCHRP 1-37A" model have been constructed utilizing the laboratory determined dynamic modulus data from each mixture in this study, to minimize the difference between the measured and predicted E* of these mixtures with different air void contents. These models can be used to predict the dynamic modulus of ATPB-VA, OGBB-OK and ATPB-ID mixtures with different air void content in the MEPDG level 2 and level 3 design.

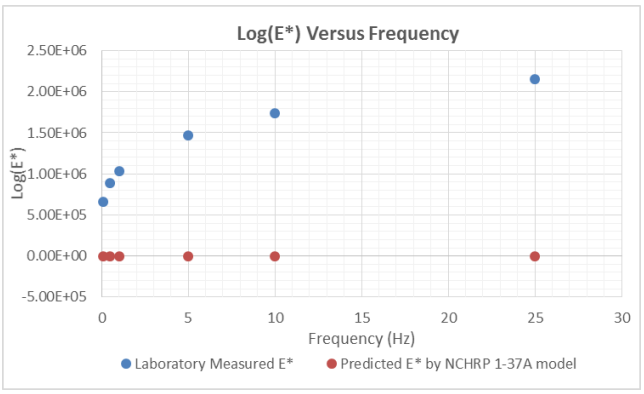

Figure 86. Comparison between measured and predicted dynamic modulus by the NCHRP 1-37A model

Constructing the modified NCHRP 1-37A model for ATPB-VA, OGBB-OK and ATPB-ID mixtures

Totally six groups of specimens with VTM levels from 20% to 28% have been used to construct the modified model for ATPB-VA mixture. Eight groups of specimens with VTM levels from 18% to 26%, and five groups of specimens with VTM levels from 22% to 28% have been used for OGBB-OK and ATPB-ID mixtures. In each group, three specimens with less than 1% deviation of the average VTM have been used. For each specimen, the dynamic modulus obtained from five different temperatures, six different frequencies have been utilized to determine the coefficients in the modified NCHRP-37A model by fitting the laboratory determined data into the model.

Since different gradations have been adopted by each state to produce the asphalt treated drainage layer mixtures, and the sieve sizes used for quality control are different, different regional models were developed firstly to predict the dynamic modulus of typically used mixtures with different VTM in each state. For example, the gradations of the aggregates used by ATPB-ID are provided with the percent passing through sieves No.8, No.4, $\frac{3}{8}$,, and $\frac{1}{2}$,, rather than the sieves incorporated in the NCHRP 1-37A model. In this study, three modified NCHRP models aiming at different mixtures used by Virginia, Oklahoma and Idaho, including regional sieve sizes as the parameters to predict dynamic modulus, have been developed as shown in Equation 23 to Equation 25. Then all the laboratory determined dynamic modulus data of the three mixtures were used to construct an overall model to predict dynamic modulus of asphalt treated open-graded mixtures through the parameters of η, f, ρ_{200}, ρ_4, $\rho_{3/8}$, $\rho_{3/4}$, V_a and V_{beff}.

The laboratory measured versus predicted E* by the calibrated NCHRP 1-37A model customized by regional sieves are shown in Figure 87 to Figure 89.

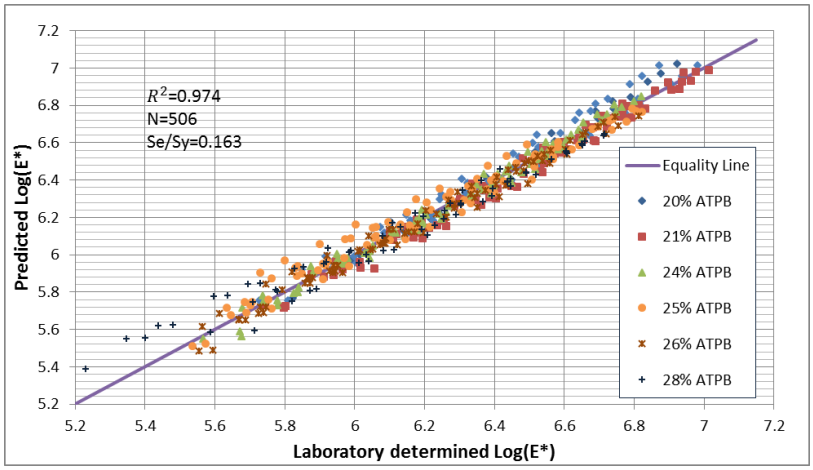

Figure 87. Comparison between the laboratory measured and predicted E* of ATPB-VA mixture by modified regional NCHRP 1-37A model

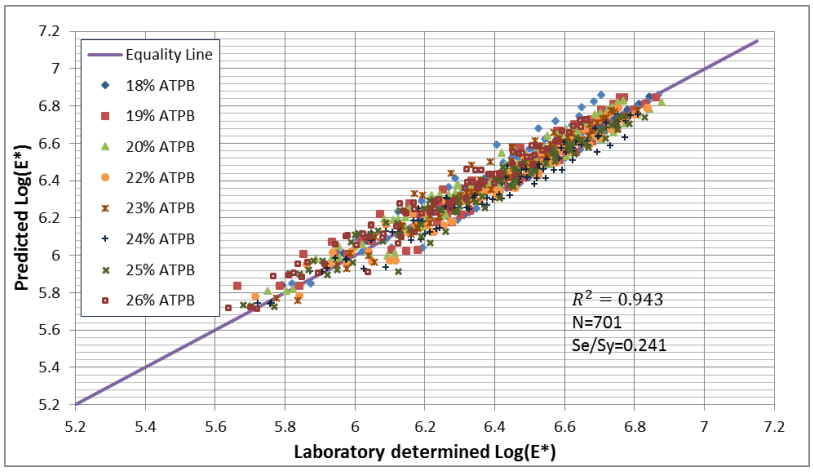

Figure 88. Comparison between the laboratory measured and predicted E* of OGBB-OK mixture by modified regional NCHRP 1-37A model

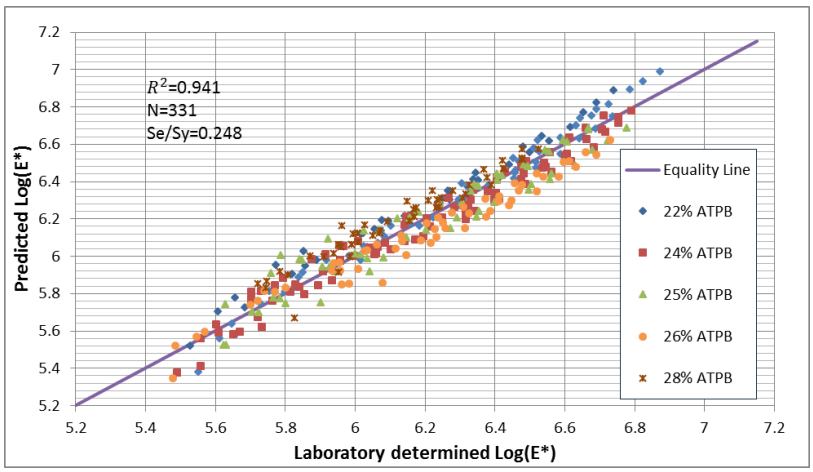

Figure 89. Comparison between the laboratory measured and predicted E* of ATPB-ID mixture by modified regional NCHRP 1-37A model

ATPB-VA:

$$\log E^* = -1.248027 + 0.029956\rho_{200} - 0.000697(\rho_{200})^2 + 0.05277\rho_8 - 0.051533V_a - 0.083203\frac{V_{beff}}{V_{beff}+V_a} + \frac{3.810034-1.934289\rho_8-3.14479\rho_{1/2}+0.3782(\rho_{1/2})^2-0.48496\rho_{3/4}}{1+e^{(-0.64184-0.197242\log(f)-0.225136\log(\eta))}} \quad (23)$$

OGBB-OK:

$$\log E^* = -2.93516 + 0.026203\rho_{200} - 0.000663(\rho_{200})^2 - 2.58\times10^{-6}\rho_4 - 0.018256V_a - 0.108905\frac{V_{beff}}{V_{beff}+V_a} + \frac{5.990667-0.00535\rho_4+0.084364\rho_{\frac{1}{2}}-1.76\times10^{-5}\left(\rho_{\frac{1}{2}}\right)^2+0.043989\rho_1}{1+e^{(-2.15219-0.202076\log(f)-0.202993\log(\eta))}} \quad (24)$$

ATPB-ID:

$$\log E^* = -1.249885 + 0.029636\rho_8 - 0.000716(\rho_8)^2 + 0.05747\rho_4 - 0.080316V_a - 0.080973\frac{V_{beff}}{V_{beff}+V_a} + \frac{3.857444-1.202505\rho_4-1.00955\rho_{3/8}+0.05103(\rho_{3/8})^2-0.65937\rho_{1/2}}{1+e^{(-0.625196-0.197549\log(f)-0.220528\log(\eta))}} \quad (25)$$

Where,

ρ_8 = accumulative % retained on #8 sieve;

ρ_1 = accumulative % retained on 1 in. sieve.

As can be seen from Figure 87 to Figure 89, the local calibrated NCHRP 1-37A models show very good fit statistics in predicting the dynamic modulus of ATPB-VA, OGBB-OK and ATPB-ID specimens. The goodness-of-fit statistics including S_e/S_y (standard error of estimate /standard deviation), the sum of squares for error (SSe), standard error (S_e) and the Coefficient of determination (R^2) of the three calibrated models have been calculated by Equations 26 to Equation 28 and the results are listed in Table 21.

$$S_e = \sqrt{\frac{\sum(y-\hat{y})^2}{(N-k)}} \quad (26)$$

$$S_y = \sqrt{\frac{\sum(y-\bar{y})^2}{(N-1)}} \quad (27)$$

$$R^2 = 1 - \frac{N-k}{N-1}\left(\frac{S_e}{S_y}\right)^2 \quad (28)$$

Where:

S_e = Standard error of estimate;

S_y = Standard deviation;

y = Measured dynamic modulus;

$\hat{y}$ = Predicted dynamic modulus;

$\bar{y}$ = Mean value of measured dynamic modulus;

N = Sample size;

k = Number of independent variables in the model;

R^2 = Correlation coefficient;

Table 21. Goodness-of-fit statistics of the calibrated local models

	S_e/S_y	SS_e	S_e	R^2	N
ATPB-VA	0.163	1.165	0.057	0.974	506
OGBB-OK	0.241	2.794	0.064	0.943	701
ATPB-ID	0.248	2.134	0.082	0.941	331

The ratio of S_e/S_y is an indicator of how the calibrated model improve the accuracy of the prediction. The smaller the ratio of S_e/S_y is, the better the prediction by the calibrated model is. The correlation coefficient R^2 also measures accuracy of the calibrated model. With the correlation coefficient closer to one, better prediction can be achieved by using the calibrated model. It has been found that R^2 is a better indicator for linear models with a large sample size while the ratio of S_e/S_y is more suitable for non-linear models, such as the empirical models, to evaluate the prediction reliability [51]. As shown in Table 21, all of the three local calibrated models exhibit quite good prediction reliability with small ratio of S_e/S_y.

Constructing the modified NCHRP 1-37A model for asphalt treated open-graded mixtures

Although the regional modified NCHRP 1-37A models have been constructed to predict the dynamic modulus of ATPB-VA, OGBB-OK and ATPB-ID mixtures with different air void contents, it is still necessary to develop an overall model which is not aiming at a specific gradation but can be used for different asphalt treated open-graded mixtures with different aggregate gradations, asphalt binder types and air void contents. To develop such a model, the laboratory-determined dynamic modulus from the three mixtures with different VTM have been utilized. Totally about 1700 points of dynamic moduli from 57 specimens under five temperatures and six frequencies have been included to develop the model.

The general modified NCHRP 1-37A model to predict the dynamic modulus of asphalt treated open-graded mixtures is shown in Figure 90. Equation 29 shows the empirical relationship between the dynamic modulus and gradations, asphalt properties and air void content.

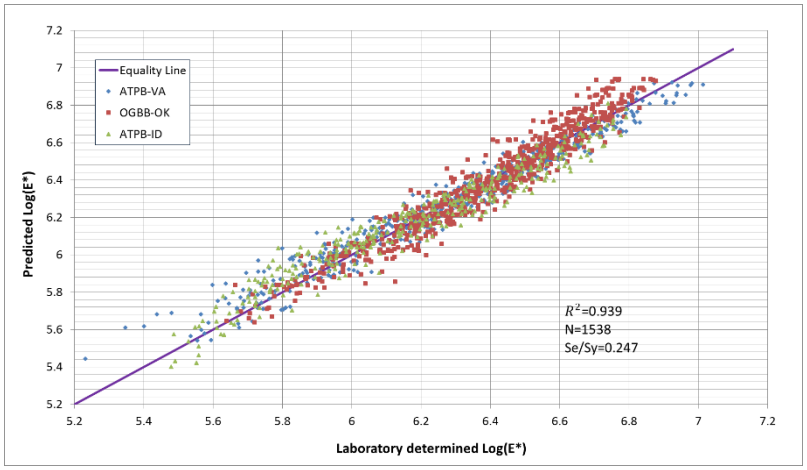

Figure 90. Comparison between the laboratory measured and predicted E* of ATPB-ID mixture by modified regional NCHRP 1-37A model

$$\log E^* = -5.363 \times 10^{-4} - 0.505\rho_{200} + 1.709(\rho_{200})^2 + 3.978 \times 10^{-4}\rho_4 - 0.132V_a$$
$$-10.382\frac{V_{beff}}{V_{beff}+V_a} + \frac{-50.640+3.506\times10^{-5}\rho_4+2.275\rho_{3/8}+0.013(\rho_{3/8})^2-6.989\rho_{3/4}}{1+e^{(-1.664-0.141\log(f)-0.0152\log(\eta))}} \quad (29)$$

The parameters used in the calibrated general model are the same as in NCHRP 1-37A model. This calibrated model, constructed based on three different asphalt treated open-graded mixtures, can be used to predict the dynamic modulus of the asphalt treated drainage layer materials in different gradations, asphalt types and air void contents. In some cases, when the gradation information is not provided in form of ρ_{200}, ρ_4, $\rho_{3/8}$, and $\rho_{3/4}$, the aggregate gradation curve should be constructed firstly using available sieve size information and the required gradation parameters in Equation 29 can be determined from the gradation curves. Table 22 lists the goodness-of-fit statistics for the calibrated general NCHRP 1-37A model.

Table 22. Goodness-of-fit statistics of the calibrated general model

S_e/S_y	SS_e	S_e	R^2	N
0.247	8.921	0.076	0.939	1538

MOISTURE SUSCEPTIBILITY OF ATPB MATERIALS

The dynamic modulus before and after moisture-environmental conditioning was selected as the indicator to evaluate the moisture-resistance performance of the ATPB-VA and OGBB-OK mixtures. However, unlike the traditional dense-graded asphalt mixtures, the ATPB adopted for drainage layers are all open-graded materials with typical VTM larger than 20% to ensure adequate permeability and facilitate drainage purposes. The gradation and air void content adopted for ATPB mixtures have already led to impaired dynamic modulus compared with traditional asphalt concrete, let alone the moisture deteriorated ATPB specimens. On the other hand, the current available dynamic modulus test standard, which is AASHTO T342-11, requires

the strain of specimen during the test to be within 50 to 150 micro-strains as much as possible, not only to remain the material within linear visco-elastic scope but also to obtain consistent test results, as stated before. Take all of these into consideration, the proposed modified dynamic modulus test especially in terms of modified conditioning time and stress level is applied to obtain reliable dynamic modulus results of ATPB materials after moisture-environmental conditioning. Although the modified conditioning time and stress level have been provided for ATPB specimens without moisture damage, it is not sure whether they are applicable on the moisture-conditioned specimens. Therefore, the modified conditioning time and the stress levels were selected again using the same procedures as described in Chapter 4, for the moisture-deteriorated ATPB specimens. Table 23 and Table 24 have listed the modified conditioning time and stress levels specialized for evaluating the dynamic modulus of moisture-deteriorated ATPB specimens in this study.

Table 23. Time to condition the moisture-deteriorated ATPB specimens at each temperature

Temperature ℃ (℉)	Time to condition the specimens from room temperature	Time to condition the specimens from last temperature
4.4 (40)	Overnight	N/A
12.7(54.9)	3 hours	2 hours
21.1 (70)	1 hour	1.5 hours
29.4(84.9)	1.5 hours	1 hour
37.8 (100)	2 hours	1 hour

Table 24. Modified stress levels specialized for evaluating the dynamic modulus of moisture-deteriorated ATPB specimens

Temperature ℃ (℉)	Frequency (Hz)	Pressure for conditioned specimens (kPa)	Pressure for unconditioned specimens (kPa)	Cycles	Recommended Pressure by AASHTO T 342-11 (kPa)
4.4 (40)	25	400	500	200	700-1400
	10	400	500	200	
	5	300	400	100	
	1	300	400	20	
	0.5	200	300	15	
	0.1	200	300	15	
12.7(54.9)	25	200	300	200	N/A
	10	200	300	200	
	5	150	250	100	
	1	150	250	20	
	0.5	100	200	15	
	0.1	100	200	15	
21.1 (70)	25	100	200	200	350-700
	10	100	200	200	
	5	75	150	100	
	1	75	150	20	
	0.5	50	100	15	
	0.1	50	100	15	

Table 24. (Continued)

Temperature ℃ (℉)	Frequency (Hz)	Pressure for conditioned specimens (kPa)	Pressure for unconditioned specimens (kPa)	Cycles	Recommended Pressure by AASHTO T 342-11 (kPa)
29.4(84.9)	25	50	100	200	N/A
	10	50	100	200	
	5	40	75	100	
	1	40	75	20	
	0.5	30	50	15	
	0.1	30	50	15	
37.8 (100)	25	30	50	200	140-250
	10	30	50	200	
	5	20	30	100	
	1	20	30	20	
	0.5	10	15	15	
	0.1	10	15	15	

Moisture-induced deterioration in dynamic modulus of ATPB mixtures

In this study, the modified dynamic modulus test has been adopted to evaluate the moisture susceptibility of the ATPB-VA and ATPB-OK mixtures. Instead of using the ECS for specimen conditioning, a simply 5-day or 10-day period of submersion in water tank at 25 ℃ has been used to imitate the moisture environment that the drainage layer may subject to in field. This simplified moisture conditioning method, although is not an accelerated approach as the ECS does, is closer to the real situation in field and can be conveniently performed to provide moisture-environmental conditioning. The conditioned specimens were then dried in room temperature and adopted in afore-mentioned modified dynamic modulus test to investigate the deterioration in dynamic modulus of ATPB mixtures caused by moisture damage. Figure 91 and Figure 92 have shown the ATPB-VA and ATPB-OK specimens conditioned in water tank and prepared for the modified dynamic modulus test.

Figure 91. Submerged specimens in water tank for conditioning

Figure 92. Conditioned specimen mounted for modified dynamic modulus test

The master curves of dynamic modulus for ATPB-VA and OGBB-OK mixtures with different air void contents have been constructed for both conditioned and unconditioned specimens, by simultaneously solve the equations 14 to 16. Figure 93 to Figure 98 have demonstrated the comparison between the dynamic modulus obtained before and after conditioning in water tank for both the ATPB-VA and ATPB-OK specimens. Three levels of air void contents including 20%, 26% and 28% for ATPB-VA specimens, 20%, 23% and 25% for ATPB-OK specimens were tested and evaluated.

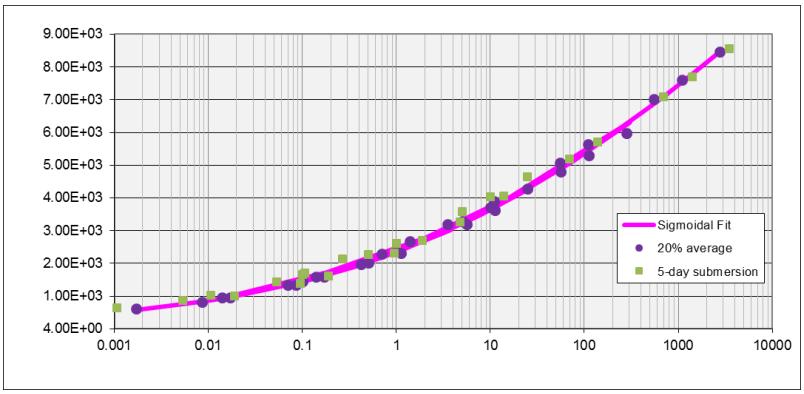

Figure 93. Dynamic modulus before and after moisture-environmental conditioning of ATPB-VA specimens with 20% air void content

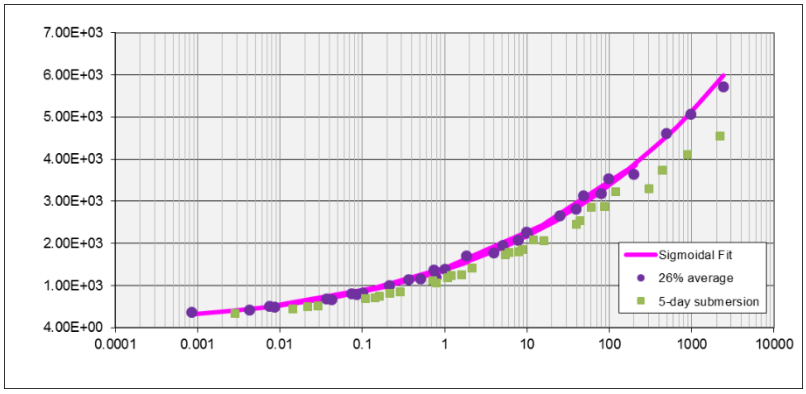

Figure 94. Dynamic modulus before and after moisture-environmental conditioning of ATPB-VA specimens with 26% air void content

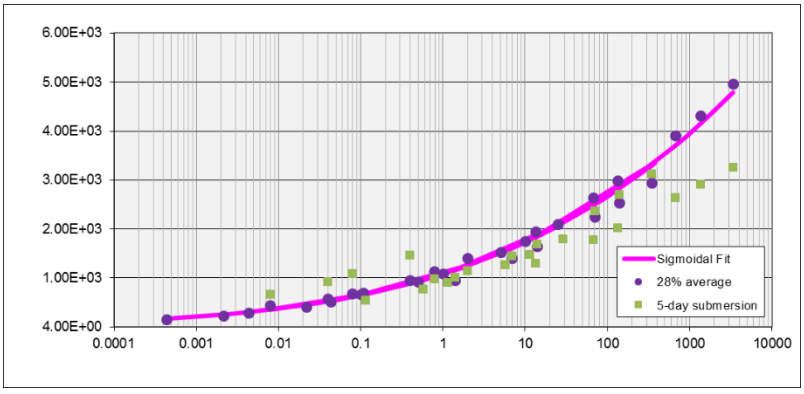

Figure 95. Dynamic modulus before and after moisture-environmental conditioning of ATPB-VA specimens with 28% air void content

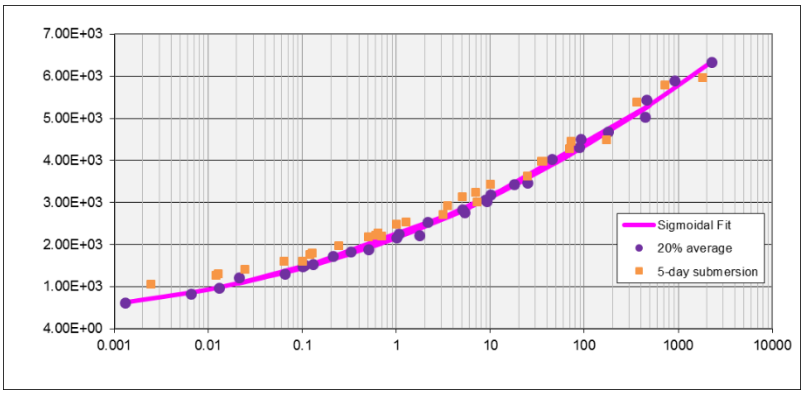

Figure 96. Dynamic modulus before and after moisture-environmental conditioning of OGBB-OK specimens with 20% air void content

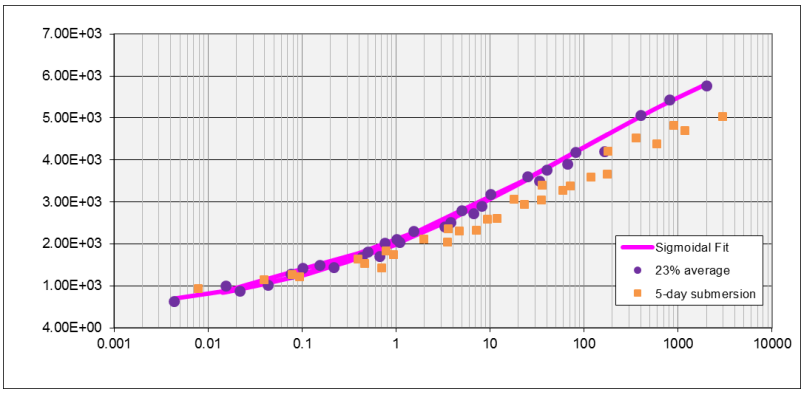

Figure 97. Dynamic modulus before and after moisture-environmental conditioning of OGBB-OK specimens with 23% air void content

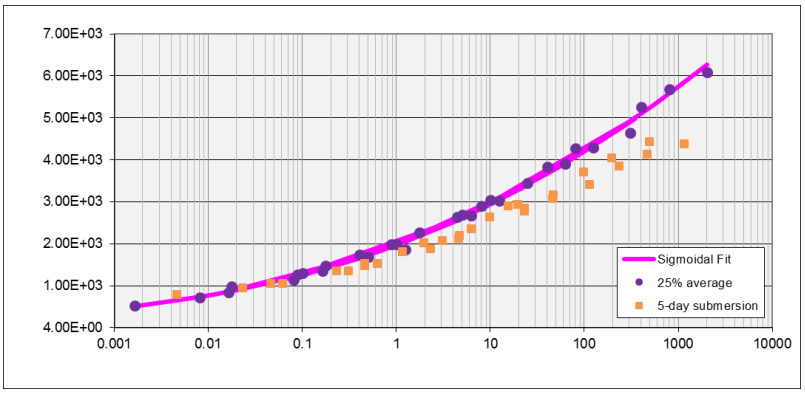

Figure 98. Dynamic modulus before and after moisture-environmental conditioning of OGBB-OK specimens with 25% air void content

As shown in Figure 93 to Figure 98, the post-conditioning specimens have exhibited different properties compared with the no-conditioning specimens, even though they are at the same level of air void content. Figure 93 to Figure 95 illustrate the dynamic modulus master curves of the ATPB-VA specimens with air void content of 20%, 26% and 28% before and after the conditioning. Although the moisture-induced dynamic modulus reduction is not significant, it still can be found that the moisture-induced deterioration on dynamic modulus is larger as the air

void content increases. The influence of the moisture on dynamic modulus of OGBB-OK specimens are shown in Figure 96 to Figure 98. It is found that the two mixtures have comparable moisture resistance performance in term of the similar extend of modulus reduction after 5-day water bath conditioning. The application of anti-stripping additives may have improved the moisture-resistance property of the two mixtures. Another interesting point is that the influence of moisture on dynamic modulus of specimens with 20% air void content is so limited for both mixtures.

Figure 99 has shown the comparison between the dynamic modulus master curves of the ATPB-VA specimen with 24% air void content under different moisture-conditioning periods. As the moisture-conditioning period elongates from 5 days to 10 days, the dynamic modulus is decreasing due to moisture damage. In addition, as can be seen from Figure 99, the difference in dynamic modulus caused by a certain change in reduced frequency decreases as the moisture-conditioning time increases.

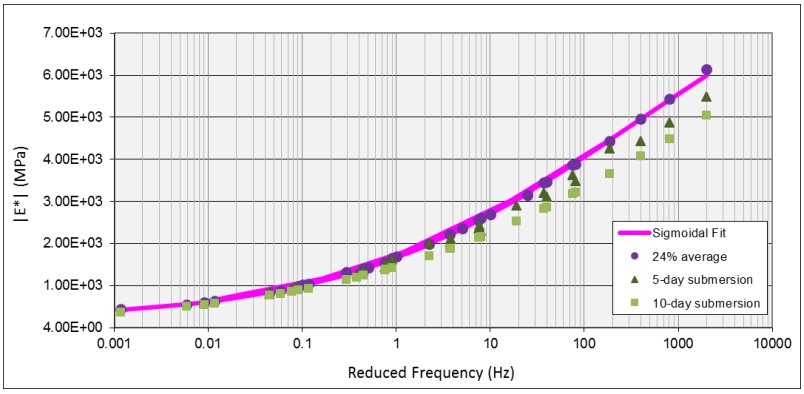

Figure 99. Dynamic modulus before and after 5-day and 10-day moisture-environmental conditioning of OGBB-OK specimens with 24% air void content

Ratio of modulus under different conditions

The ratio of modulus, as defined in Equation 30, is a measurement of how much the dynamic modulus has been affected by moisture-induced deterioration. As the dynamic modulus is known to be significantly influenced by temperature, frequency, and VTM, the ratio of modulus is also possibly influenced by these variables. Whether the ratio of modulus increases or decreases with these variables will indicate which modulus, the unconditioned or conditioned, has a larger changing rate due to the variable. That is, whether the unconditioned or the conditioned modulus is more “sensitive” to the variable. Figure 100 has demonstrated the influence of dynamic modulus test temperature and VTM on the ratio of modulus for ATPB-VA and OGBB-OK specimens. It is important to note that the ratio of modulus may slightly exceed one in few cases possibly due to the experimental error. Especially when the specimens have good moisture-resistance performance and the difference between the dynamic modulus before and after conditioning is not significant, the experimental error may exceed the influence of moisture damage causing the ratio of modulus larger than one. However, considering the ratio of modulus is only slightly larger than one in few cases, the laboratory results are still good enough to be analyzed.

$$Retained\ \% = \frac{Dyn.Modulus\ After\ ECS}{Dyn.Modulus\ Before\ ECS} \times 100\% \quad (30)$$

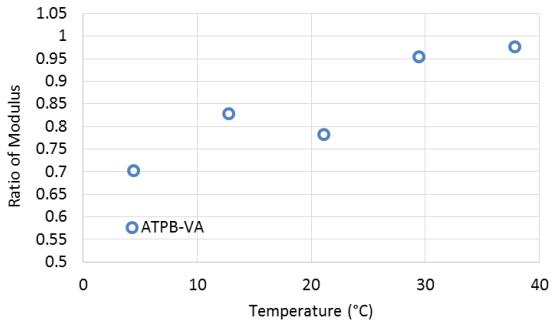

(a) Ratio of modulus versus temperature under 25 Hz frequency for ATPB-VA specimen (26% VTM)

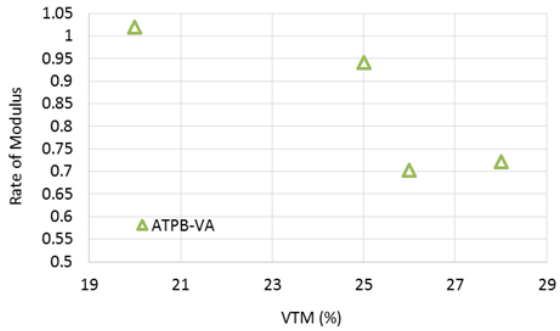

(b) Ratio of modulus versus VTM under 25 Hz frequency at 4.4 ℃ for ATPB-VA specimens

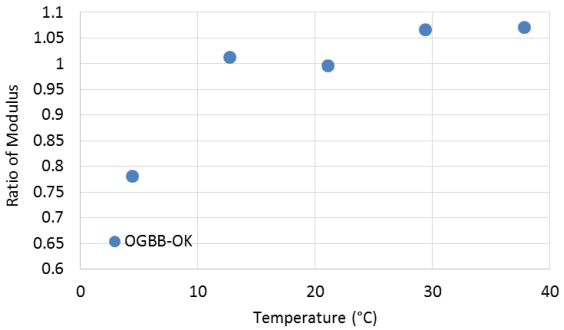

(c) Ratio of modulus versus temperature under 25 Hz frequency for OGBB-OK specimen (23% VTM)

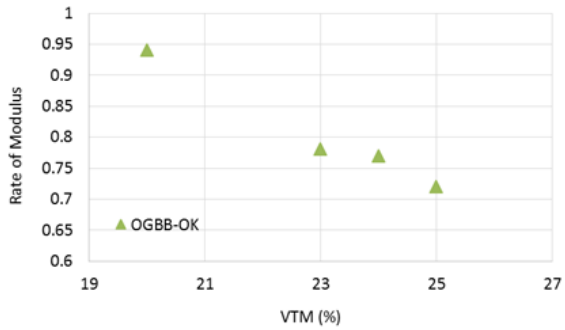

(d) Ratio of modulus versus VTM under 25 Hz frequency at 4.4 ℃ for OGBB-OK specimens

Figure 100. Ratio of modulus versus temperature and VTM

With increasing temperature or VTM, the dynamic moduli of both the unconditioned and conditioned specimens are changing accordingly, which further influences the ratio of modulus. The changes in ratio of modulus indicate the changing rate in dynamic modulus of the unconditioned and conditioned specimens caused by the variables like temperature, VTM and so forth. For detailed illustration, as shown in Figure 100 (a) and (c), when the VTM and frequency remain unchanged, the ratio of modulus is increasing as the test temperature increases. This is because when the temperature rises, both the unconditioned and conditioned dynamic modulus decrease while the decreasing rate of the conditioned modulus is not as large as that of the unconditioned one. As a result, the ratio of modulus increases. In Figure 100 (c) and (d), the unconditioned and conditioned dynamic modulus all decrease as the VTM increases, but with higher decreasing rate of conditioned modulus, the ratio of modulus is decreasing as the VTM increases. From Figure 100, it is concluded that the water-bath conditioning has led to the ATPB-VA and ATPB-OK specimens less sensitive to temperature but more sensitive to VTM. That is, as the temperature increases, the drop in dynamic modulus of moisture-deteriorated specimen is not as large as that of no moisture-deteriorated specimen. However, as the VTM

increases, the drop in dynamic modulus of moisture-deteriorated specimen is larger compared with no moisture-deteriorated specimen. In addition, the smallest ratio of modulus for both the ATPB-VA and OGBB-OK specimens are about 70%, standing between the 85% and 55% corresponding to well-performed and poor performed mixtures as reported by NCHRP Project 9-34.

Unlike the monotonically increasing ratio of modulus with increasing loading frequency as obtained in NCHRP Project 9-34, the relationship between ratio of modulus and loading frequency has exhibited different trends even for the same mixture in this study. There is no fixed changing tendency to conclude the influence of loading frequency on the ratio of modulus, because either situations when the ratio of modulus increases or decreases as the loading frequency increases can be observed. This may indicate the possibility that the influence of the loading frequency can be more significant on either unconditioned or conditioned specimen. Figure 101 has demonstrated both the increasing and decreasing ratio of modulus versus increasing loading frequency observed from ATPB-VA specimens.

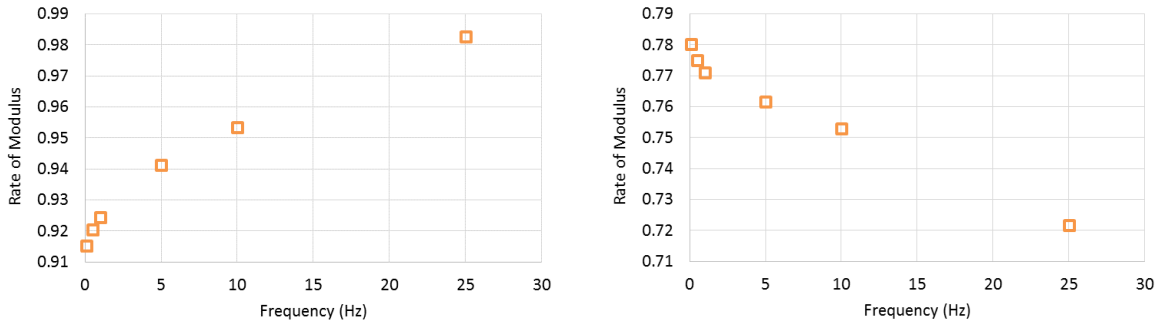

(a) Ratio of modulus versus frequency under 12.7 ℃ for ATPB-VA specimen (25% VTM)

(b) Ratio of modulus versus frequency under 4.4 ℃ for ATPB-VA specimen (28% VTM)

Figure 101. Ratio of modulus versus loading frequency for ATPB-VA specimens

To sum up, the evaluation on the moisture-related reduction in dynamic modulus of the ATPB-VA and OGBB-OK mixtures in this study has demonstrated acceptable performance of these two mixtures in resisting moisture damage. A comparison between the dynamic modulus of the conditioned and unconditioned specimens of both ATPB-VA and OGBB-OK mixture has shown that:

- Exposure to moisture for five days does deteriorate the mechanical property of asphalt stabilized drainage layer materials in term of dynamic modulus.
- As the air void content increases, the moisture-induced decrease in dynamic modulus tend to be larger, although the difference is not significant for 5-day conditioning.
- For the ATPB-VA and OGBB-OK mixtures used in this study, generally the ratio of modulus grows with the increasing temperature but decreases with the increasing air void content, indicating that the drainage layer materials may become more sensitive to VTM but less sensitive to temperature after conditioned in moisture environment. That is, the influence of VTM on the dynamic modulus of moisture-deteriorated specimen is more significant compared with the un-deteriorated specimen, while the influence of

temperature on the dynamic modulus of moisture-deteriorated specimen is less significant compared with the un-deteriorated specimen. Therefore, the drainage layers with large VTM are more susceptible to moisture damage in term of reduced dynamic modulus and mechanical performance.

- With a typical minimum ratio of modulus to be 0.7, the ATPB-VA and ATPB-OK mixtures used in this study are considered to have acceptable performance in moisture resistance, based on the findings in NCHRP Project 9-34.

COMPRESSIVE STRENGTH OF OGPCCB-OK MIXTURES

Totally 24 OGPCCB-OK specimens have been fabricated with the air void content ranging from 26% to 34%. Due to a combination effects of the gradation adopted by the OGPCCB-OK and the compaction way of hand-rodding, the smallest air void content can be achieved for OGPCCB-OK specimen is 26%. After the fabrication, the specimens were cured and stored until they reached 7-day, 14-day, 21-day or 28-day ages and then the compressive strength at different ages were determined. The compressive strength of OGPCCB-OK specimens with 26% to 34% air void content are shown in Table 25 and Figure 102.

Table 25. Air void content and compressive strength of specimens with 7-day, 14-day, 21-day and 28-day age

	# of specimen	Air void content (%)	Compressive loading at failure (bl)	Cross sectional area (in^2)	Compressive strength (psi)
7-day age	S1	28.07	6000	12.57	477.33
	S2	31.38	6800	12.57	540.97
	S3	27.30	8800	12.57	700.08
	S4	34.27	5600	12.57	445.51
	S7	32.17	9800	12.57	779.63
	S8	33.04	4000	12.57	318.22
14-day age	S5	28.47	11200	12.57	891.01
	S6	32.91	5400	12.57	429.59
	S9	29.30	7200	12.57	572.79
	S10	30.49	7600	12.57	604.61
	S11	29.71	8400	12.57	668.26
	S12	29.29	8600	12.57	684.17
21-day age	S13	28.10	11800	12.57	938.74
	S14	32.07	6800	12.57	540.97
	S15	33.16	8800	12.57	700.08
	S16	29.08	11600	12.57	922.83
	S17	34.82	8200	12.57	652.35
	S18	26.51	9200	12.57	731.90
28-day age	S26	30.43	8000	12.57	636.44
	S28	27.10	12400	12.57	986.48
	S29	29.38	9800	12.57	779.63
	S31	32.34	9000	12.57	715.99
	S32	34.64	6800	12.57	540.97
	S33	32.24	6000	12.57	477.33

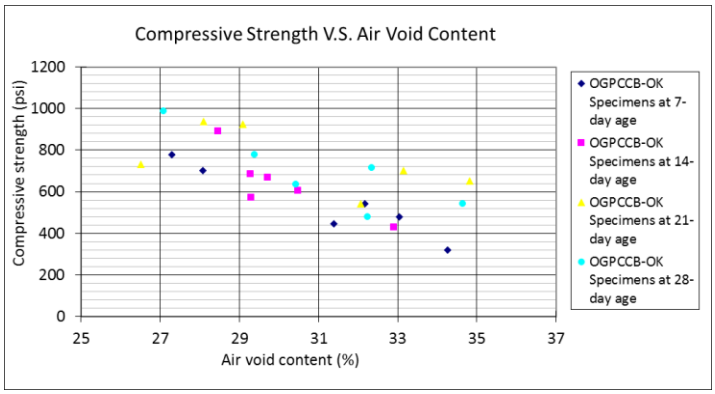

Figure 102. The relationship between the compressive strength and the air void content for specimens with 7-day, 14-day 21-day and 28-day age

As in Figure 102, obvious decreasing in the compressive strength can be observed as the air void content increases. When it comes to the influence of the age, generally the compressive strength of the OGPCCB-OK specimen increases with the age. The difference can reach more than 200 psi from 7-day to 28-day ages. In addition, compared with the default level 3 inputs of Portland Cement Concrete (PCC) in MEPDG, the compressive strengths of OGPCCB-OK specimens determined in laboratory are much lower. The compressive strength at 7-day, 14-day, 21-day and 28-day ages of OGPCCB-OK specimens are all below 1,000 psi with air void content larger than 27%, while the typical compressive strength of PCC in MEPDG is from 2,500psi to 7,000psi. As a result, if the drainage layer will be considered as a structural layer and included in the structural design in MEPDG, proper default compressive strength of the cement treated open-graded mixtures should be used. Based on the results from laboratory test in this study, the recommended default compressive strength of the OGPCCB-OK mixtures ranges from 400 psi to 1000 psi.

CHAPTER 6 FEM SIMULATION ON STRUCTURAL PERFORMANCE OF THE DRAINAGE LAYER

Generally, the structural performance of the drainage layer has not been considered by most pavement analysis and design procedures. However, as part of the pavement structure, the drainage layer typically incorporated as part of the base or subbase course also performs structural contribution to the system. Due to its particular material properties compared with regular dense-graded asphalt concrete, the stress and strain distribution within the pavement structure may change a lot when a drainage layer is used. Finite Element Method (FEM) is used to investigate the structural contribution and the location effect of the drainage layer. The MEPDG is used to determine the upper and lower bounds of the optimal air void content in terms of both sufficient permeability and good structural performance.

STRUCTURAL CONTRIBUTION AND LOCATION EFFECTS

Prony Series Parameters

The Prony series are used to mechanically describe the time-temperature dependent properties of asphalt mixtures and incorporate the realistic material properties into FEM simulations conveniently. Equation 31 shows the storage modulus (imaginary part) in form of frequency domain Prony series. Since this mathematical model will be more accurate to describe the laboratory testing data when more terms are included, enough terms should be adopted to make full use of the laboratory data and to accurately describe the material properties. According to our investigation, by increasing the terms in Prony series from 5 to 11, the model will be approaching the original test data significantly as shown in Figure 103. Other figures shown the 5-term and 11-term Prony series to describe the laboratory dynamic modulus data of ATPB-VA, OGBB-K and ATPB-ID specimens can be found in Appendix B.

$$E'(\omega) = G_0\left[1 - \sum_{i=1}^{N} \overline{g_i^P}\right] + G_0 \sum_{i=1}^{N} \frac{\omega^2 \tau_i^2 \overline{g_i^P}}{\omega^2 \tau_i^2 + 1} \quad (31)$$

Where,

$E'(\omega)$ is the imaginary part of the complex modulus, or storage modulus,

G_0, $\overline{g_i^P}$, τ_i are all coefficients.

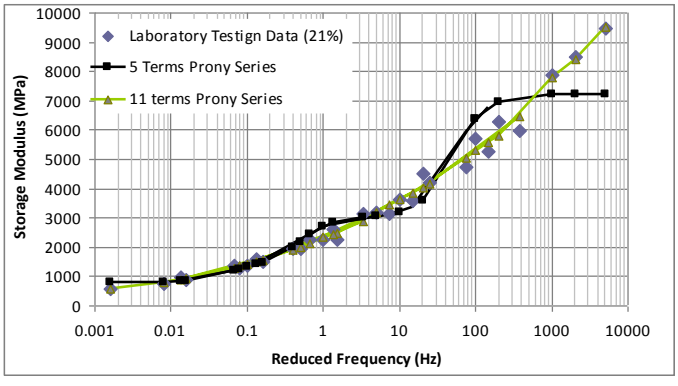

Figure 103. The Prony series with 5 and 11 terms to describe the original test data (21% VTM, ATPB-VA mixture)

For the accuracy consideration, the 11-term Prony series were used to describe the viscoelastic properties of the ATPB-VA, OGBB-OK and ATPB-ID materials based on laboratory dynamic modulus test results. The fitted parameters of the Prony series are presented in Table 26 for the ATPB-VA mixture. The parameters of the 11-term Prony series for OGBB-OK and ATPB-ID mixtures are included in Appendix B. These parameters will be used in the FEM simulation to describe the time-temperature properties of the asphalt treated drainage layer materials.

Table 26. 11-terms Prony Series Parameters for ATPB-VA Mixture

21%				25%		28%	
G_0	11443.02			G_0	8247.85	G_0	7012.767
τ_1	0.00002	$\overline{g_1{}^P}$	0.05978797	$\overline{g_1{}^P}$	0.09527796	$\overline{g_1{}^P}$	0.11011482
τ_2	0.0002	$\overline{g_2{}^P}$	0.23127016	$\overline{g_2{}^P}$	0.26520895	$\overline{g_2{}^P}$	0.27961182
τ_3	0.002	$\overline{g_3{}^P}$	0.22926499	$\overline{g_3{}^P}$	0.22973498	$\overline{g_3{}^P}$	0.24373027
τ_4	0.02	$\overline{g_4{}^P}$	0.14527118	$\overline{g_4{}^P}$	0.14440705	$\overline{g_4{}^P}$	0.12057071
τ_5	0.2	$\overline{g_5{}^P}$	0.11769956	$\overline{g_5{}^P}$	0.10241869	$\overline{g_5{}^P}$	0.09290047
τ_6	2	$\overline{g_6{}^P}$	0.08488443	$\overline{g_6{}^P}$	0.06658912	$\overline{g_6{}^P}$	0.05308622
τ_7	20	$\overline{g_7{}^P}$	0.05326667	$\overline{g_7{}^P}$	0.03571431	$\overline{g_7{}^P}$	0.04091311
τ_8	200	$\overline{g_8{}^P}$	0.03180873	$\overline{g_8{}^P}$	0.01558389	$\overline{g_8{}^P}$	0.03003996
τ_9	2000	$\overline{g_9{}^P}$	0.00000087	$\overline{g_9{}^P}$	0.02071041	$\overline{g_9{}^P}$	0.00989047
τ_{10}	20000	$\overline{g_{10}{}^P}$	0.02637300	$\overline{g_{10}{}^P}$	0.01653045	$\overline{g_{10}{}^P}$	0.01658425
τ_{11}	200000	$\overline{g_{11}{}^P}$	0.00634667	$\overline{g_{11}{}^P}$	0.00428506	$\overline{g_{11}{}^P}$	0.00255253

FEM Simulation of structural contribution and location effect of the drainage layer

Compared with static loading and multi-layer elastic theory, FEM simulation considering dynamic loading and realistic material properties are more accurate and can provide the closest pavement responses to field measured results [52, 53]. A flexible pavement model with typical structure based on the structure adopted by Franklin Turnpike Extension at Lynchburg, Virginia has been set up and analyzed by Program Abaqus/Standard. The pavement model is 5 meters along the direction of moving traffic. The configuration of the pavement model and the contact area are shown in Figure 104.

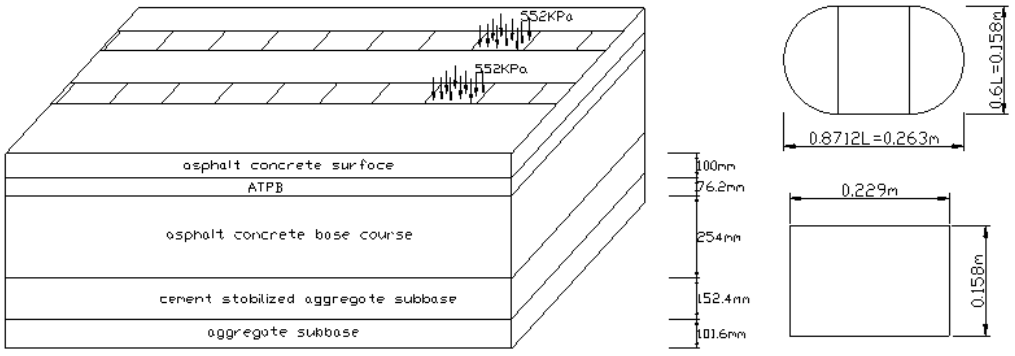

Figure 104. Configuration of the Pavement Model and Contact Area

The air void content of the ATPB drainage layer was assumed to be 25% in the simulation. The Prony series parameters in Table 26 and Appendix B representing the viscoelastic properties of the ATPB drainage layer were used in Dynamic/Implicit analysis. A moving half-sinusoidal traffic loading was applied on the surface of the pavement model at speed of 40 mph.

In addition to the modulus of the drainage layer, the modulus of other layers would also influence the pavement responses and the stress or strain distribution within the structure, therefore totally two scenarios with different moduli of the layers have been set up in the simulation. The comparison between the two scenarios can be used to see how the modulus of other layers influence the pavement responses, and to what extent the pavement responses are influenced. Table 27 and 28 lists the material properties used in the two scenarios. In scenario I, the modulus of all the other layers are much lower as compared with scenario Π. The magnitude of the tire-pavement contact pressure is 552Kpa based on 80KN single-axle load for scenario I, and 700KPa of contact pressure regarding heavy traffic is used in scenario Π. In the following section of structural contribution and location effect, scenario Π material properties have been adopted. In the section regarding influence of air void content, both the two scenarios are discussed.

Table 27. Summary of Material Parameters in scenario I

Layer	Thickness	Elastic modulus(MPa)	Poisson's Ratio
AC surface layer	4''	1800	0.30
AC Base	10''	1200	0.30
ATPB	3''	352 (long term)	0.30
Cement treated subbase 1	6''	1200	0.30
Aggregate subbase 2	4''	500	0.35

Table 28. Summary of Material Parameters in scenario Π

Layer	Thickness	Elastic modulus(MPa)	Poisson's Ratio
AC surface layer	4''	3500	0.30
AC Base	10''	3000	0.30
ATPB	3''	352 (long term)	0.30
Cement treated subbase 1	6''	1400	0.30
Aggregate subbase 2	4''	200	0.35

Figure 105 has shown the simulated inelastic strain at the bottom of the drainage layer under moving traffic loading. As in Figure 105, there are still two tracks of inelastic strain at the bottom of the drainage layer when the wheel loading has passed, indicating the time-dependent viscoelastic property of the ATPB material.

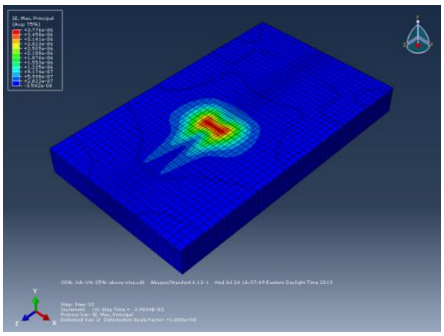

Figure 105. Inelastic strain at the bottom of ATPB when it is above the base from scenario I

Figure 106 and Figure 107 present the stress and vertical deformation on the surface of pavement versus time. The maximum stress and vertical deformation happens at about 0.001 seconds after the wheel loading reaches the maximum values. As the wheel loading passes away, the stress and strain dissipate dramatically. The damping of the stress, however, is much faster than that of the deformation as found in other study. [51]

Although no notable differences were observed in stress and deformation on the surface of the pavement in time domain, large differences were found along the depth right below the wheel at the end of the traffic loading, as shown in Figure 108 to Figure 111. In Figure 108, the ATPB drainage layer inside a pavement structure is a location where stress reaches the maximum value. The vertical deformations under wheel loading are comparable when the drainage layer is located above or below the base as shown in Figure 109. The total vertical deformation at surface under wheel loading is slightly larger when the drainage layer is located above the base. The horizontal tensile stress at the top of the drainage layer is always the largest no matter the drainage layer is located above or below the base course as illustrated in Figure 110. Figure 111 demonstrates that the vertical stress within the surface and drainage layer is larger in above-base case.

The pavement structure without the ATPB drainage layer is also simulated. The mechanical properties of other pavement materials are kept the same. With increasing depth below the pavement surface, the stress inside an undrained pavement is concentrated at the top layers and then decreases successively with depth while the drained pavement will observe sudden stress increase in the drainage layer as shown in Figure 108. The no-drainage-layer case has the largest vertical deformation at the moment of applying wheel loads as present in Figure 109, indicating that the ATPB drainage layer does undertake part of the load no matter where it locates, although the structural contribution of the drainage layer is not significant.

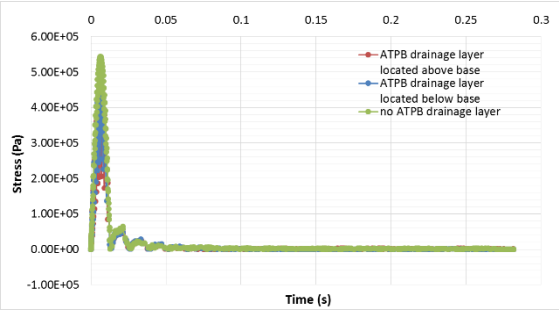

Figure 106. Chart. Stress on the pavement surface versus time

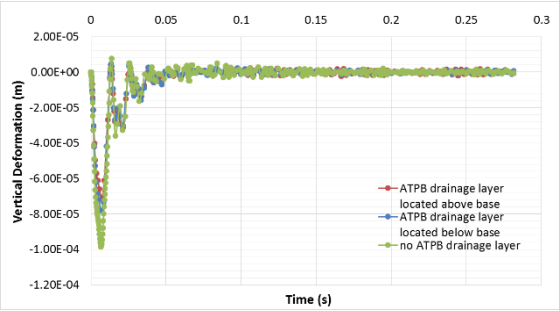

Figure 107. Chart. Vertical deformation on the pavement surface versus time

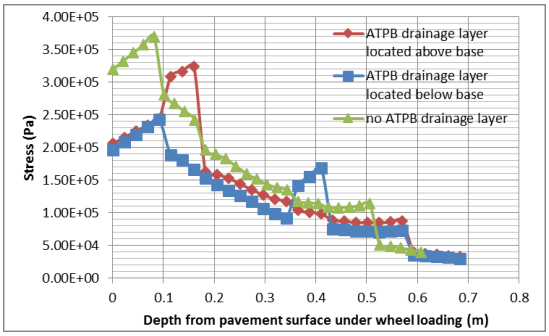

Figure 108. Chart. Stress along the depth under traffic loading

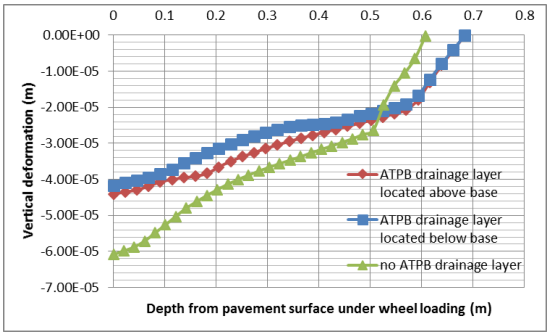

Figure 109. Chart. Vertical deformation along the depth under traffic loading

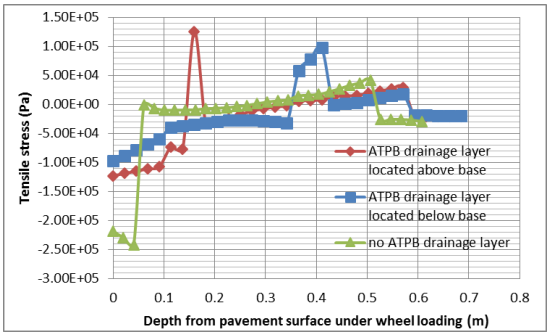

Figure 110. Chart. Tensile stress along the depth under traffic loading

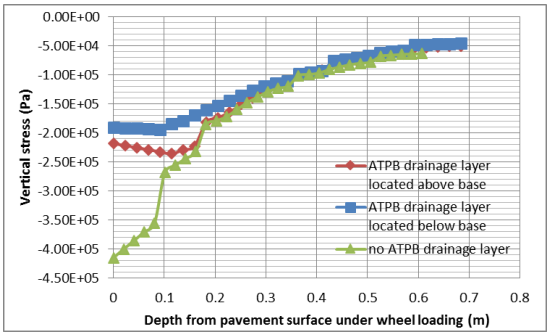

Figure 111. Chart. Vertical stress along the depth under traffic loading

THE INFLUENCE OF THE DRAINAGE LAYER'S AIR VOID CONTENT ON PAVEMENT RESPONSES

The air void content is a vital parameter that influence the mechanical properties of the stabilized drainage layers, given a mixture with specified asphalt binder and aggregates. Accordingly, when considering the structural contribution of the drainage layer, the influence of the air void content should not be neglected. The FEM simulations have been conducted to

investigate the pavement responses with drainage layers of different air void contents under moving traffic loading.

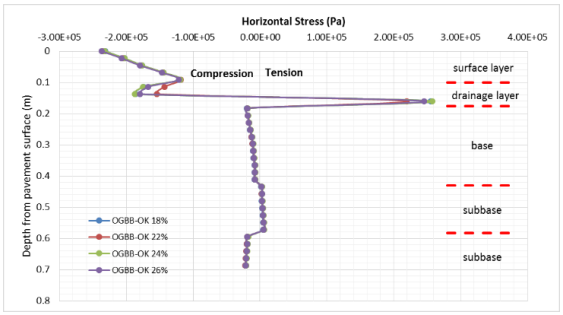

Figure 112. The horizontal stress distribution along the depth under traffic loading with above-base drainage layer (OGBB-OK)

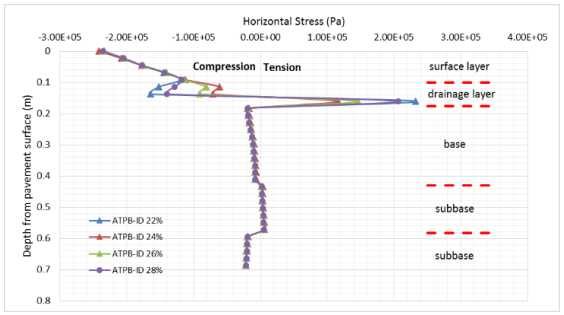

Figure 113. The horizontal stress distribution along the depth under traffic loading with above-base drainage layer (ATPB-ID)

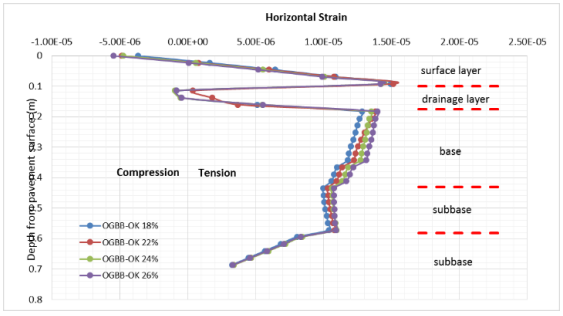

Figure 114. The horizontal strain distribution along the depth under wheel at the maximum traffic loading with above-base drainage layer (OGBB-OK)

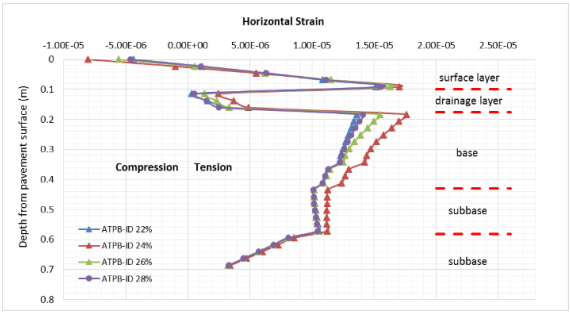

Figure 115. The horizontal strain distribution along the depth under wheel at the maximum traffic loading with above-base drainage layer (ATPB-ID)

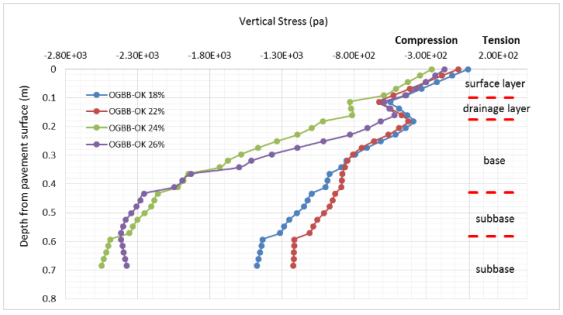

Figure 116. The vertical strain distribution along the depth under wheel at the end of traffic loading with above-base drainage layer (OGBB-OK)

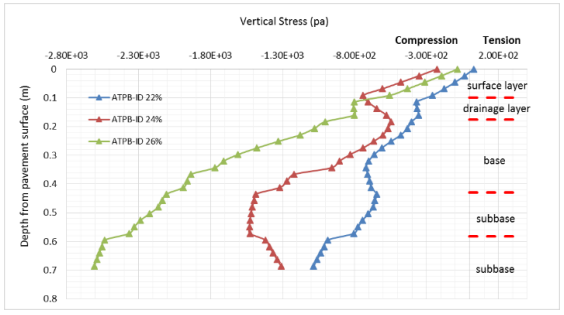

Figure 117. The vertical strain distribution along the depth under wheel at the end of traffic loading with above-base drainage layer (ATPB-ID)

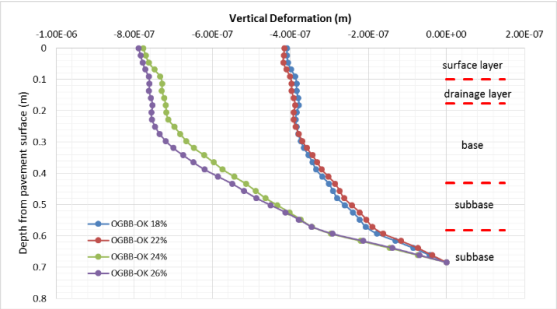

Figure 118. The vertical deformation distribution along the depth under wheel at the end of traffic loading with above-base drainage layer (OGBB-OK)

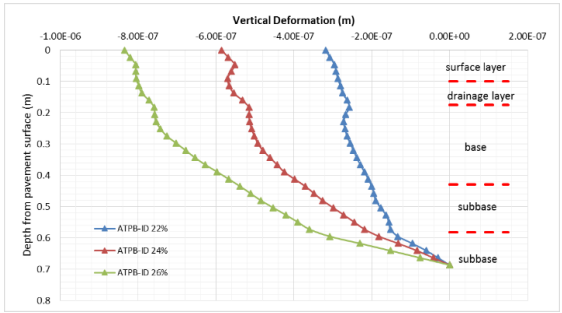

Figure 119. The vertical deformation distribution along the depth under wheel at the end of traffic loading with above-base drainage layer (ATPB-ID)

Figure 112 to Figure 119 show the pavement responses under traffic loading when the drainage layer is located above the base. All the negative values represent the compression and all the positive values represent tensile stresses. Figure 112 and Figure 113 present the horizontal stress below one tire at the moment when the traffic loading reaches the maximum value. Compression horizontal stress has been observed within the surface layer while the horizontal stress is changing to tensile stress within the drainage layer. This is very similar to a typical flexible pavement responses under traffic loading, when the top of the surface layer subjects to compressive stress and the bottom of the surface layer undergoes tensile stress. However, the existence of drainage layer has moved the tensile stress from the surface layer to itself. The maximum tensile stress occurs in the drainage layer and then dissipates rapidly. Compressive horizontal stress occupies most of the underlying layers.

Figure 112 and Figure 113 also give a comparison between the situations when the drainage layers are of different air void contents. It is found that the stress within the drainage layer is not a monotone-changing function as the air void content changes. This may be attribute to the experimental error of the dynamic modulus or air void content, which are inputs for the simulation. However, generally the pavement with a mechanically stronger drainage layer, or the drainage layer with lower air void content, will have reduced tensile stress within itself.

Figure 114 and Figure 115 have shown the horizontal strain developed along the depth under one tire when the wheel loading reaches the maximum value. Within the surface layer, the horizontal strain transfers from compression to tension with depth. The distribution of horizontal strain within the drainage layer follows the similar trend. Compressive strain has been observed at the top of the drainage layer while tensile strain at the bottom. Typically reducing the air void content in drainage layer will also reduce the tensile strain within the underlying layers.

At this moment when the wheel loading reaches the maximum value, the maximum compressive stress is at the top of the surface layer, and is getting smaller as going deeper below the surface. The influence of the air void content in drainage layer is insignificant compared with the influence of the traffic loading. To present the effects of the air void content more clearly, the distribution of vertical stress and deformation along the depth under one tire when the traffic loading just passed by have been shown in Figure 116 to Figure 119.

At this moment when the traffic loading has just passed by, the distribution of the vertical stress along depth has shown different configuration. The traffic loading at pavement surface reduced to zero and the vertical stress within the surface layer has reduced significantly to almost

zero, but the vertical stress within the underlying layers is dissipating much slowly. Generally, the compressive stress is getting larger as the air void content of the drainage layer increases. The distribution of the vertical strain follows the same trend as that of the vertical stress. Pavement with lower air void content in drainage layer will achieve smaller strains and consequently, smaller deflection on the pavement surface as shown in figure 118 and Figure 119.

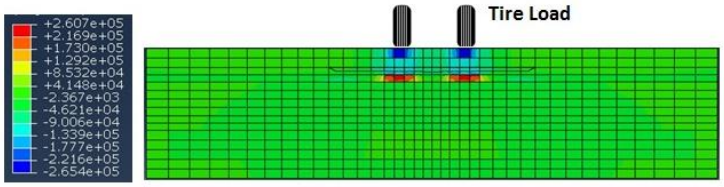

Figure 120. Horizontal Stress distribution under traffic loading of the pavement incorporated with the ATPB-ID drainage layer of 28% air void content

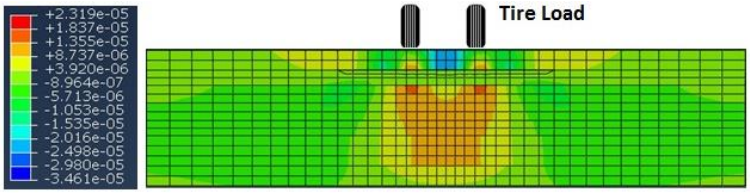

Figure 121. Horizontal Strain distribution under traffic loading of the pavement incorporated with the ATPB-ID drainage layer of 28% air void content

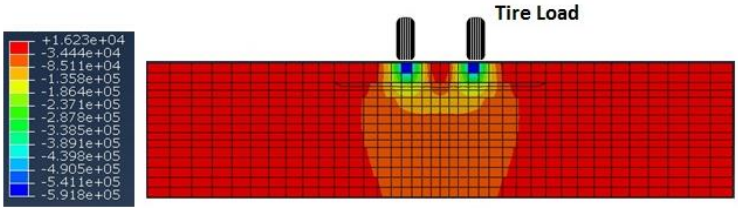

Figure 122. Vertical Stress distribution under traffic loading of the pavement incorporated with the ATPB-ID drainage layer of 28% air void content

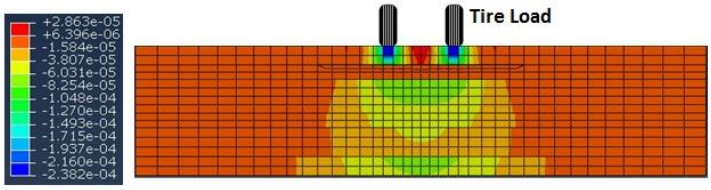

Figure 123. Vertical Strain distribution under traffic loading of the pavement incorporated with the ATPB-ID drainage layer of 28% air void content

Figure 120 to Figure 123 present the pavement responses under one axle when the traffic loading reaches the maximum value. It can be found that underneath the tire load, the surface layer subjects to compressive stress and strain. Outside the tire load, especially between the two tires, compressive horizontal stress and strain and tentile vertical stress and strain are observed. When the drainage layer is located right below the surface layer, tensile horizontal stress and strain occur at the bottom of it. The vertical stress and strain within the drainage layer and the

underlying layers below tires are compressive. Higher compressive strain has been found at the top of base and subbase.

Figure 124 to Figure 131 have presented the pavement responses along the depth below the wheel loading when the drainage layer is located below the base course. As shown in Figure 124 and Figure 125, the bottom of the drainage layer is the location within the pavement structure where the horizontal tensile stress reaches the maximum value. Compared with the situation when the drainage layer is above the base course, it can be found that the tensile stress within the drainage layer has reduced significantly. As shown in Figure 126 and Figure 127, no compressive horizontal strain occurs in the drainage layer when it is below the base. However, the tentile strain at the bottom of the surface layer, which is also the maximum tensile strain within the pavement structure, has increased dramatically compared with the above-base situation. As a result, the horizontal strain within the base course which is directly below the surface also increased a lot. The influence of the air void content is not significant when the traffic loading reaches the maximum value as in above-base case. Figure 128 to Figure 131 presenting the stress and deformation distribution when the traffic loadig just passed by can be used to investigate the influence of air void content. Very similar results have been observed as the above-base situation, that is, generally the increase in air void content will result in increasing vertical stress and deformation. However, exception may exist due to complex material properties and the experiment errors.

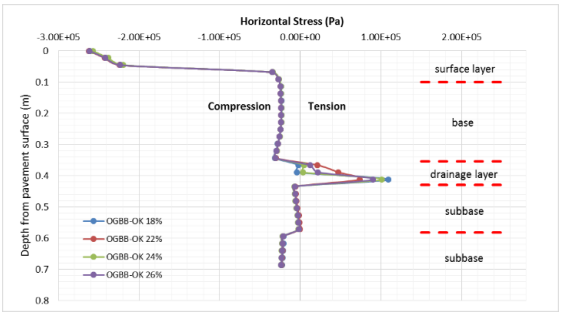

Figure 124. The horizontal stress distribution along the depth under traffic loading with below-base drainage layer (OGBB-OK)

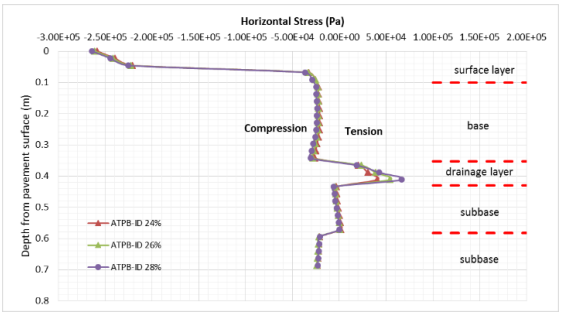

Figure 125. The horizontal stress distribution along the depth under traffic loading with below-base drainage layer (ATPB-ID)

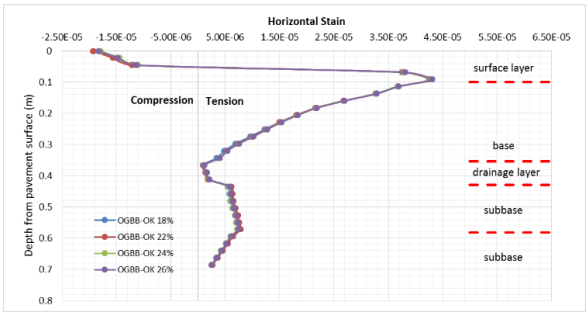

Figure 126. The horizontal strain distribution along the depth under traffic loading with below-base drainage layer (OGBB-OK)

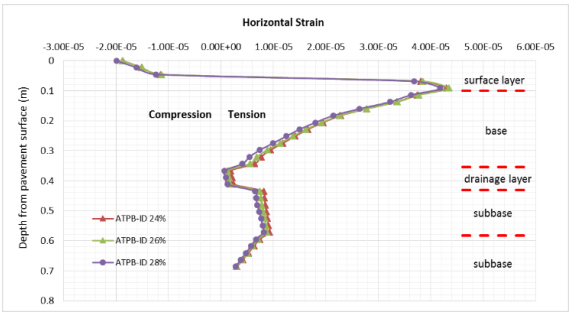

Figure 127. The horizontal strain distribution along the depth under traffic loading with below-base drainage layer (ATPB-ID)

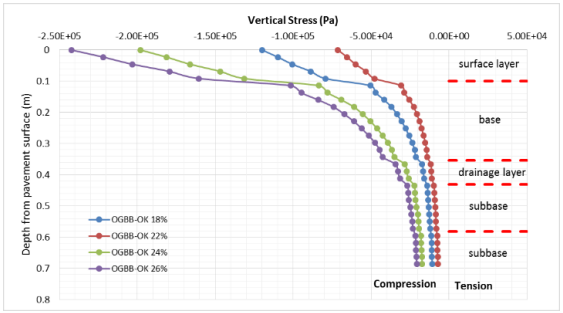

Figure 128. The vertical stress distribution along the depth under traffic loading with below-base drainage layer (OGBB-OK)

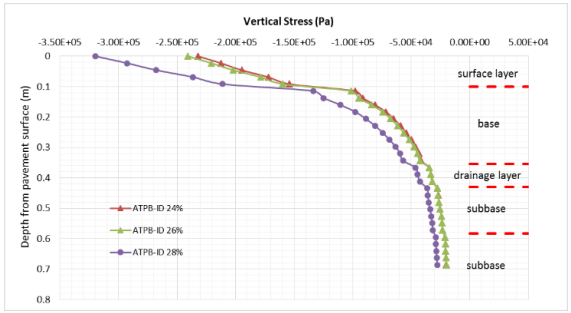

Figure 129. The vertical stress distribution along the depth under traffic loading with below-base drainage layer (ATPB-ID)

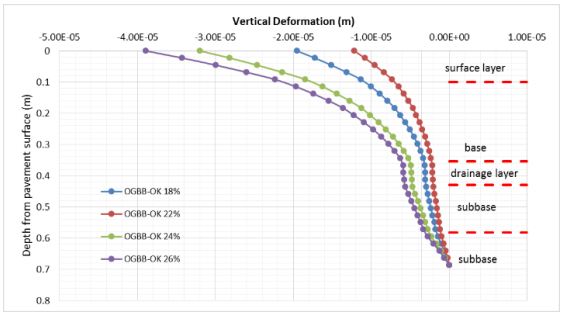

Figure 130. The vertical deformation distribution along the depth under traffic loading with below-base drainage layer (OGBB-OK)

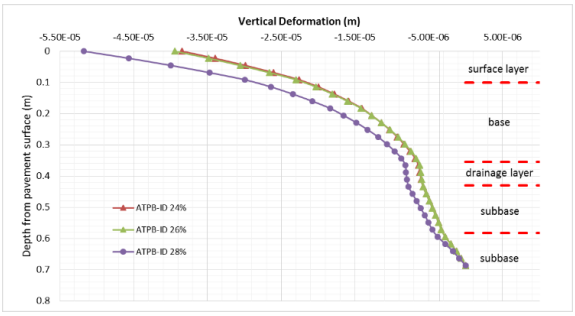

Figure 131. The vertical deformation distribution along the depth under traffic loading with below-base drainage layer (ATPB-ID)

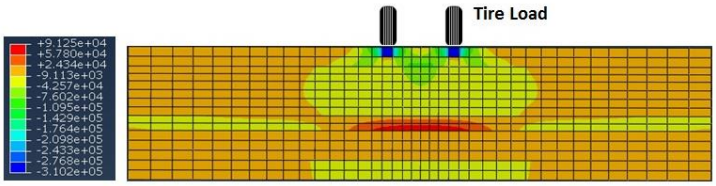

Figure 132. Horizontal stress distribution under traffic loading of the pavement incorporated with the OGBB-OK drainage layer of 28% air void content

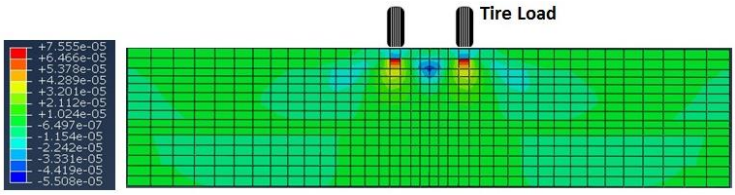

Figure 133. Horizontal strain distribution under traffic loading of the pavement incorporated with the ATPB-ID drainage layer of 28% air void content

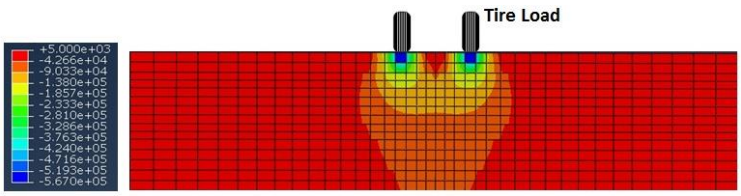

Figure 134. Vertical stress distribution under traffic loading of the pavement incorporated with the ATPB-ID drainage layer of 28% air void content

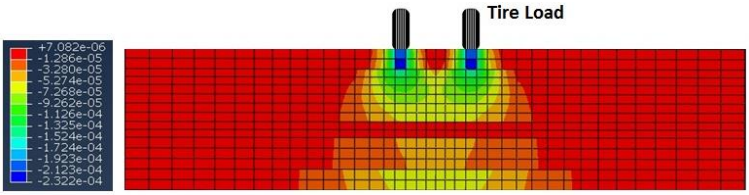

Figure 135. Vertical strain distribution under traffic loading of the pavement incorporated with the ATPB-ID drainage layer of 28% air void content

Figure 132 to Figure 135 present the stress and strain distribution under the wheel loading when the drainage layer is located below the base. Compared with the situation when the drainage layer is located above the base, it can be found that the drainage layer has moved the tensile horizontal stress to the place where it locates. As a resilt, the drainage layer is under tensile horizontal stress no matter it is above or below the base. In addition, the vertical strain within the drainage layer is very small wherever it locates. The layer right below the drainage layer will have increased compressive vertical strain.

All the above results are obtained from the Scenario I simulations on OGBB-OK and ATPB-ID drainage layers with different air void contents. The results of Scenario Π simulation, with ATPV-VA drainage layer and increased modulus of the surface and base, are shown as follows. Figure 136 to Figure 140 have presented the influence of the air void content in scenario Π with the ATPB-VA mixtures used as the drainage layer above the base. Figure 141 to Figure 145 have presented the influence of the air void content in scenario Π when the ATPB-VA drainage layer is located below the base. The moment when the traffic loading has just passed by is selected as the base for the comparison. Although the modulus of the surface and base have been increased and the modulus of the lower subbase has been reduced, similar stress and deformation distribution has been obtained as in scenario I. The major difference only lies in the magnitude of the stress, strain and deformation. According to the FEM analysis of scenario I and scenario Π with different layer modulus and drainage layer air void content, it can be concluded that:

- Horizontal tensile stress occurs at the bottom of the drainage layer, no matter it is located above or below the base.
- The horizontal and vertical strain within the drainage layer is much lower than that within the adjacent layers, which are approching zero within the FEM model adopted in this study.

- If the modulus of drainage layer is smaller than the adjacent base course, moving the drainage layer from the top of base to the bottom of base can reduce the total surface deformation. Given the ATPB-VA drainage layer properties and the typical pavement structure in this study, this location effect on the total surface deformation is very limited.
- The drainage layer does contribute as a structural layer to the pavement but the influence is limited.
- Generally, increase the air void content of the drainage layer will cause increase in stress, strain and total deformation within the pavement structure.

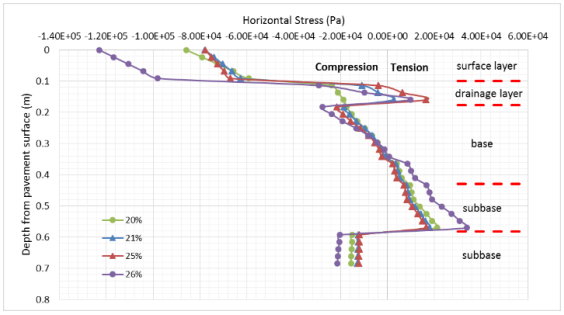

Figure 136. The horizontal stress distribution along the depth under traffic loading with above-base drainage layer (ATPB-VA)

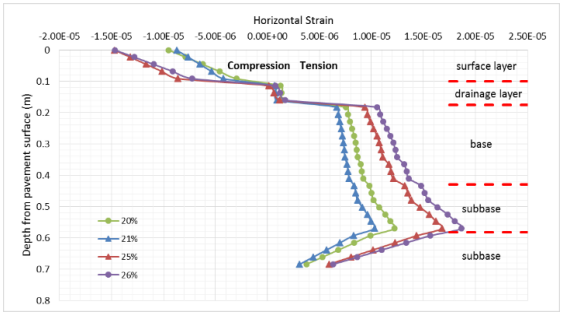

Figure 137. The horizontal strain distribution along the depth under traffic loading with above-base drainage layer (ATPB-VA)

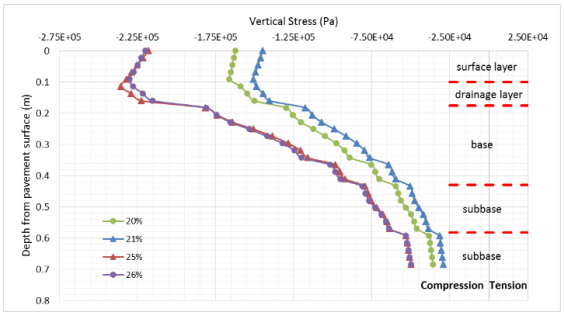

Figure 138. The vertical stress distribution along the depth under traffic loading with above-base drainage layer (ATPB-VA)

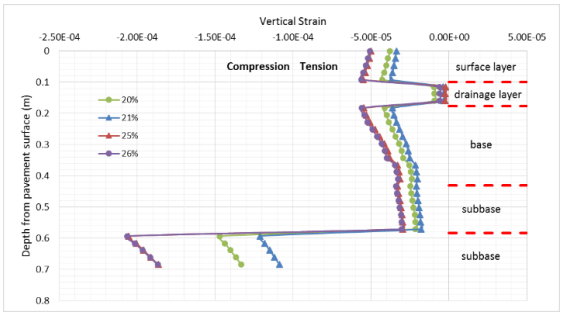

Figure 139. The vertical strain distribution along the depth under traffic loading with above-base drainage layer (ATPB-VA)

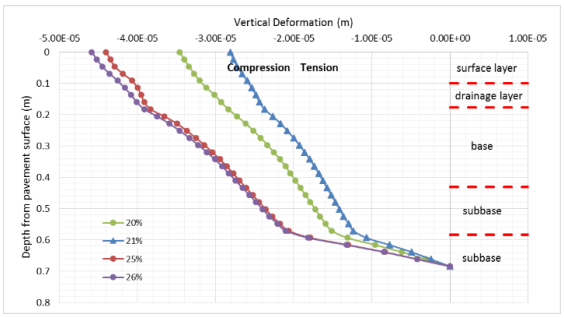

Figure 140. The vertical deformation distribution along the depth under traffic loading with above-base drainage layer (ATPB-VA)

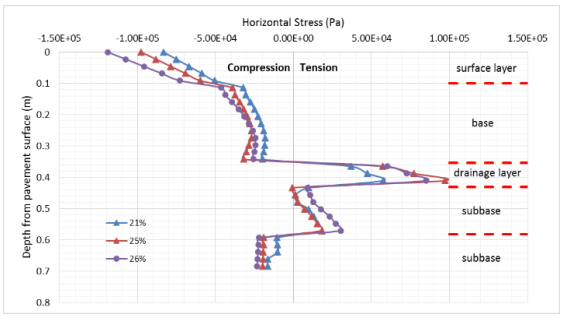

Figure 141. The horizontal stress distribution along the depth under traffic loading with below-base drainage layer (ATPB-VA)

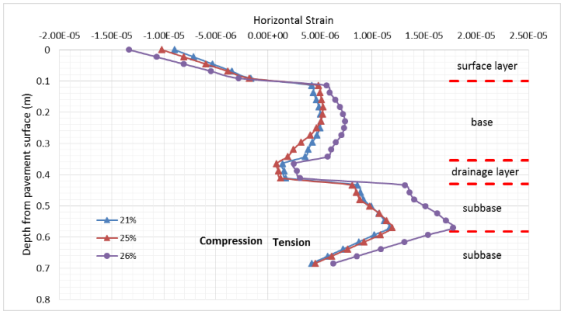

Figure 142. The horizontal strain distribution along the depth under traffic loading with below-base drainage layer (ATPB-VA)

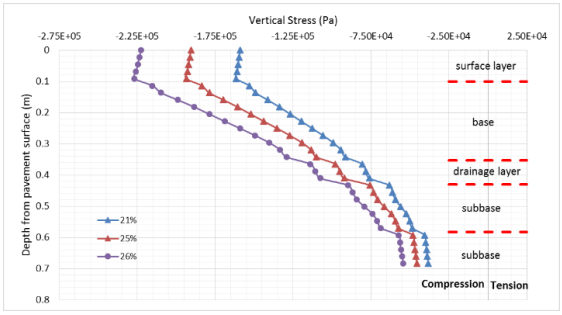

Figure 143. The vertical stress distribution along the depth under traffic loading with below-base drainage layer (ATPB-VA)

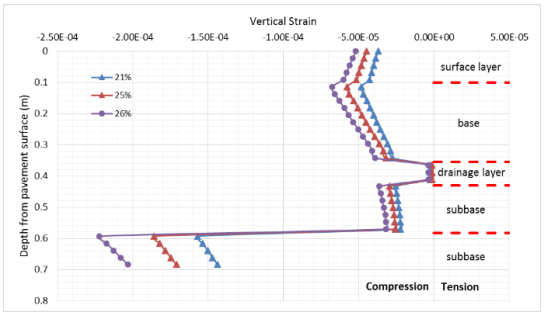

Figure 144. The vertical strain distribution along the depth under traffic loading with below-base drainage layer (ATPB-VA)

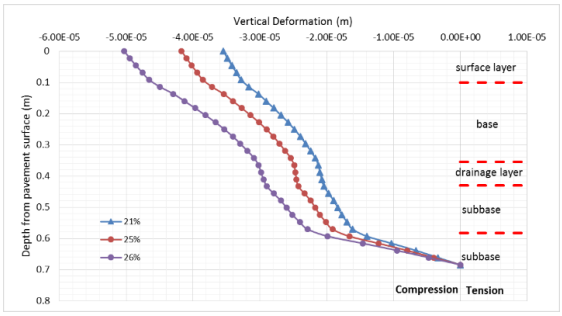

Figure 145. The vertical deformation distribution along the depth under traffic loading with below-base drainage layer (ATPB-VA)

THE INFLUENCE OF THE VIHECLE'S SPEED ON THE RESPONSES OF DRAINED PAVEMENT

The vehicle speed is another factor that will influence the responses of the pavement incorporated with a drainage layer. To investigate the influence of the vehicle speed, the pavement model with a drainage layer located above the base course is subject to wheel loading at speed of 20mph, 40mph and 60mph respectively. A comparison between the pavement

responses under different moving loading speeds has been presented from Figure 146 to Figure 150.

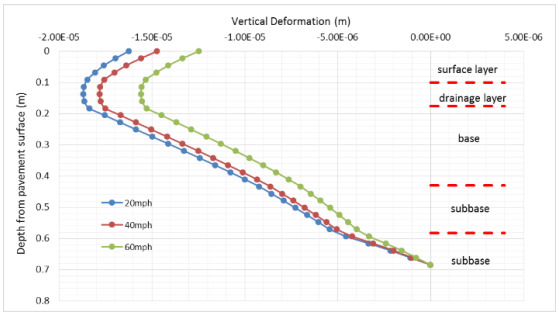

Figure 146. The vertical deformation distribution along the depth under traffic loading with above-base drainage layer (ATPB-VA)

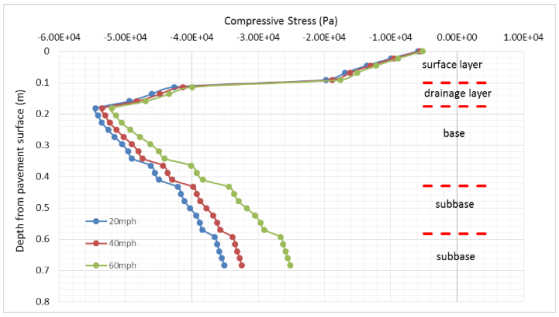

Figure 147. The compressive stress distribution along the depth under traffic loading with above-base drainage layer (ATPB-VA)

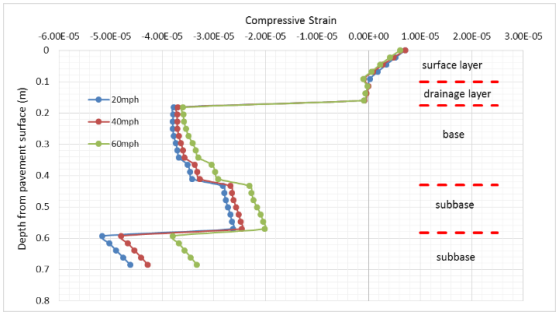

Figure 148. The compressive strain distribution along the depth under traffic loading with above-base drainage layer (ATPB-VA)

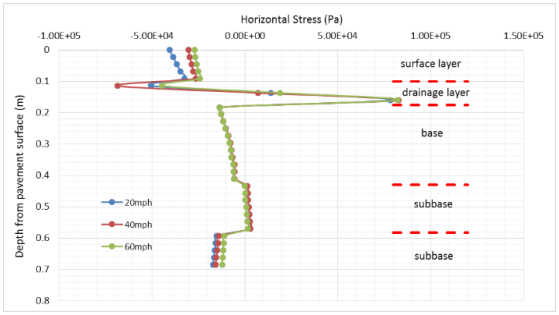

Figure 149. The horizontal stress distribution along the depth under traffic loading with above-base drainage layer (ATPB-VA)

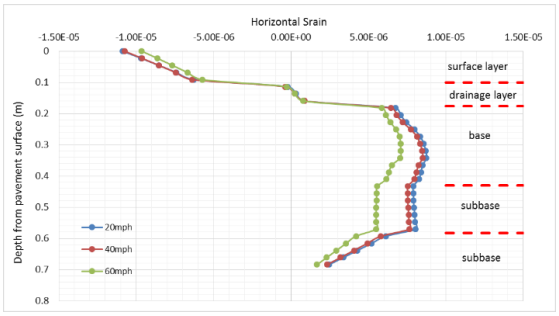

Figure 150. The horizontal strain distribution along the depth under traffic loading with above-base drainage layer (ATPB-VA)

As can be seen from Figure 146 to Figure 150, generally the stress, strain and vertical deformation are all the largest when the moving wheel loading is at the lowest speed of 20mph. As the speed of the wheel loading increases to 40mph or 60mph, the vertical deformation, stress and strain drops. Particularly the differences caused by increase in speed from 40mph to 60mph are much more significant than that from 20mph to 40mph. The influence of the vehicle speed

obtained from the simulation on drained pavement has shown conclusions in agreement with the findings from previous research. That is, the influences of traffic loading on a pavement structure is more significant with smaller speed, given the same level of loading magnitude.

THE OPTIMAL AIR VOID CONTENT

The functions of the drainage layer inside the pavement structure are multiple. Besides the main function of removing entrapped water out of the structure, the drainage layer also contributes to the structural performance, although this structural contribution was not often considered in the past. The air void content of drainage layer is the vital parameter influencing not only the permeability, but also the mechanical properties. Increasing in the air void content typically improves the permeability of the drainage layer, but may also reduce the strength and other mechanical properties. Therefore, the selection of the air void content of the drainage layer is a tradeoff between permeability and mechanical properties. There should be the optimal air void content ranges for the drainage layer, with which the drainage layer will not only satisfy the structural requirements but also obtain the adequate permeability.

According to FHWA, the trend of drainage layers in the 1990s, which is to apply a very high permeability of 8,000 to 10,000 ft/day, has been replaced today. It is found that there is no need to use drainage layers with such high permeability at the price of scarifying stability of the pavement. In addition, the amount of water that can infiltrate into the well-maintained pavement is not as high as the permeability. Nowadays the typical permeability of the drainage layer is from 500 ft/day to 800 ft/day [55]. The ACPA has also reported the same trend for unstabilized permeable subbases [56]. Taking this into consideration, the criteria of permeability to determine the lower bound of the optimal air void content has been selected to be 500 ft/day.

Based on laboratory permeability test results, to ensure a permeability of 500 ft/day, the air void content of the ATPB-VA drainage layer should be larger than 24.5%, as shown in Figure 151. For the OGBB-OK and ATPB-ID drainage layers, the minimum air void contents to ensure permeability of 500 ft/day are 21% and 24%, as shown in Figure 152 and Figure 153. On the other hand, the drainage layer should have adequate strength and stability as part of the pavement structure. As the air void content increases to achieve good performance in permeability, the strength and stability of the drainage layer deteriorate. To determine the upper bound of the air void content of the drainage layer at which the stability requirement in term of permanent deformation can be satisfied, MEPDG has been used to predict the potential rutting depth at a twenty-year pavement service life. Then the lower bound derived from permeability requirement and the upper bound determined from stability consideration will be utilized to establish the optimal air void content ranges for the drainage layer.

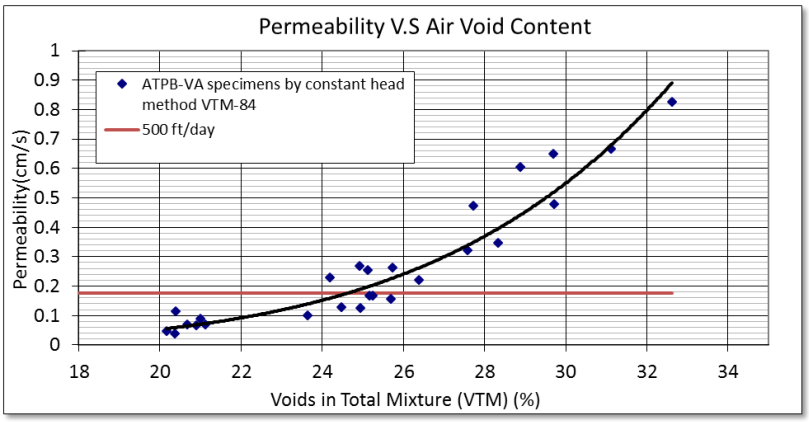

Figure 151. The lower bound of the optimal air void content for ATPB-VA drainage layer

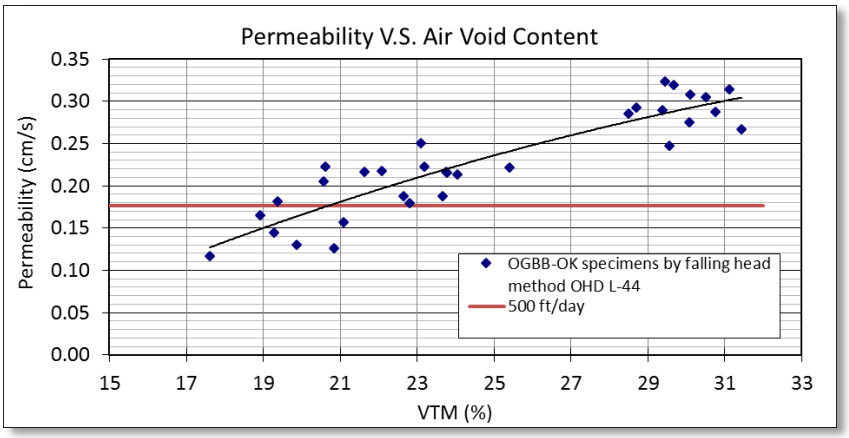

Figure 152. The lower bound of the optimal air void content for OGBB-OK drainage layer

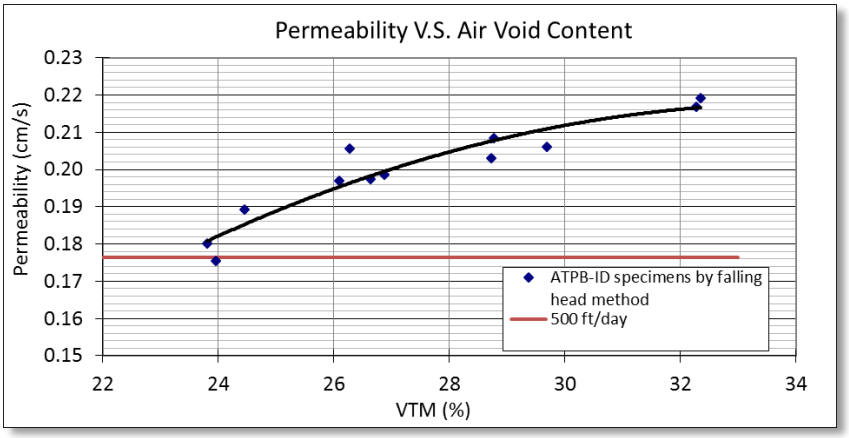

Figure 153. The lower bound of the optimal air void content for ATPB-ID drainage layer

Based on AASHTO 2008 standard, the rutting criteria for interstate pavements is 0.4 inches (1.016cm) and 0.5 inches (1.27cm) for primary pavements. A total rutting limit of 0.5 inches on average before adjustment of reliability is recommended by Witczak [57]. The MEPDG recommended a total rutting threshold of 0.75 inches after adjustment for reliability. Take into

consideration all of these rutting criteria, a rutting threshold of 0.75 inches after adjustment of reliability has been adopted to determine the upper bound of the optimal air void content ranges.

The pavement structure used in the MEPDG analysis is selected to be the same as the one adopted by Franklin Turnpike Extension at Lynchburg, Virginia. Figure 154 presents the pavement structure and Table 29 lists the parameters used in the MEPDG level 3 design. The asphalt treated drainage layer is considered as asphalt concrete with the air void content ranging from 20% to 35% in the analysis. The gradations of aggregates adopted by ATPB-VA mixture in this study and the laboratory-determined effective binder contents have been used as inputs for the drainage layer in this analysis. The other inputs for the surface layer, base and subbase follow the typical values for each mixture type. The climate data from Lynchburg, VA climate station has been used in the analysis for the ATPB-VA mixture.

In MEPDG, it is absolutely mandatory that the minimum and maximum test temperatures as recommended in AASHTO standard which are designed for the dense-graded asphalt concrete be used in the level 1 design. However, the laboratory-determined dynamic modulus of the ATPB-VA mixture utilized the modified temperatures different from the AASHTO standard. As a result, the laboratory-determined dynamic modulus cannot be used as the level 1 inputs in this analysis. On the other hand, because there is no specific prediction models adopted by the MEPDG to consider the mechanical properties of the drainage layer, the analysis by MEPDG presented here has used the uncalibrated NCHRP 1-37A model to predict the dynamic modulus of the drainage layer. According to the comparison between laboratory-determined and predicted dynamic modulus by NCHRP 1-37A model, the uncalibrated model will underestimate the dynamic modulus of ATPB materials, as stated in Chapter 5. Therefore the results obtained from this analysis is estimated to be conservative.

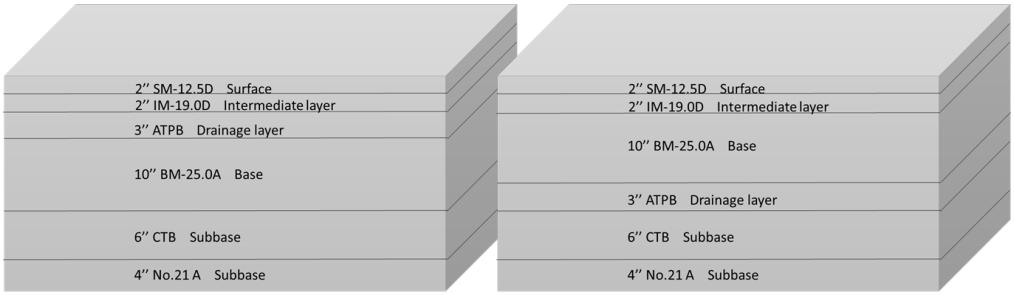

Figure 154. Pavement structure used in MEPDG analysis

Table 29. Parameters used in MEPDG level 3 design

	Gradation			
Surface layer: Virginia SM-12.5D	Cumulative % Retained 3/4 inch sieve	Cumulative % Retained 3/8 inch sieve	Cumulative % Retained #4 sieve	% Passing #200 sieve
	0.0	15.3	49.8	5.2
	Effective Binder content (%)	11.0	Total unit weight (pcf)	146.13
	Air voids (%)	7.0	Asphalt Binder:	Superpave Binder Grading: PG 70-22

Table 29. (Continued)

Base: Virginia IM-19.0D	Gradation			
	Cumulative % Retained 3/4 inch sieve	Cumulative % Retained 3/8 inch sieve	Cumulative % Retained #4 sieve	% Passing #200 sieve
	5.0	27.0	47.0	5.0
	Effective Binder content (%)	6.5	Total unit weight (pcf)	140
	Air voids (%)	8.0	Asphalt Binder:	Superpave Binder Grading: PG 70-22
Base: Virginia BM-25.0A	Gradation			
	Cumulative % Retained 3/4 inch sieve	Cumulative % Retained 3/8 inch sieve	Cumulative % Retained #4 sieve	% Passing #200 sieve
	8.8	58	71.3	5.8
	Effective Binder content (%)	10.0	Total unit weight (pcf)	155.93
	Air voids (%)	6.9	Asphalt Binder:	Superpave Binder Grading: PG 64-22

As shown in Figure 155, when the drainage layer is located above the base course, the increase in air void content will distinctly increase the permanent deformation during the 20-year service life of the pavement. The pavement incorporated with the ATPB-VA drainage layer of 25% air void content can just survive based on the analysis of 80% reliability. Besides the criteria of permanent deformation, the surface down cracking is the most susceptible parameter that may exceed the criteria based on the analysis. Figure 156 shows the predicted surface down cracking during the 20-year service life when the drainage layer is located above the base. It is found that the ATPB mixtures with less than 35% air void content all satisfy the surface down cracking requirement with 80% reliability.

As previously stated, the lower bound of the optimal air void content of the ATPB-VA drainage layer has been determined through the laboratory permeability test to be 24.5%, which is the threshold of air void content to reach the 500 ft/day minimum permeability requirement. On the other hand, considering the MEPDG analysis results are conservative due to underestimated dynamic modulus of the drainage layer, and the pavement structure with the drainage layer of 25% air void content can survive to 20 years without exceeding the rutting requirement, it is suggested that the optimal air void content of the above-base ATPB-VA drainage layer within the given pavement structure to be 25%, to achieve both good permeability and structural performance.

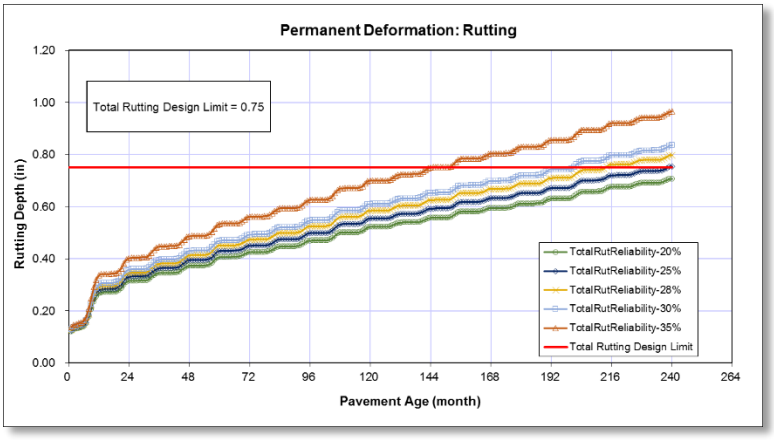

Figure 155. Predicted rutting during 20-year service life of pavement with above-base ATPB-VA drainage layer of different air void contents

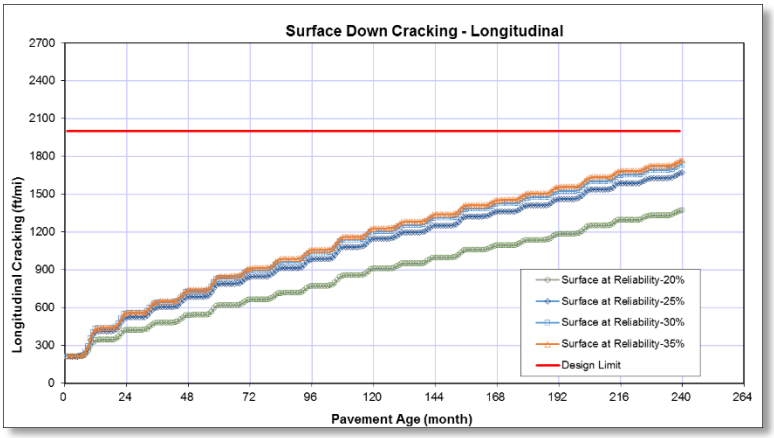

Figure 156. Predicted surface down cracking during 20-year service life of pavement with above-base ATPB-VA drainage layer of different air void contents

The situation when the drainage layer is located below the base layer has also been analyzed in MEPDG. Under the 10'' base layer, the influence of the air void content of ATPB drainage layer on the permanent deformation is not significant at all, as shown in Figure 157. In fact, the calculated rutting depth within the ATPB layer is always zero in below-base case even though the VTM increases. The reason behind this may related with the location of the ATPB drainage layer. When it is placed under the 10-in AC base, the plastic strain produced by the traffic loading is so small in the ATPB layer and consequently the rutting depth as a function of plastic strain can be neglected. This is in consistent with the fact that the majority of all the rutting in the HMA layer occurs within the top 3 to 5 inches [58]. As a result, with the air void content of the drainage layer ranging from 20% to 35%, the rutting depth would not exceed 0.75'' within the given pavement structure during the 20-year service life, according to the 80%-reliability analysis results. The other indicators of pavement performance including surface down cracking, IRI and so forth all satisfy the requirements when the drainage layer is located below the base. Therefore, it is assumed that as long as the pavement with the ATPB drainage layer located above the base can satisfy all the criteria in M-E design, the pavement with the drainage layer located below the base is also acceptable, given the same material properties. Finally, the

optimal air void content is determined to be 25% according to the analysis results of the pavement structure with the ATPB-VA drainage layer above the base by MEPDG.

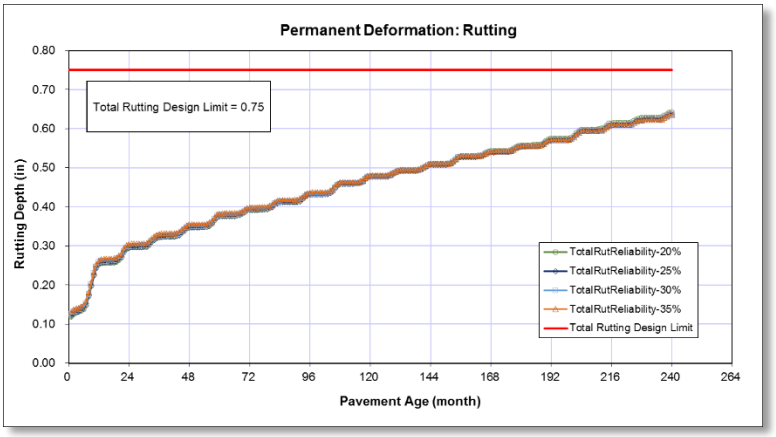

Figure 157. Predicted rutting during 20-year service life of pavement with below-base ATPB-VA drainage layer of different air void contents

The MEPDG analysis has also been conducted on OGBB-OK and ATPB-ID drainage layer materials. Figure 158 to Figure 161 have presented the MEPDG analysis results of the rutting depth and surface-down cracking during the pavement service life for OGBB-OK and ATPB-ID drainage layers. It has shown that the conservative upper bound of the optimal air void content of the OGBB-OK drainage layer is 24%, if the same pavement structure is used. For the ATPB-ID drainage layer, the upper bound of the optimal air void content is 28%, with the same pavement structure. Considering the lower bound of the OGBB-OK and ATPB-ID drainage layers are 21% and 24% determined from minimum permeability requirement, the optimal air void content ranges are determined to be 21% to 24% for the OGBB-OK drainage layer, and 24% to 28% for the ATPB-ID drainage layer if the same pavement structure is used.

However, in practice, the pavement structures used in Oklahoma and Idaho may vary with the given pavement structure adopted here, which is derived from the Virginia's project. Therefore the optimal air void content ranges of the OGBB-OK and ATPB-ID drainage layers provided here may be inapplicable under other cases. However, although further investigation is needed when different pavement structure is applied, the same procedures as adopted in this study can be used to determine the optimal air void content of the other cases.

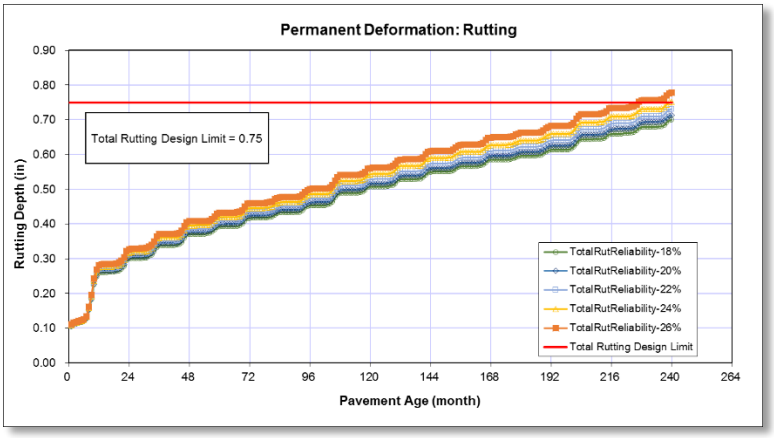

Figure 158. Predicted rutting during 20-year service life of pavement with above-base OGBB-OK drainage layer of different air void contents

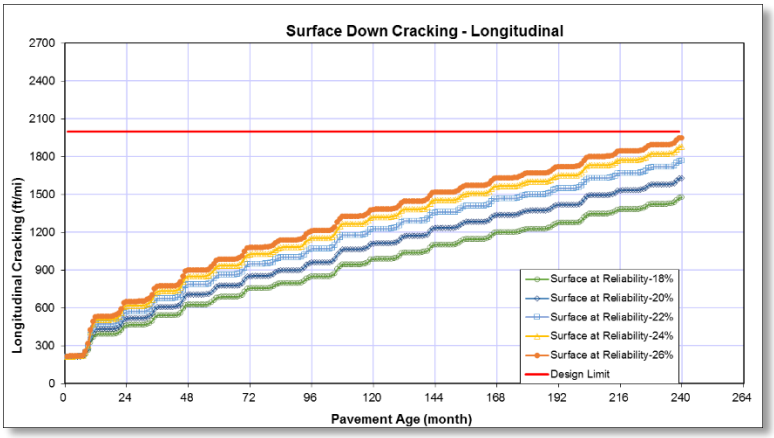

Figure 159. Predicted surface-down cracking during 20-year service life of pavement with above-base OGBB-OK drainage layer of different air void contents

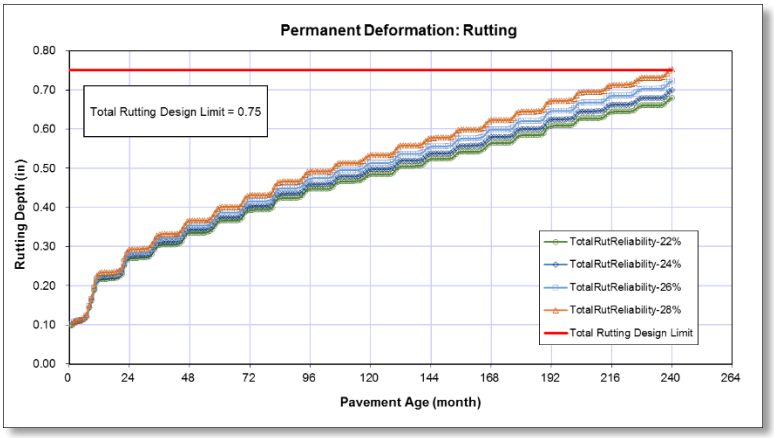

Figure 160. Predicted rutting during 20-year service life of pavement with above-base ATPB-ID drainage layer of different air void contents

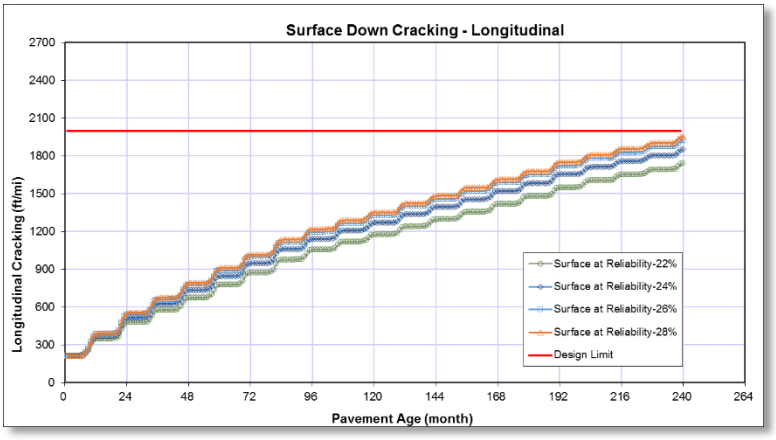

Figure 161. Predicted surface-down cracking during 20-year service life of pavement with above-base ATPB-ID drainage layer of different air void contents

CHAPTER 7. CONCLUSIONS AND RECOMMENDATIONS

To characterize the properties of the typical drainage layers adopted in VA, OK and ID, an on-line survey has been conducted to collect information about the current status of drainage layers in participating states. Typical drainage layer materials were collected from the three states and specimens were compacted in laboratory. The dimensional method, Parafilm method and CoreLok vacuum sealing method have been used to quantify the VTM of the specimens. With the comparison among these methods by statistical analysis, the most suitable method to determine the VTM of drainage layer materials with large air void content has been provided. It is recommended that for the sake of cost efficiency, the Parafilm method is good to test specimens of less than 24% VTM while the CoreLok method should be applied for specimens of VTM larger than 24%. However, when large variations between the real and target air void content exist, or the batch of specimens have wide ranges of air void contents, consistency in test method is important and the Vacuum sealing method is recommended once the air void content is possible to exceed 24%. To characterize the permeability properties of the drainage layer materials, constant head method or the falling head method customized with larger inlet tube have been adopted. The relationship between permeability and air void content, and the minimum air void content to satisfy the typical permeability requirement (500 ft/day) have been obtained. To investigate the mechanical properties of the drainage layer, the modified dynamic modulus test were proposed and followed to determine the dynamic modulus of the ATPB mixtures with different VTMs. It is found that the modified stress levels and test temperatures have significantly improved the applicability of the traditional dynamic modulus test on the ATPB materials. The dynamic modulus master curves were constructed based on the laboratory-determined dynamic moduli, which can be used as level 1 inputs for the M-E pavement design to consider the structural contribution of the drainage layer. In addition, the modified NCHRP 1-37A local models to predict the dynamic modulus of ATPB-VA, OGBB-OK, ATPB-ID mixtures, and the modified NCHRP 1-37A model to predict the dynamic modulus of ATPB mixtures, have been provided. These models can be applied by each participating state to predict the dynamic modulus of the ATPB materials and used as the level 2 and 3 inputs in M-E pavement design.

The FEM simulation has also been conducted to investigate the location effects and the structural contribution of the drainage layer in pavement structure, and to investigate the influence of the drainage layer's air void content on pavement performance. It has been found that the horizontal tensile stress occurs at the bottom of the drainage layer; The horizontal and vertical strain within the drainage layer is much lower than that within the adjacent layers; moving the drainage layer from the top of the base to the bottom of the base can reduce the total vertical deformation on surface but the difference is very limited given the material properties and pavement structure applied in this study; and generally, increase the air void content of the drainage layer will cause increase in stress, strain and total deformation within the pavement structure.

Finally, the optimal air void content of the drainage layer to achieve not only required permeability, but also good structural performance has been determined. The minimum air void content to satisfy the permeability requirement of 500 ft/day has been used as the lower bound of the optimal air void content. The upper bound of the optimal air void content was determined by limiting the 20-year rutting depth within 0.75 inches at 80% reliability level in the M-E

pavement design of a typical drained pavement structure. Considering the M-E pavement analysis results tend to be conservative, the optimal air void content of the drainage layer is recommended to be 25%, 21% to 24%, and 24% to 28% for VA, OK and ID, but should be used with adequate verification for different pavement structures.

To sum up, the primary objectives of the pooled fund study have been achieved. The properties of the typical ATPB and CTPB drainage layer materials of the participating states have been investigated by selected or modified methods. The new dynamic modulus procedure works well on ATPB-VA, OGBB-OK and ATPB-ID materials and is recommended for application on other ATPB materials. The laboratory-determined dynamic modulus can be used as M-E design level 1 input and the modified NCHRP 1-37A models can be used as level 2 and level 3 inputs to incorporate the drainage layer into M-E pavement design. The FEM simulations have shown the pavement responses with the different drainage-layer locations and air void contents. The optimal air void content were also recommended for the ATPB-VA drainage layer within the pavement structure given in this study. For OGBB-OK and ATPB-ID drainage layers, the same method can be applied to quantify the ranges of the optimal air void content, based on the specific pavement structures adopted in each state.

APPENDIX A. DYNAMIC MODULUS DATA OF ATPB-VA, OGBB-OK AND ATPB-ID SPECIMENS WITH DIFFERENT AIR VOID CONTENTS

Totally 57 specimens of ATPB-VA, OGBB-OK and ATPB-ID mixtures with different air void contents ranging from 18% to 32% have been tested following the modified dynamic modulus test. The dynamic modulus master curves shown in Chapter 5 are all derived from average of three specimens. The selected laboratory test data of the specimens with different levels of air void content from each mixture are presented here. Firstly, the stress and strain data during the modified dynamic modulus test of one specimen presentative of each air void content level are presented. Then the dynamic modulus master curves of each specimen within the same level of air void content are provided. The sigmoidal fit shown in the dynamic modulus master curves are all obtained from the average of three specimens.

ATPB-VA 20%:

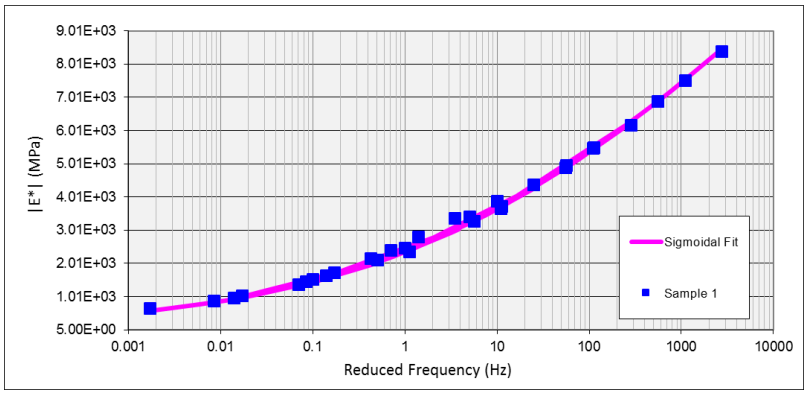

Figure 162. Dynamic modulus master curve of ATPB-VA specimen A1

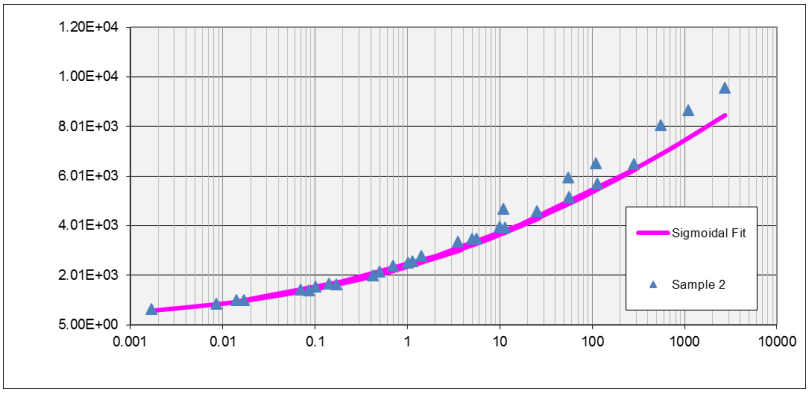

Figure 163. Dynamic modulus master curve of ATPB-VA specimen A2

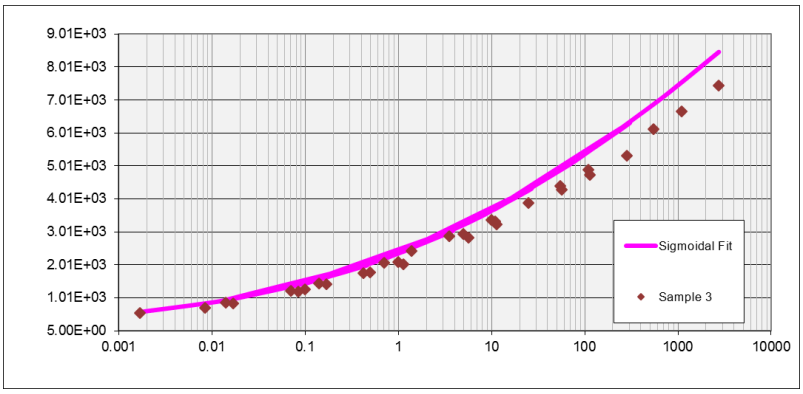

Figure 164. Dynamic modulus master curve of ATPB-VA specimen A3

ATPB-VA 21%:

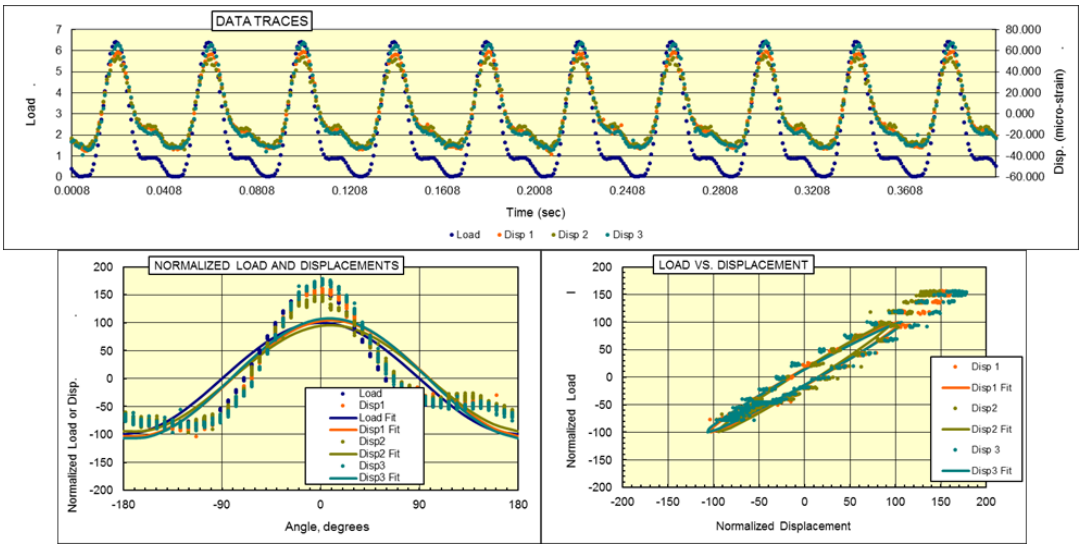

Figure 165. Dynamic modulus data of the ATPB-VA specimen A5 representative of 21% air void content

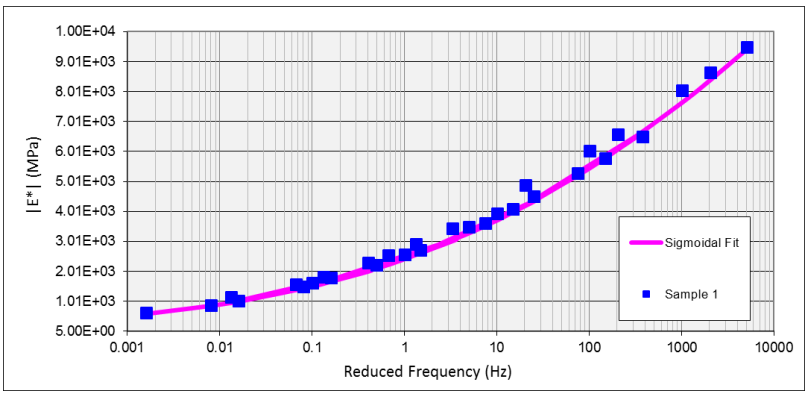

Figure 166. Dynamic modulus master curve of ATPB-VA specimen A5

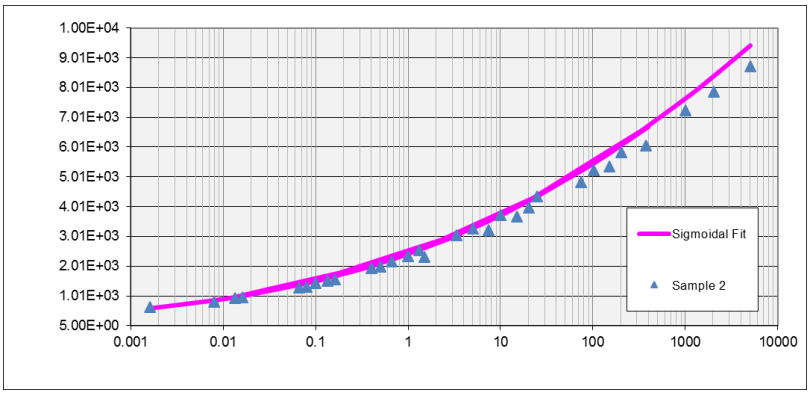

Figure 167. Dynamic modulus master curve of ATPB-VA specimen A6

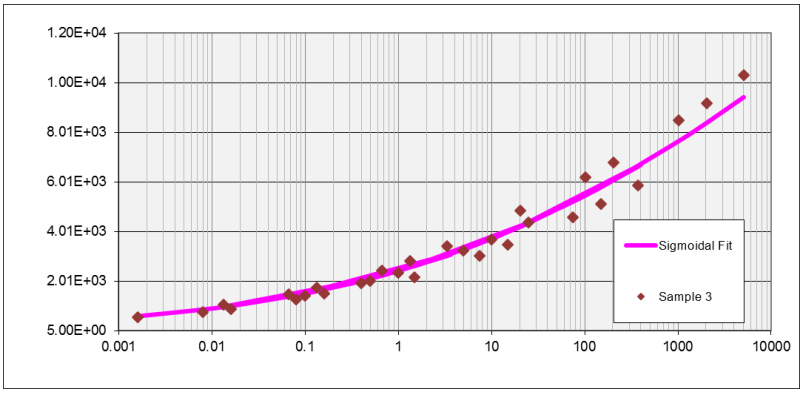

Figure 168. Dynamic modulus master curve of ATPB-VA specimen A1-1

ATPB-VA 24%:

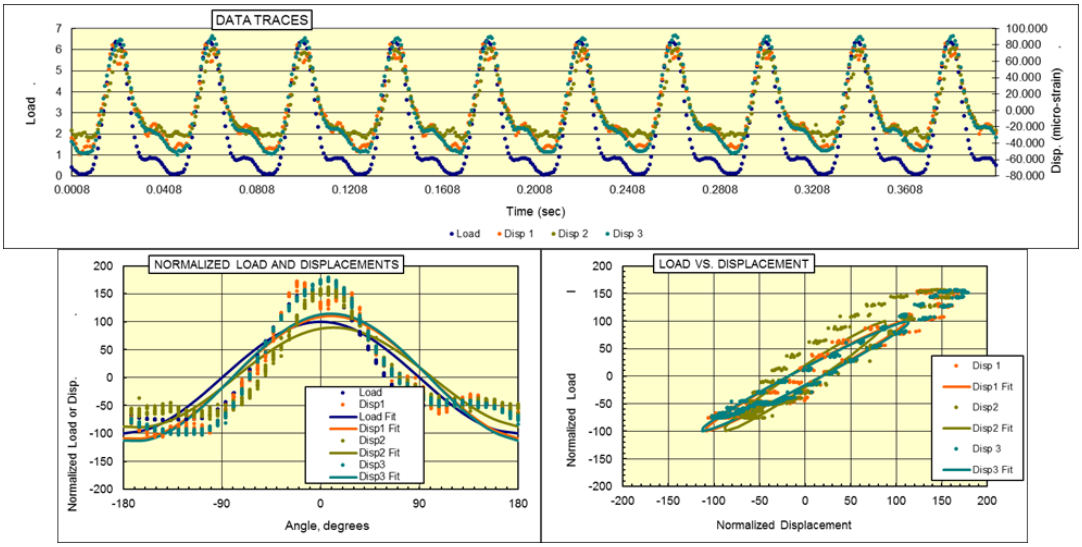

Figure 169. Dynamic modulus data of the ATPB-VA specimen B2 representative of 24% air void content

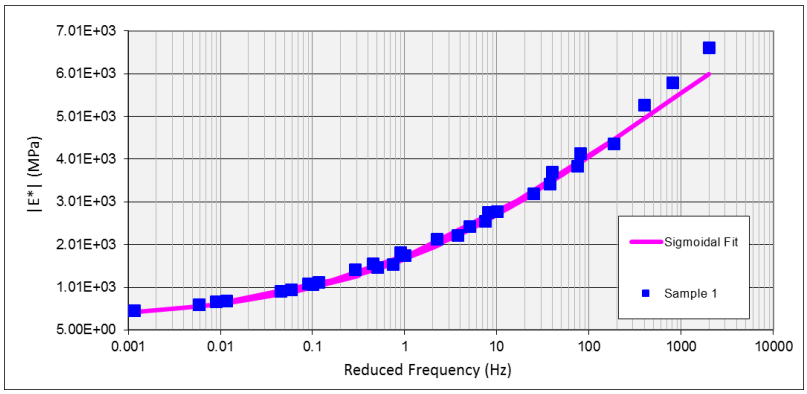

Figure 170. Dynamic modulus master curve of ATPB-VA specimen B2

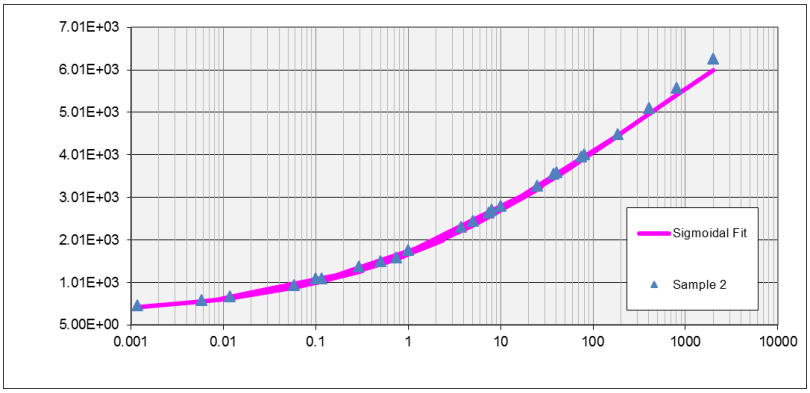

Figure 171. Dynamic modulus master curve of ATPB-VA specimen B3

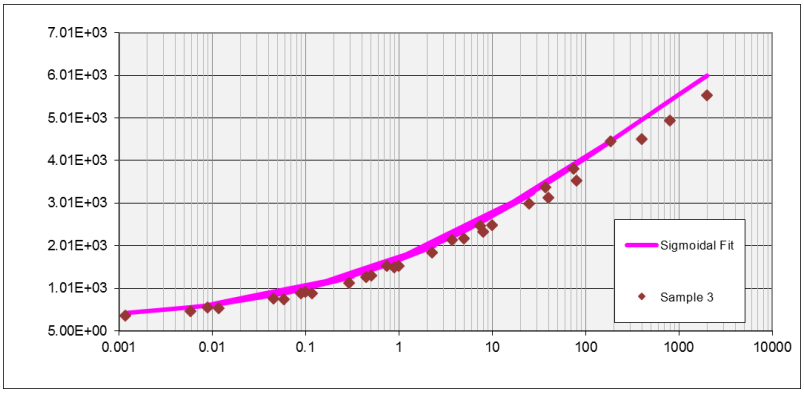

Figure 172. Dynamic modulus master curve of ATPB-VA specimen B2-2

ATPB-VA 25%:

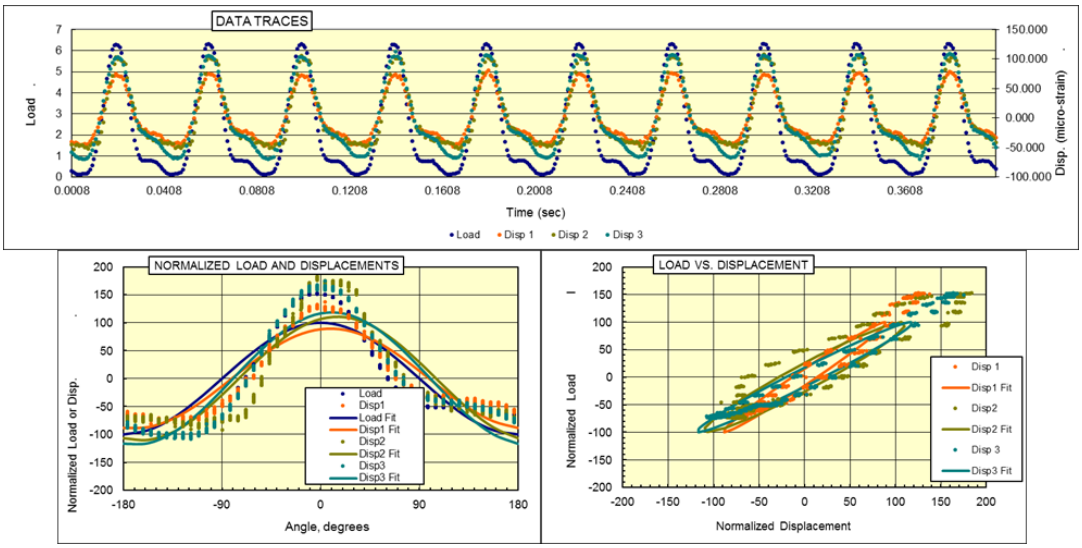

Figure 173. Dynamic modulus data of the ATPB-VA specimen B4 representative of 25% air void content

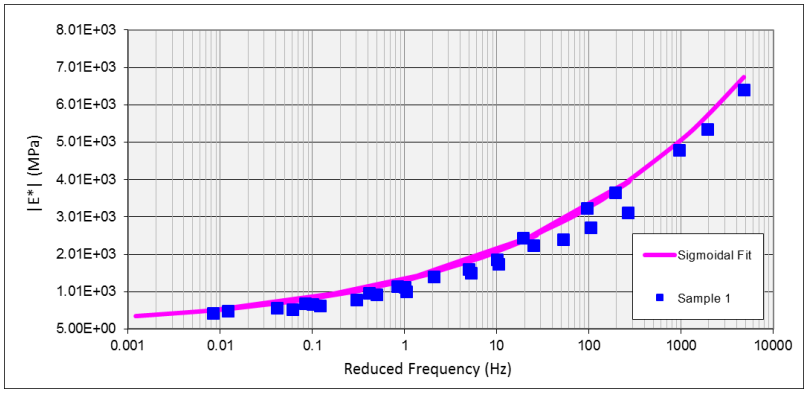

Figure 174. Dynamic modulus master curve of ATPB-VA specimen B4

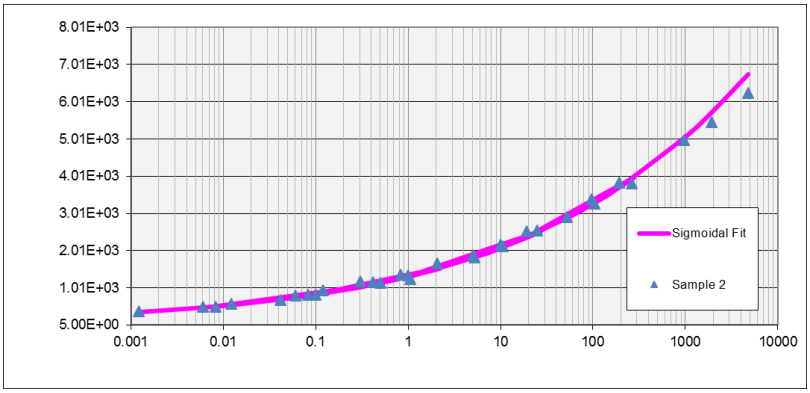

Figure 175. Dynamic modulus master curve of ATPB-VA specimen B1-1

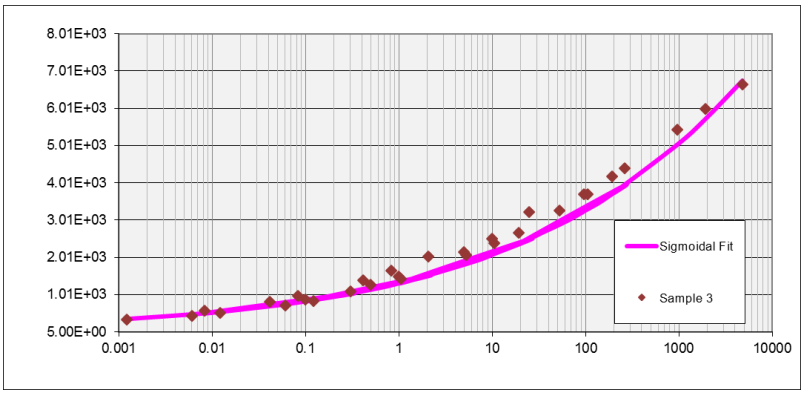

Figure 176. Dynamic modulus master curve of ATPB-VA specimen B1-2

ATPB-VA 26%:

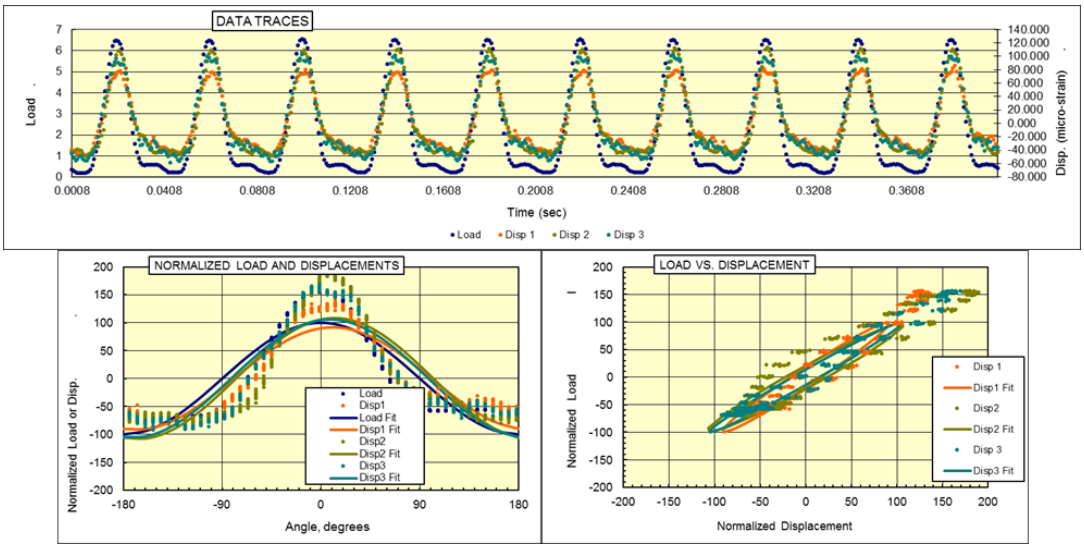

Figure 177. Dynamic modulus data of the ATPB-VA specimen B1 representative of 26% air void content

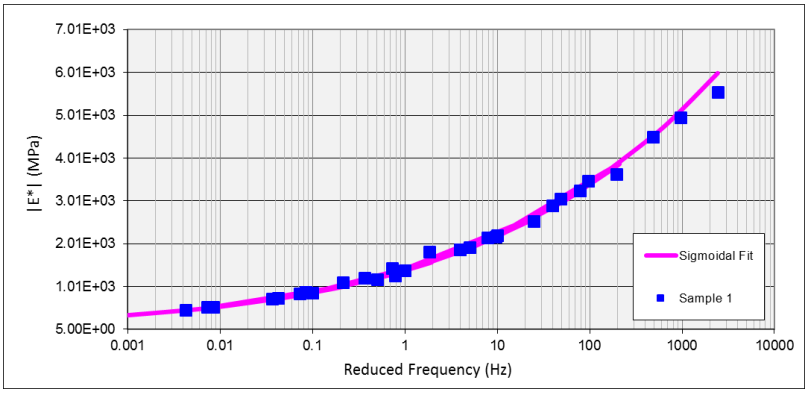

Figure 178. Dynamic modulus master curve of ATPB-VA specimen B1

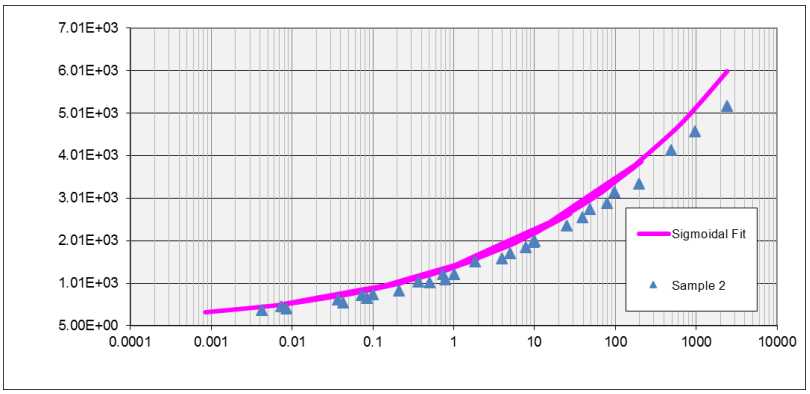

Figure 179. Dynamic modulus master curve of ATPB-VA specimen B5

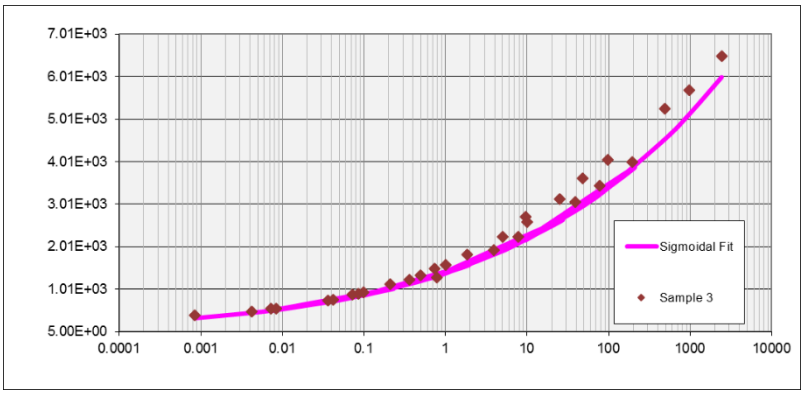

Figure 180. Dynamic modulus master curve of ATPB-VA specimen B6

ATPB-VA 28%:

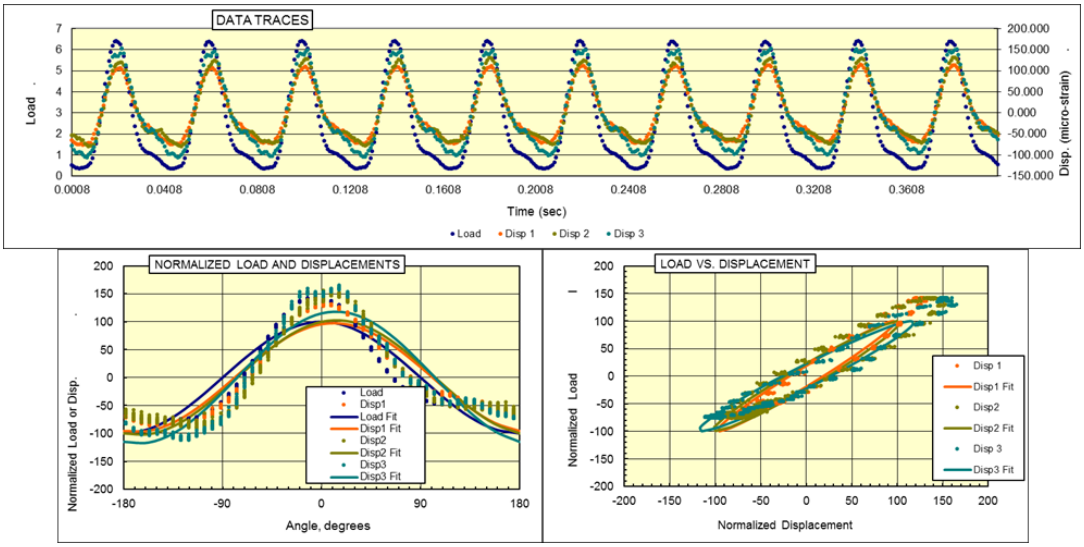

Figure 181. Dynamic modulus data of the ATPB-VA specimen C1-1 representative of 28% air void content

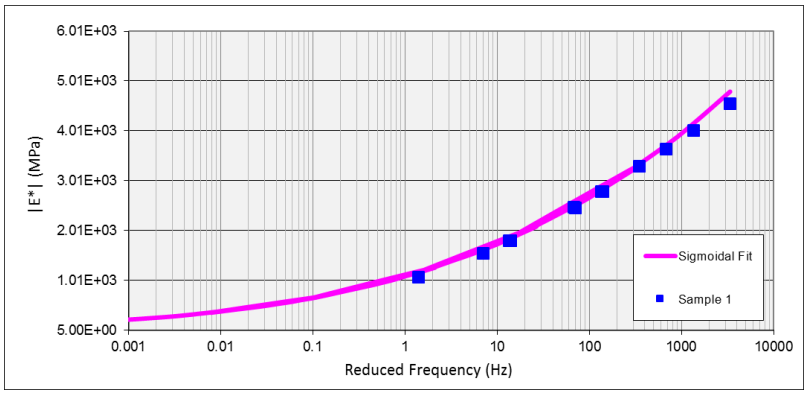

Figure 182. Dynamic modulus master curve of ATPB-VA specimen C3

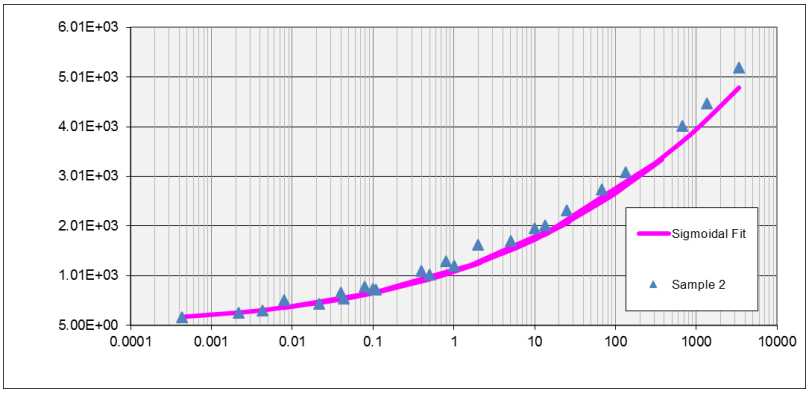

Figure 183. Dynamic modulus master curve of ATPB-VA specimen C4

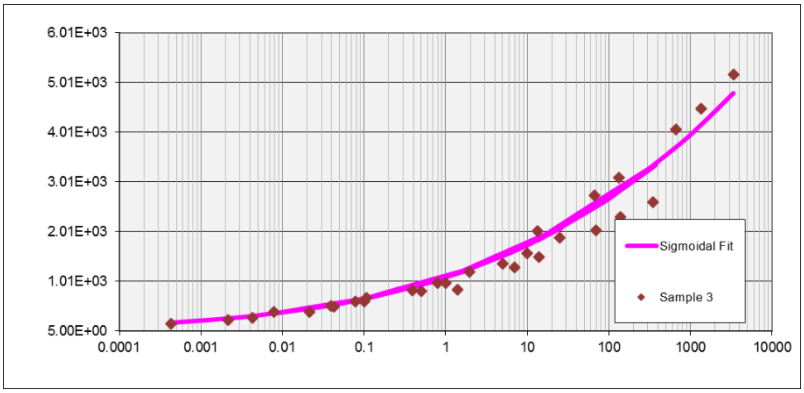

Figure 184. Dynamic modulus master curve of ATPB-VA specimen C1-1

OGBB-OK 18%:

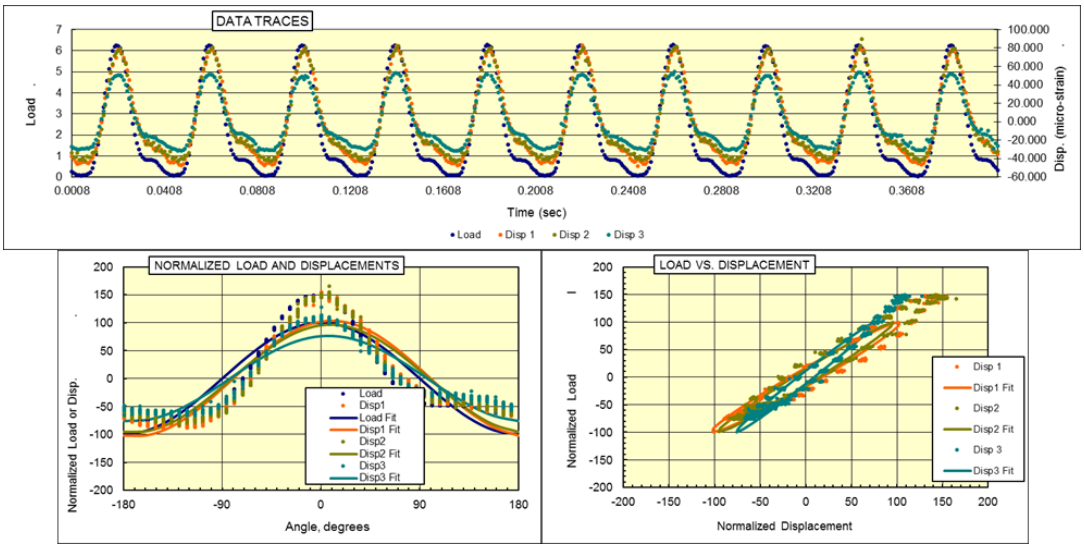

Figure 185. Dynamic modulus data of the OGBB-OK specimen E6 representative of 18% air void content

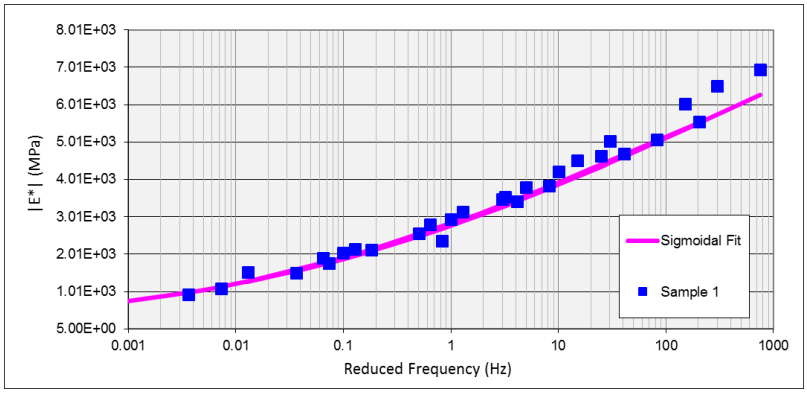

Figure 186. Dynamic modulus master curve of OGBB-OK specimen E1

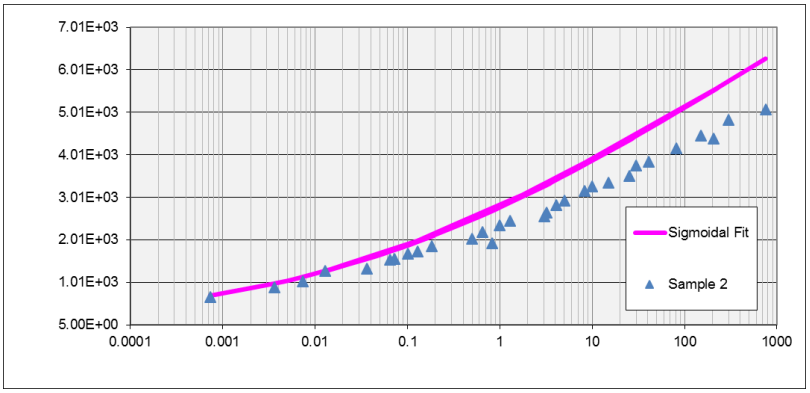

Figure 187. Dynamic modulus master curve of OGBB-OK specimen E3

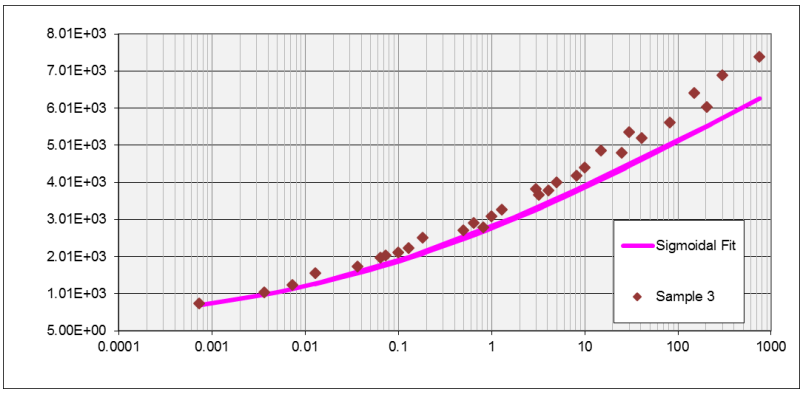

Figure 188. Dynamic modulus master curve of OGBB-OK specimen E6

OGBB-OK 19%:

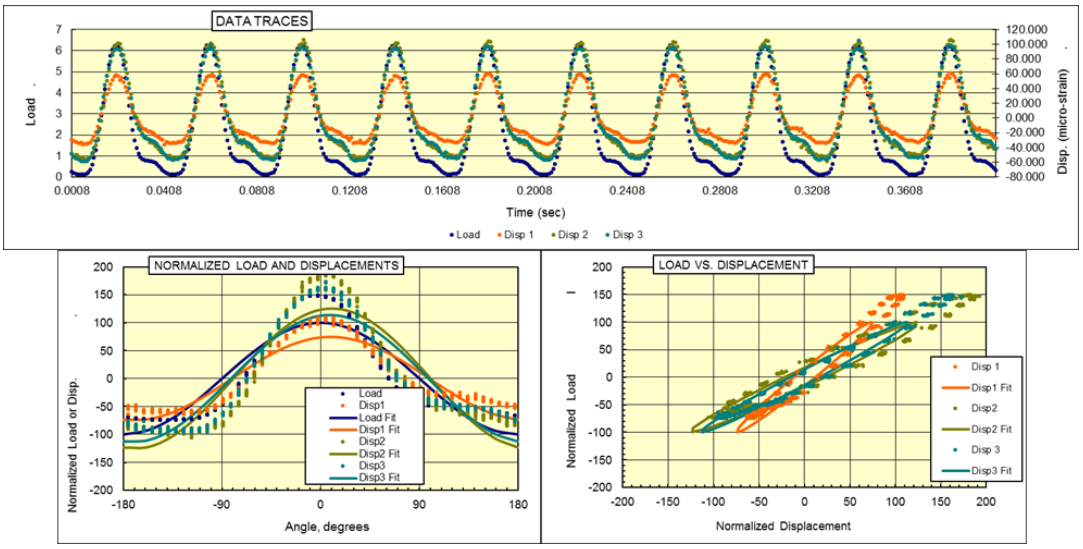

Figure 189. Dynamic modulus data of the OGBB-OK specimen E2 representative of 19% air void content

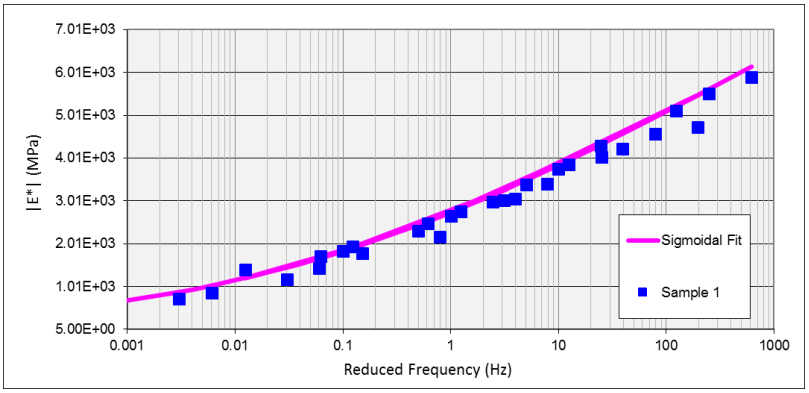

Figure 190. Dynamic modulus master curve of OGBB-OK specimen E2

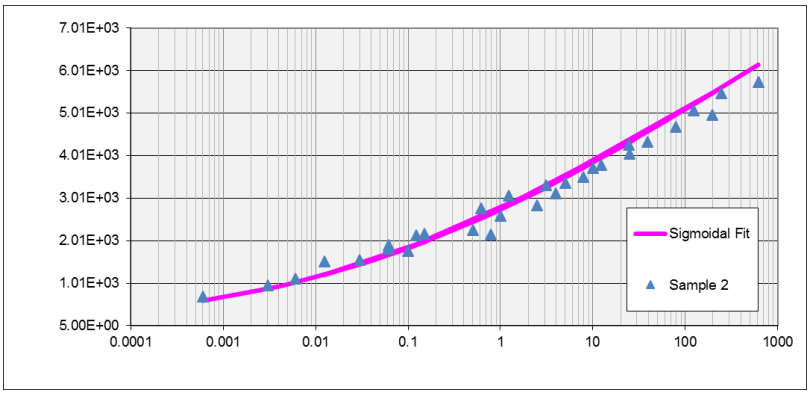

Figure 191. Dynamic modulus master curve of OGBB-OK specimen E4

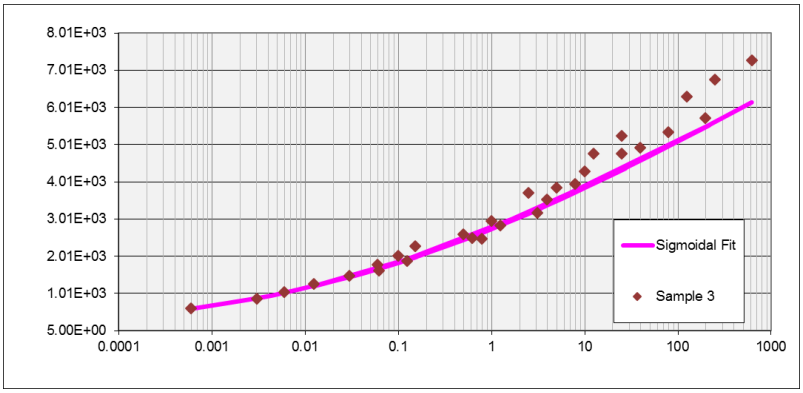

Figure 192. Dynamic modulus master curve of OGBB-OK specimen E5

OGBB-OK 20%:

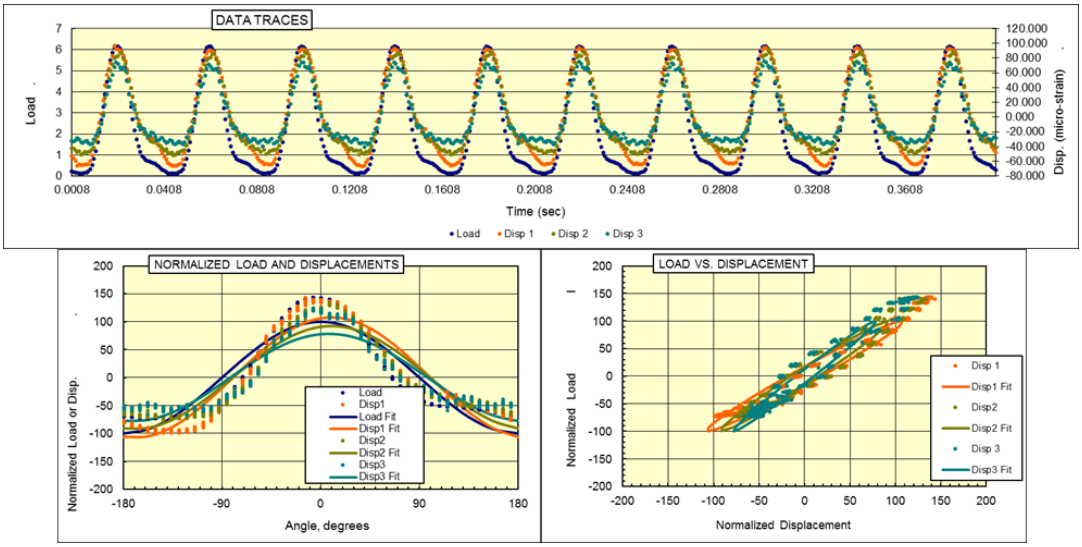

Figure 193. Dynamic modulus data of the OGBB-OK specimen F3 representative of 20% air void content

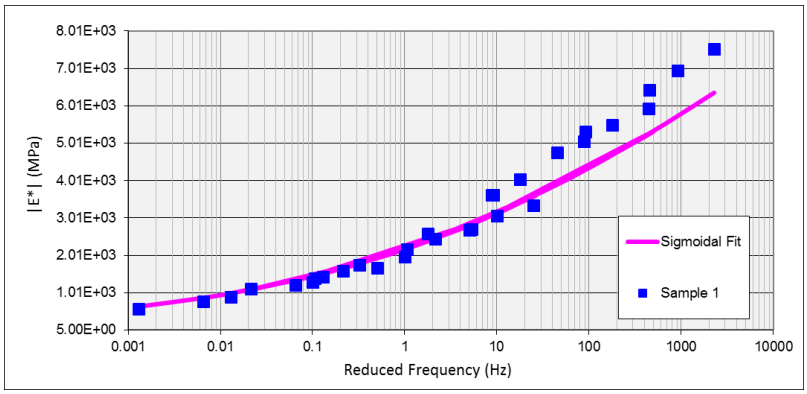

Figure 194. Dynamic modulus master curve of OGBB-OK specimen E7

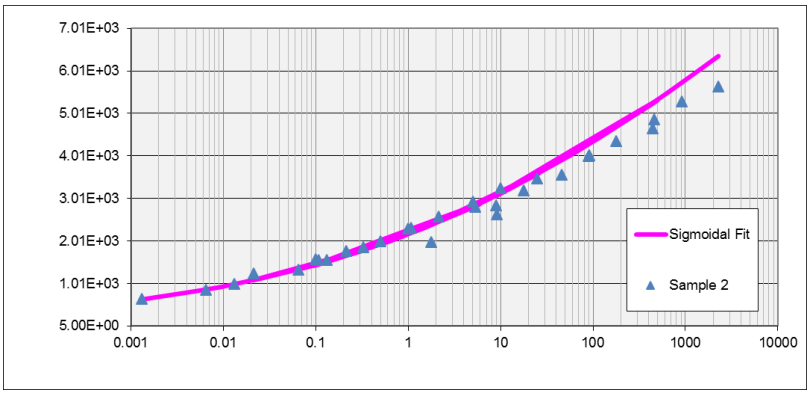

Figure 195. Dynamic modulus master curve of OGBB-OK specimen E8

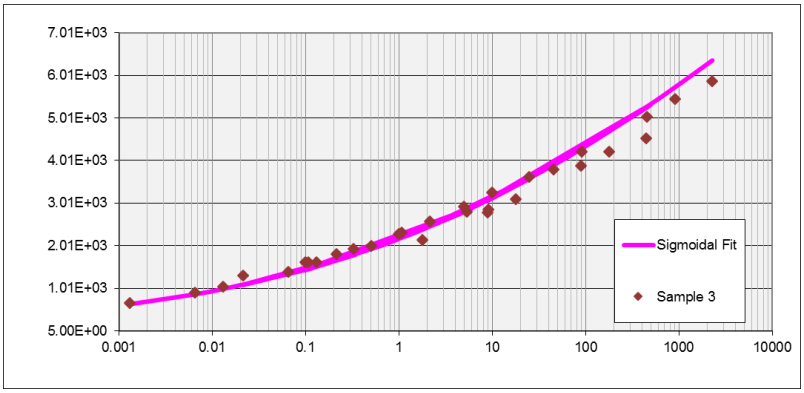

Figure 196. Dynamic modulus master curve of OGBB-OK specimen F3

OGBB-OK 22%:

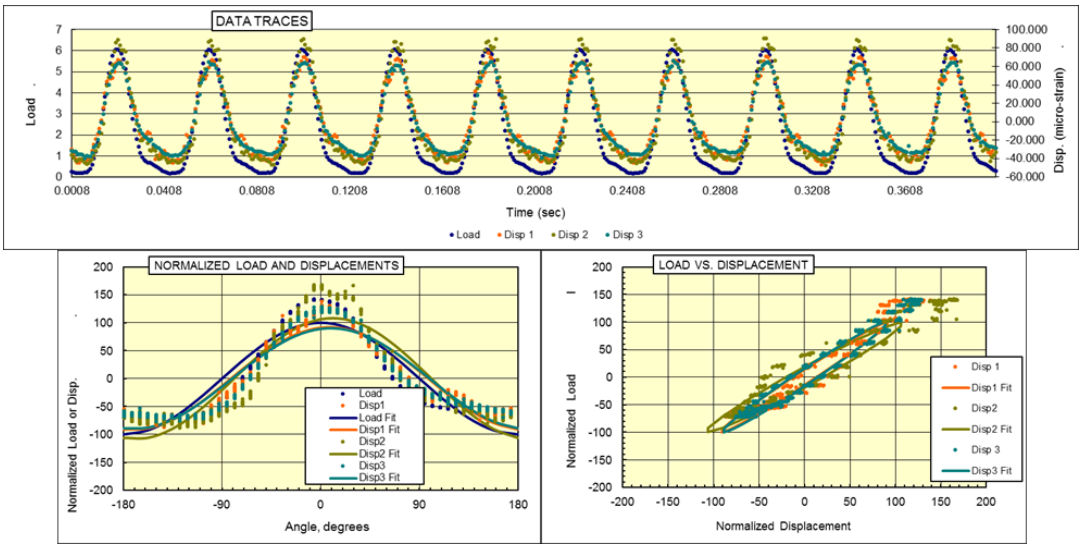

Figure 197. Dynamic modulus data of the OGBB-OK specimen F1 representative of 22% air void content

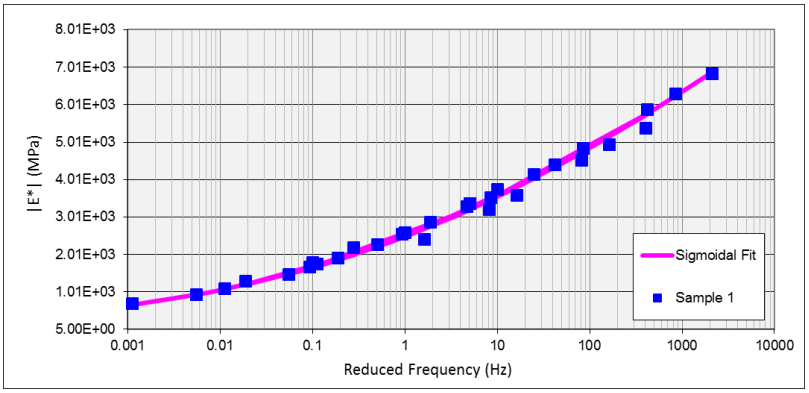

Figure 198. Dynamic modulus master curve of OGBB-OK specimen F1

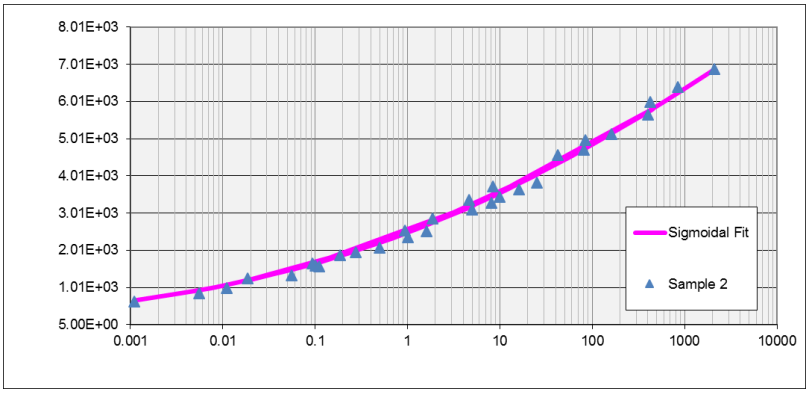

Figure 199. Dynamic modulus master curve of OGBB-OK specimen F7

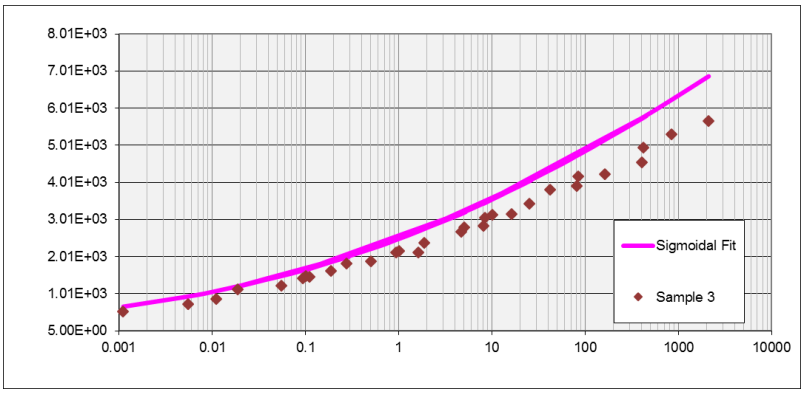

Figure 200. Dynamic modulus master curve of OGBB-OK specimen G3

OGBB-OK 23%:

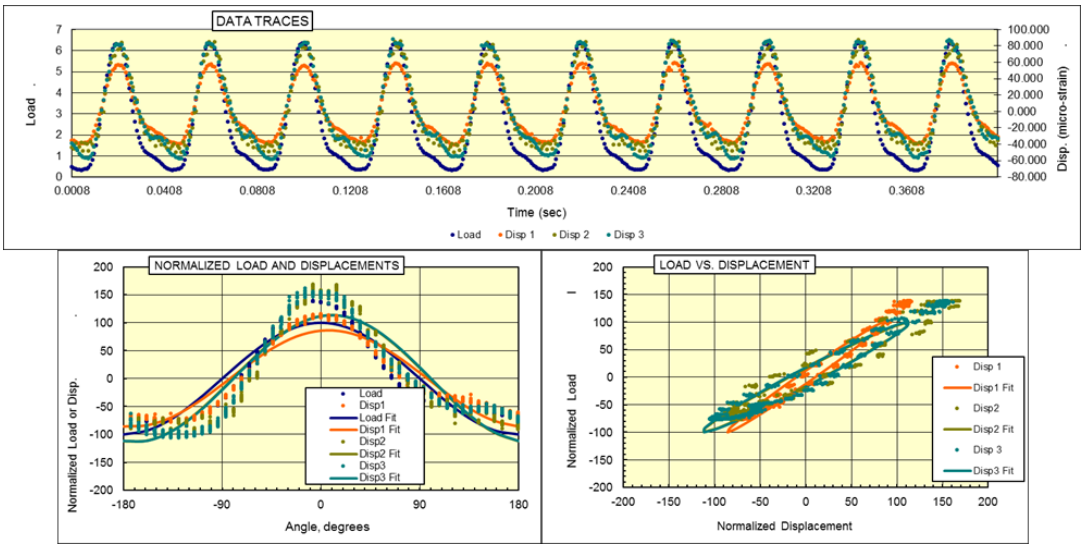

Figure 201. Dynamic modulus data of the OGBB-OK specimen G1 representative of 23% air void content

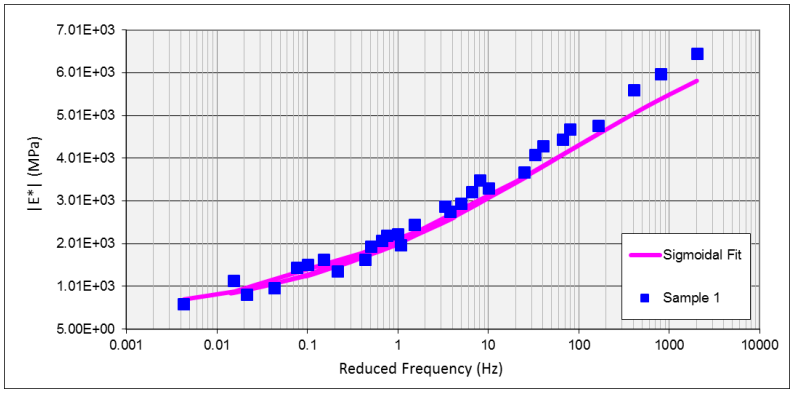

Figure 202. Dynamic modulus master curve of OGBB-OK specimen G1

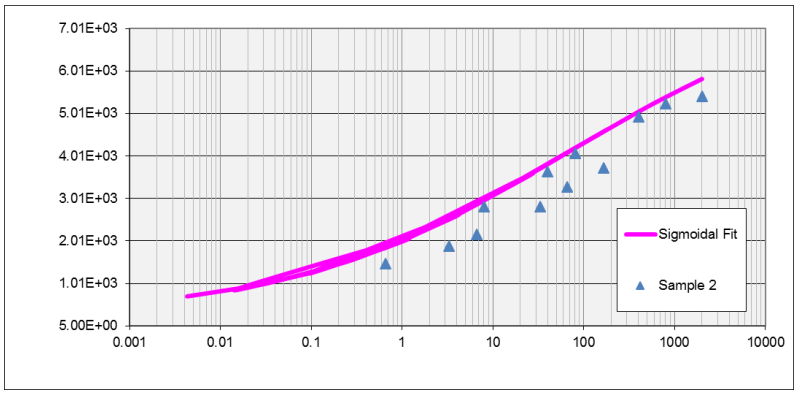

Figure 203. Dynamic modulus master curve of OGBB-OK specimen G2

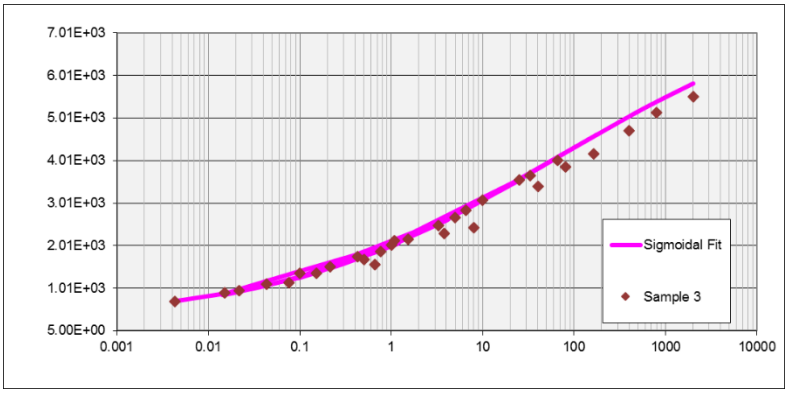

Figure 204. Dynamic modulus master curve of OGBB-OK specimen G7

OGBB-OK 24%:

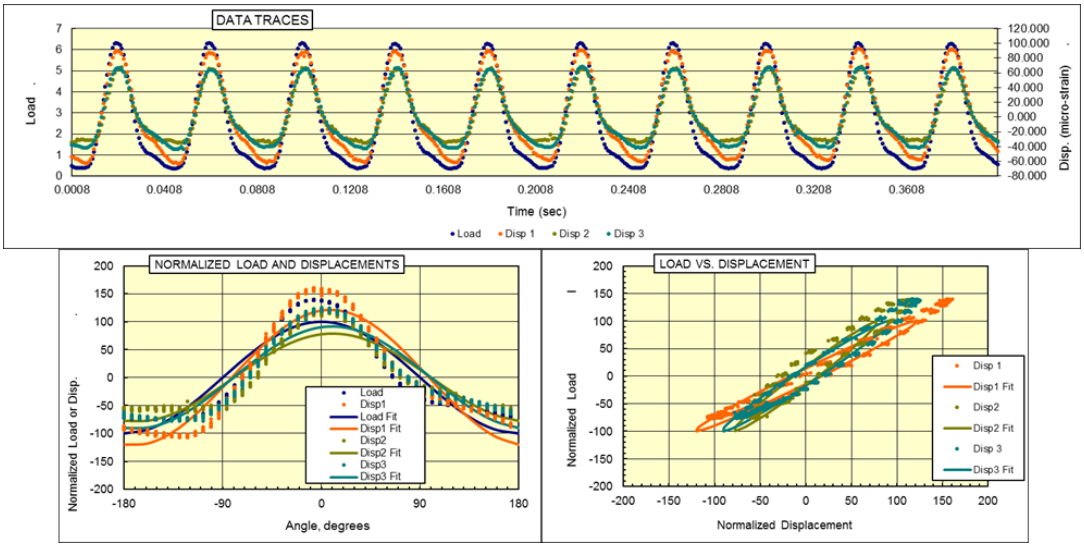

Figure 205. Dynamic modulus data of the OGBB-OK specimen H31 representative of 24% air void content

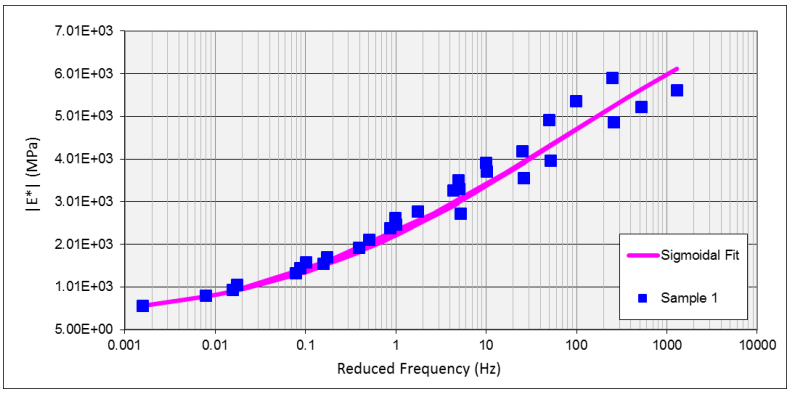

Figure 206. Dynamic modulus master curve of OGBB-OK specimen H1

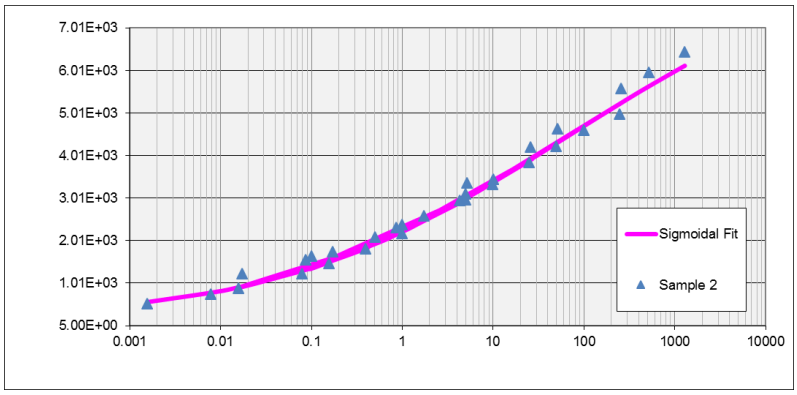

Figure 207. Dynamic modulus master curve of OGBB-OK specimen H3

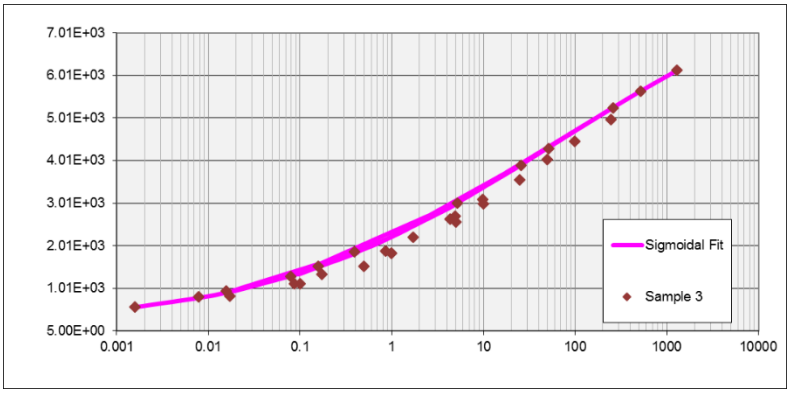

Figure 208. Dynamic modulus master curve of OGBB-OK specimen H5

OGBB-OK 25%:

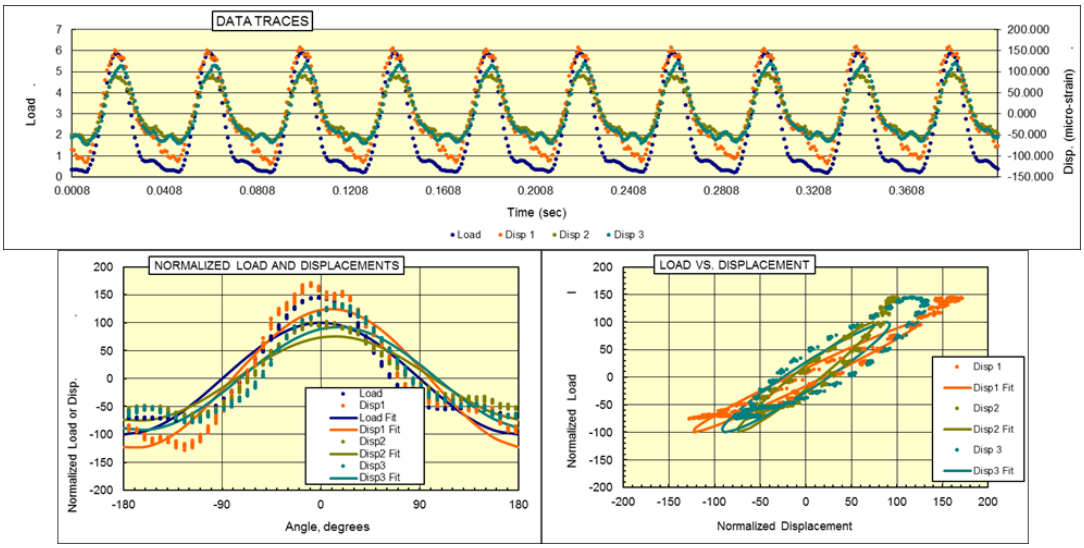

Figure 209. Dynamic modulus data of the OGBB-OK specimen H4 representative of 25% air void content

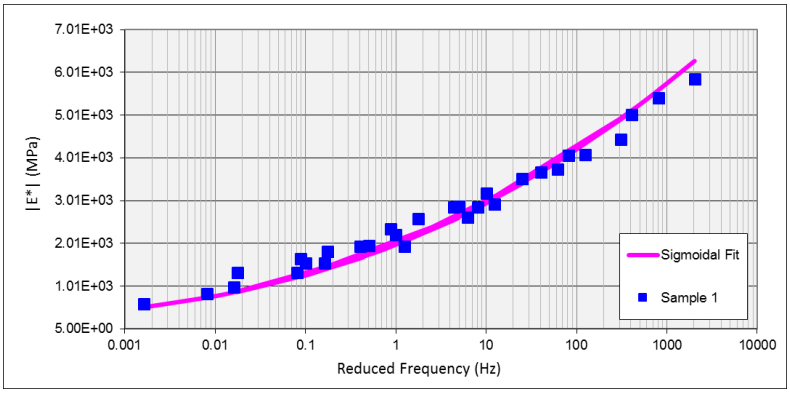

Figure 210. Dynamic modulus master curve of OGBB-OK specimen H4

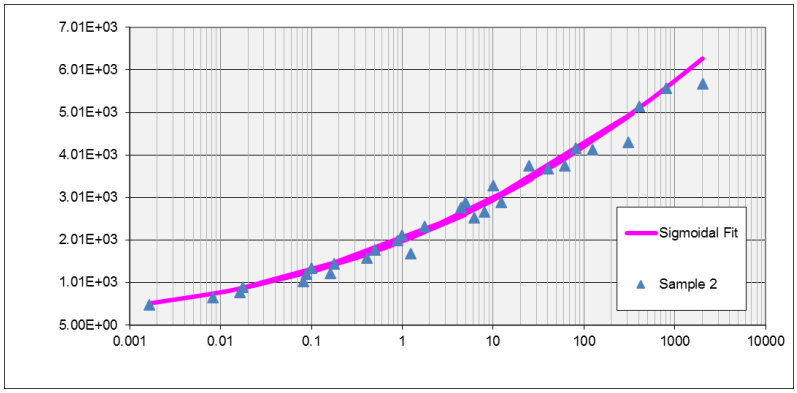

Figure 211. Dynamic modulus master curve of OGBB-OK specimen H7

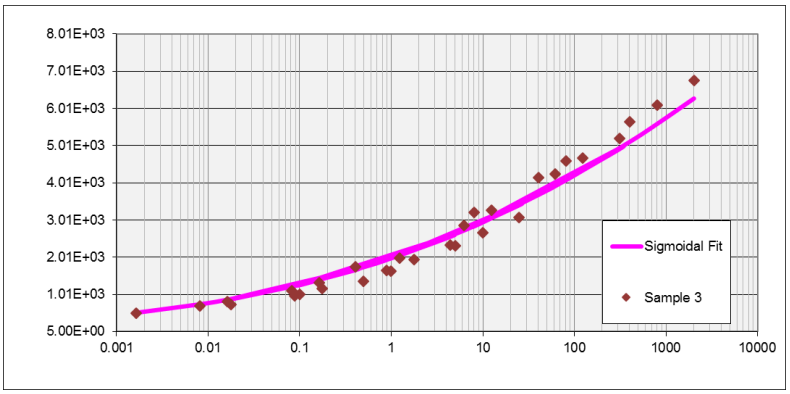

Figure 212. Dynamic modulus master curve of OGBB-OK specimen I3

OGBB-OK 26%:

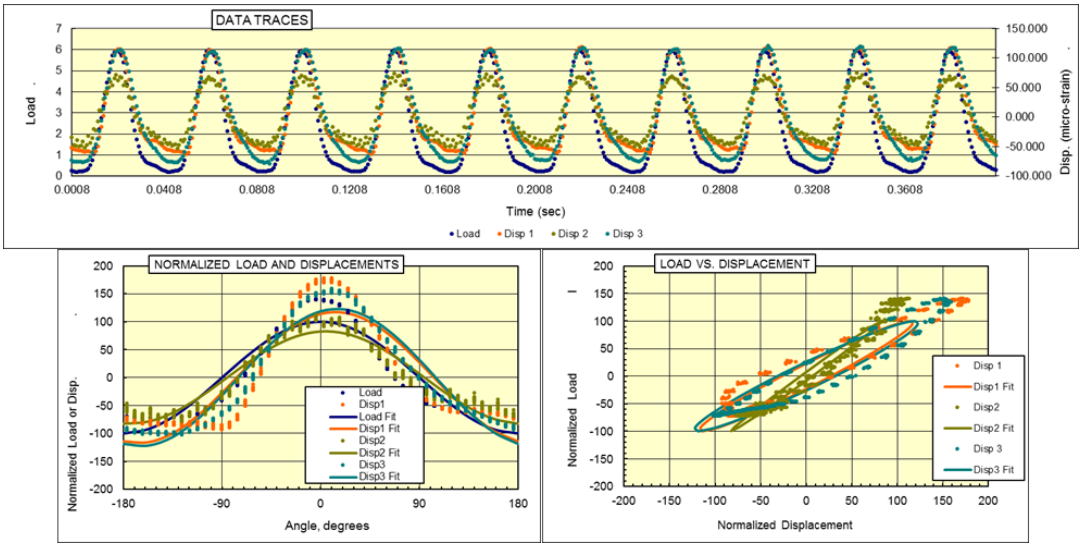

Figure 213. Dynamic modulus data of the OGBB-OK specimen I4 representative of 26% air void content

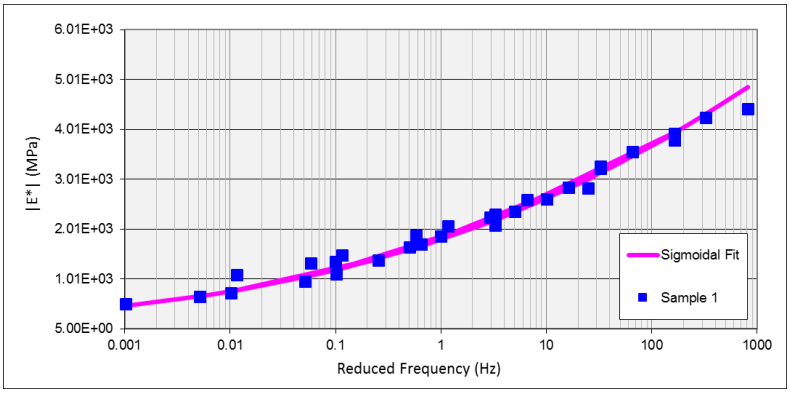

Figure 214. Dynamic modulus master curve of OGBB-OK specimen I2

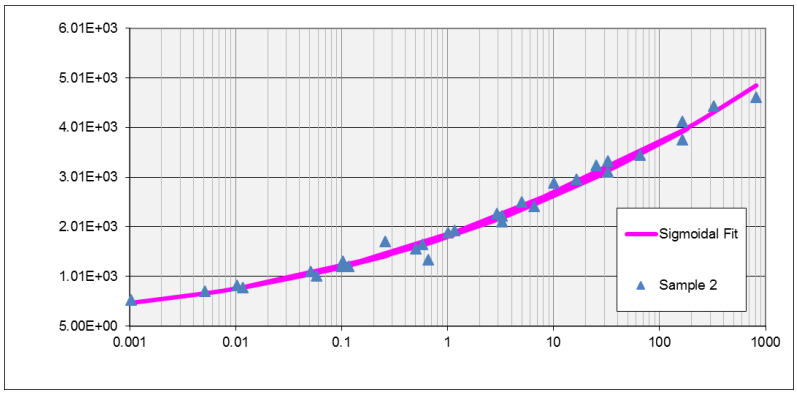

Figure 215. Dynamic modulus master curve of OGBB-OK specimen I4

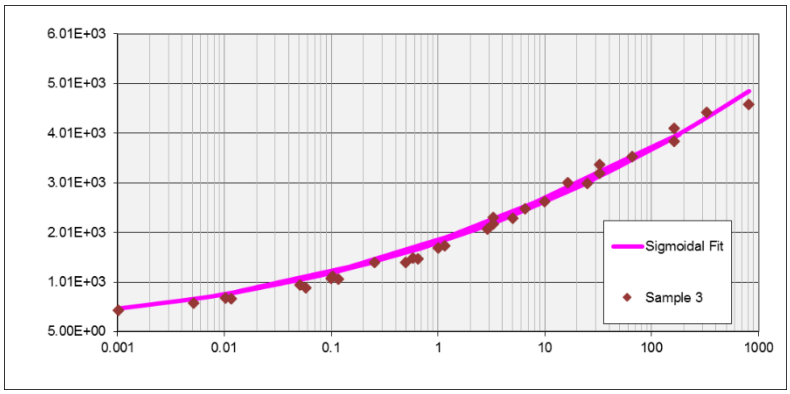

Figure 216. Dynamic modulus master curve of OGBB-OK specimen I5

ATPB-ID 22%:

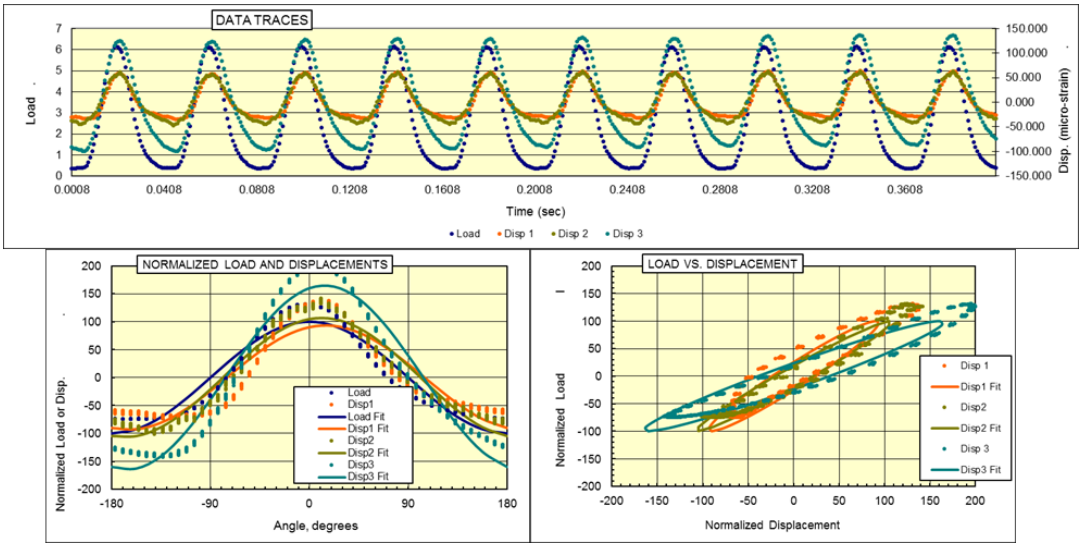

Figure 217. Dynamic modulus data of the OGBB-OK specimen Q2 representative of 22% air void content

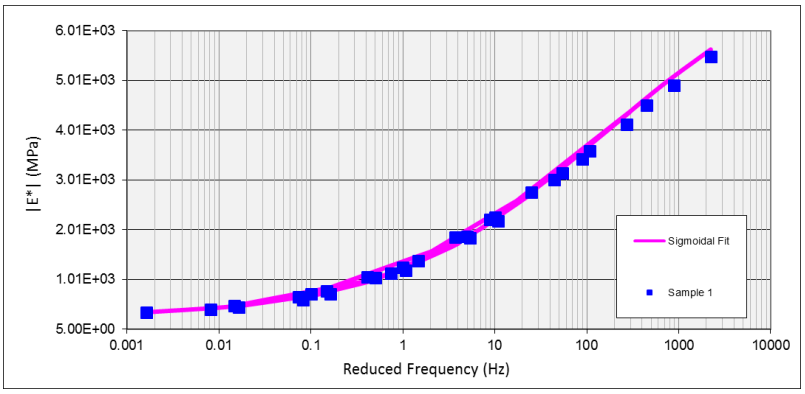

Figure 218. Dynamic modulus master curve of ATPB-ID specimen Q1

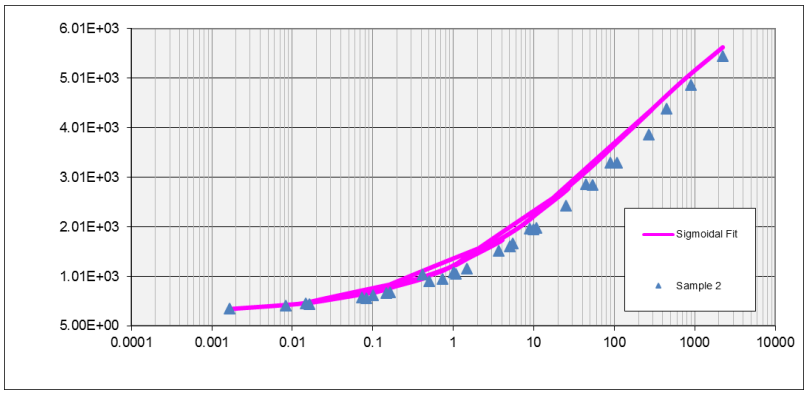

Figure 219. Dynamic modulus master curve of ATPB-ID specimen R2

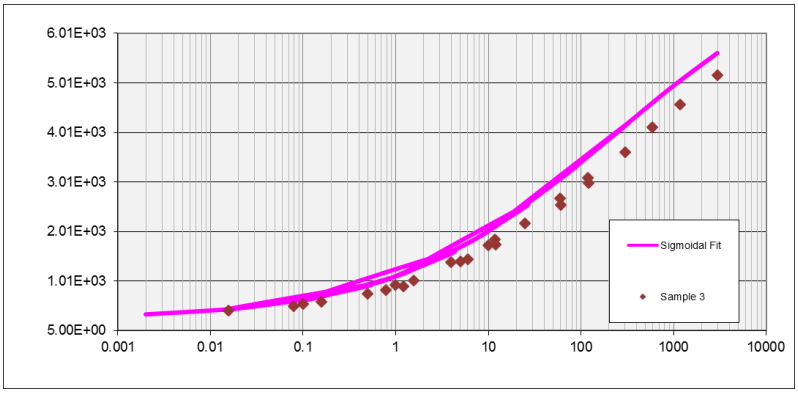

Figure 220. Dynamic modulus master curve of ATPB-ID specimen Q2

ATPB-ID 24%:

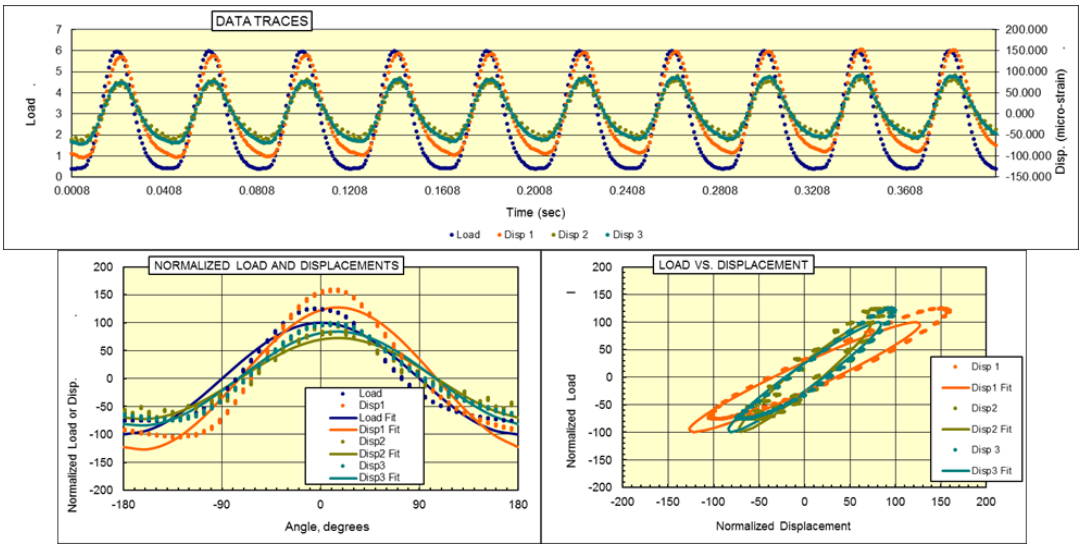

Figure 221. Dynamic modulus data of the OGBB-OK specimen R5 representative of 24% air void content

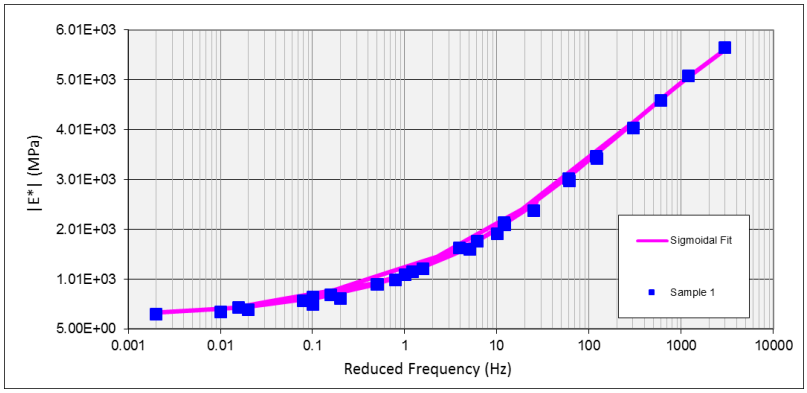

Figure 222. Dynamic modulus master curve of ATPB-ID specimen R1

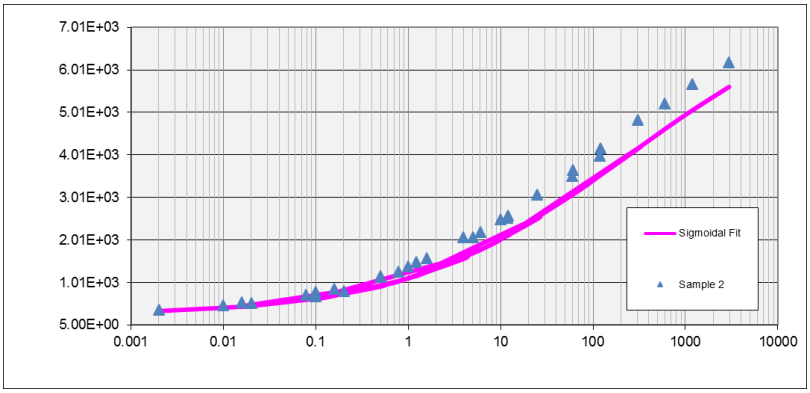

Figure 223. Dynamic modulus master curve of ATPB-ID specimen R5

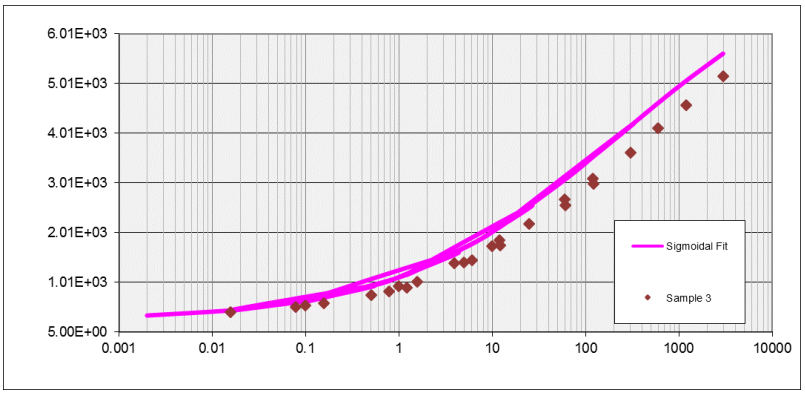

Figure 224. Dynamic modulus master curve of ATPB-ID specimen R4

ATPB-ID 25%:

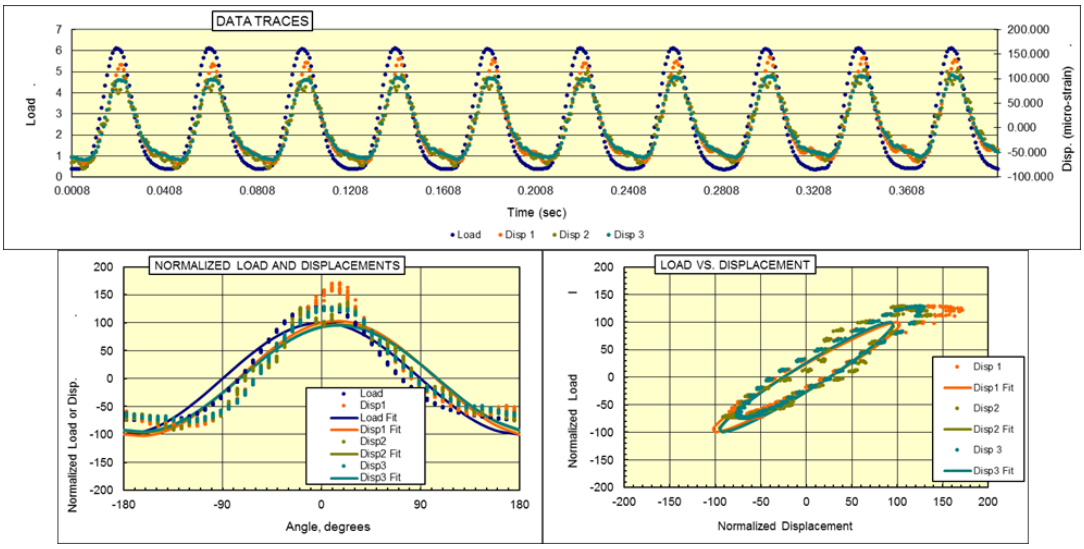

Figure 225. Dynamic modulus data of the OGBB-OK specimen S2 representative of 25% air void content

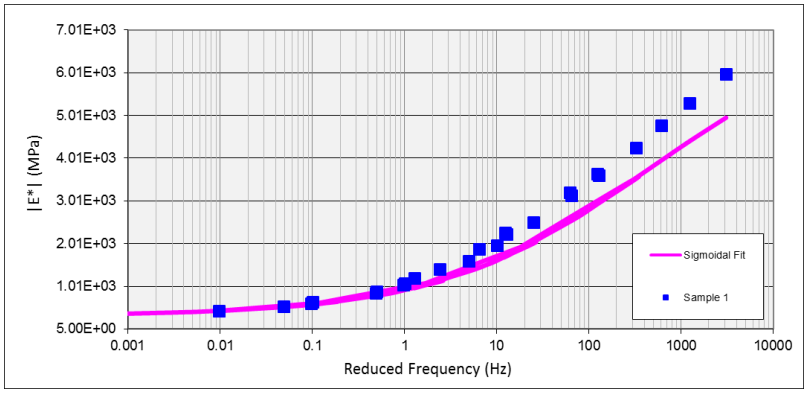

Figure 226. Dynamic modulus master curve of ATPB-ID specimen S1

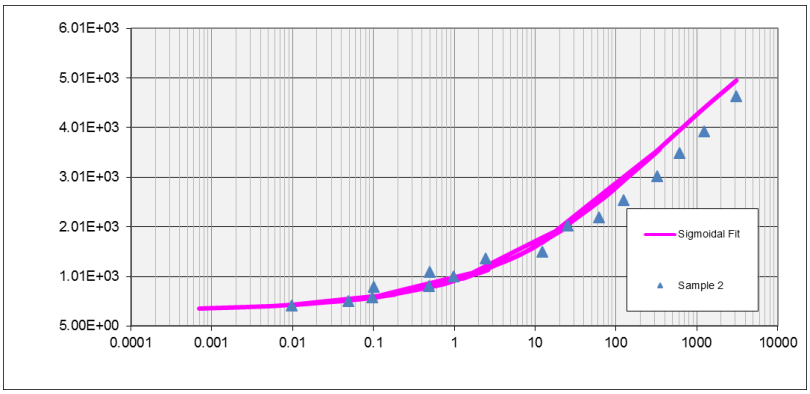

Figure 227. Dynamic modulus master curve of ATPB-ID specimen S2

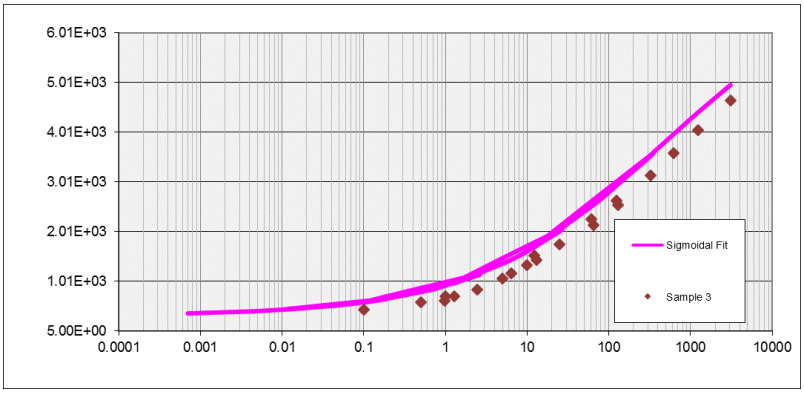

Figure 228. Dynamic modulus master curve of ATPB-ID specimen S3

ATPB-ID 26%:

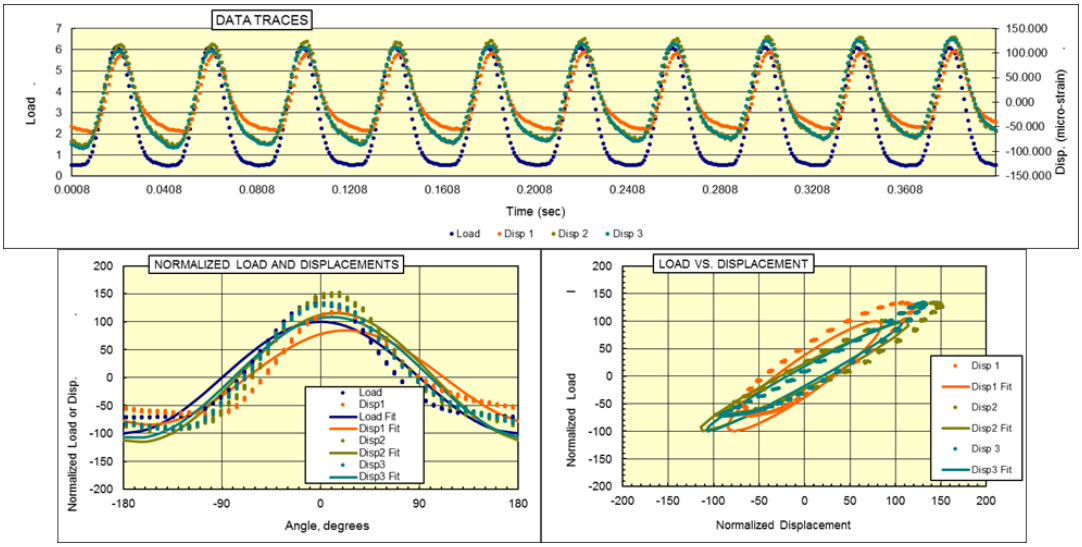

Figure 229. Dynamic modulus data of the OGBB-OK specimen T4-1 representative of 26% air void content

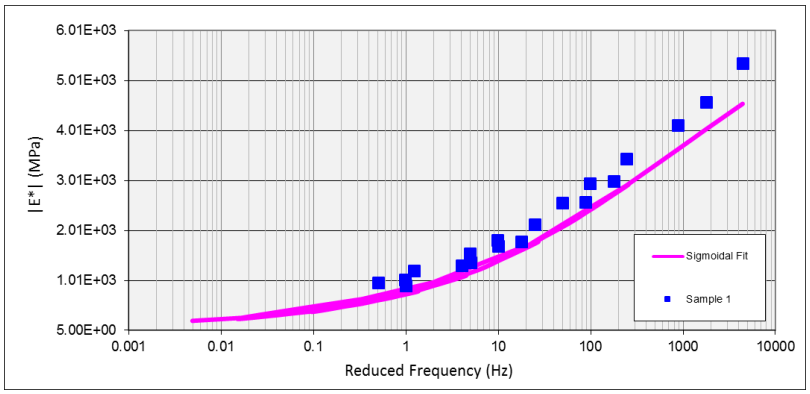

Figure 230. Dynamic modulus master curve of ATPB-ID specimen T1

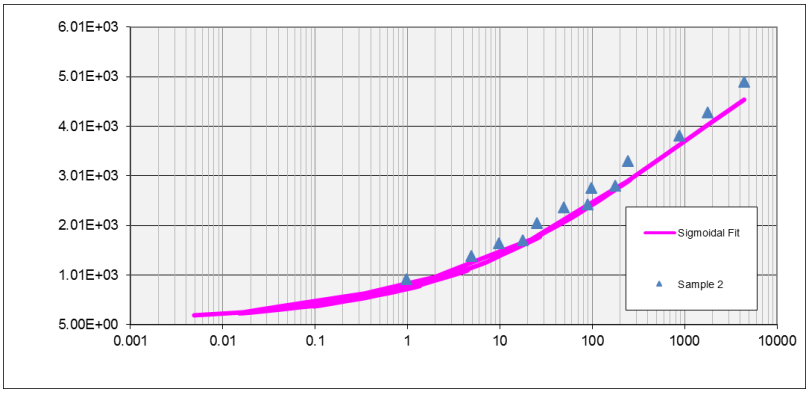

Figure 231. Dynamic modulus master curve of ATPB-ID specimen T2

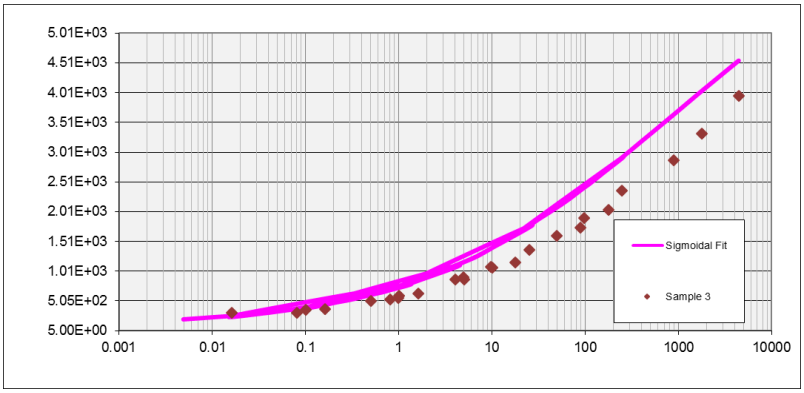

Figure 232. Dynamic modulus master curve of ATPB-ID specimen T4-1

ATPB-ID 28%:

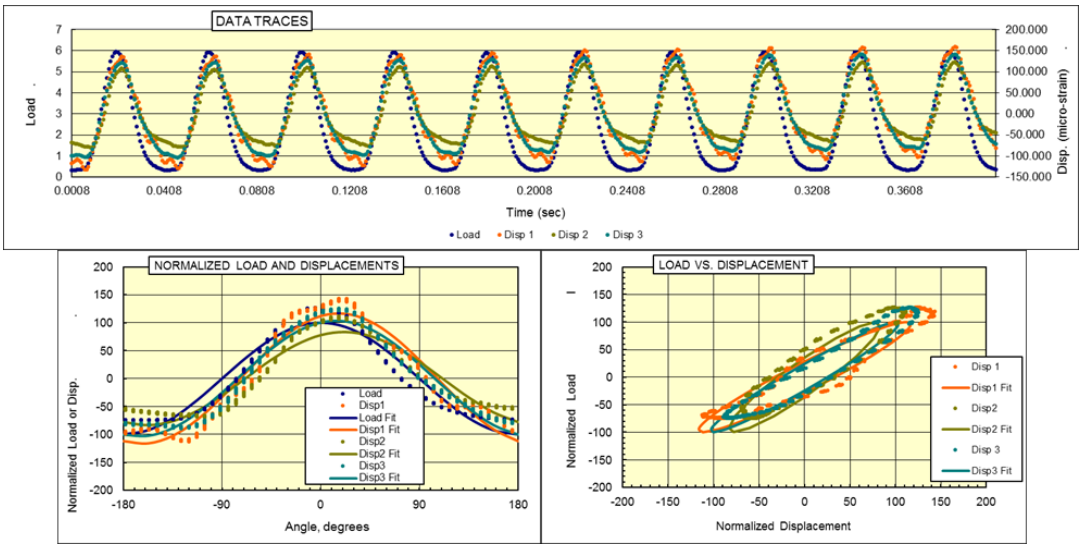

Figure 233. Dynamic modulus data of the OGBB-OK specimen U4 representative of 28% air void content

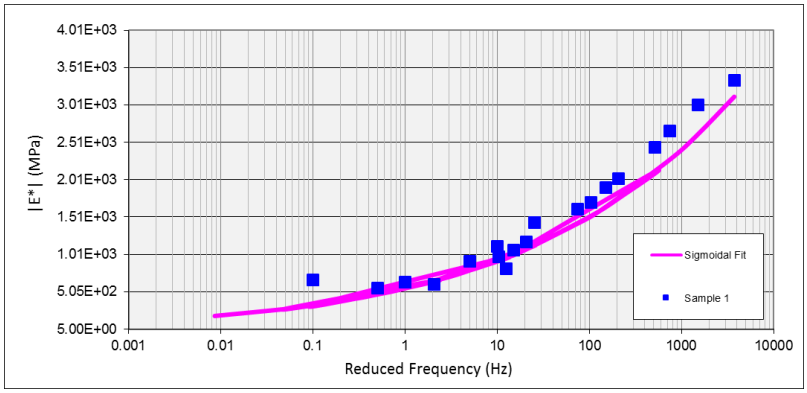

Figure 234. Dynamic modulus master curve of ATPB-ID specimen U4

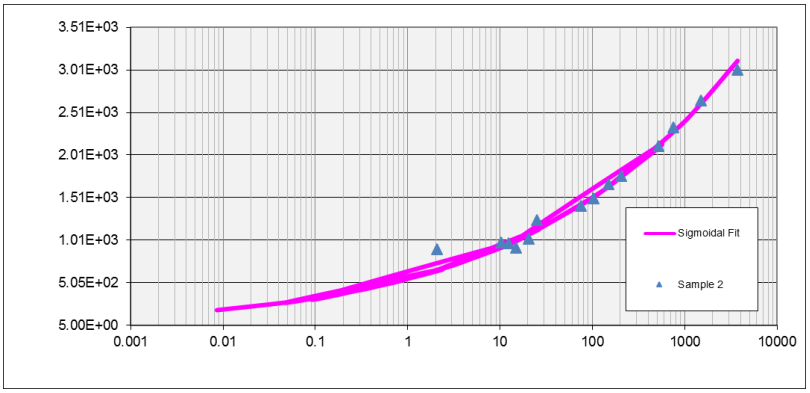

Figure 235. Dynamic modulus master curve of ATPB-ID specimen U2

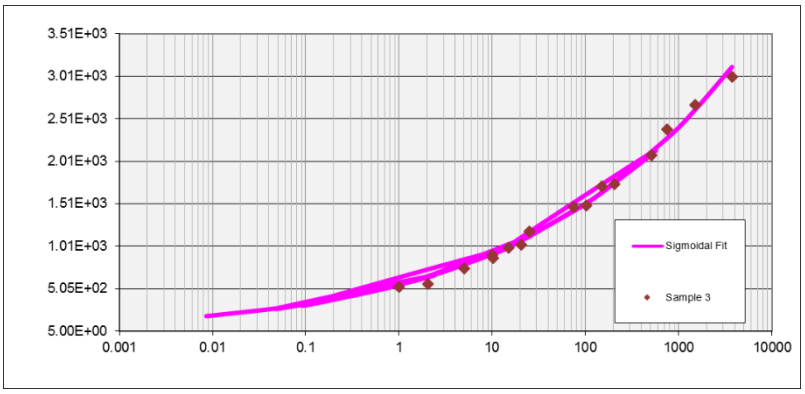

Figure 236. Dynamic modulus master curve of ATPB-ID specimen U5

APPENDIX B. PRONY SERIES PARAMETERS USED IN FEM SIMULATION

PRONY SERIES OF ATPB-VA MIXTURES

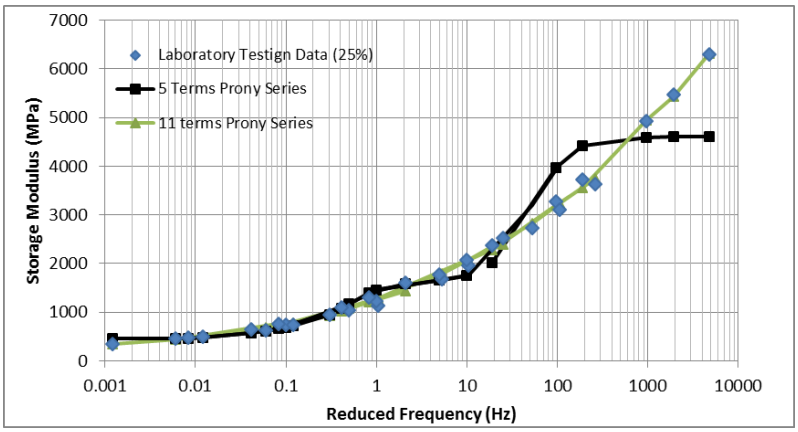

Figure 237. Comparison between 5-term and 11-term Prony series of ATPB-VA mixture of 25% air void content

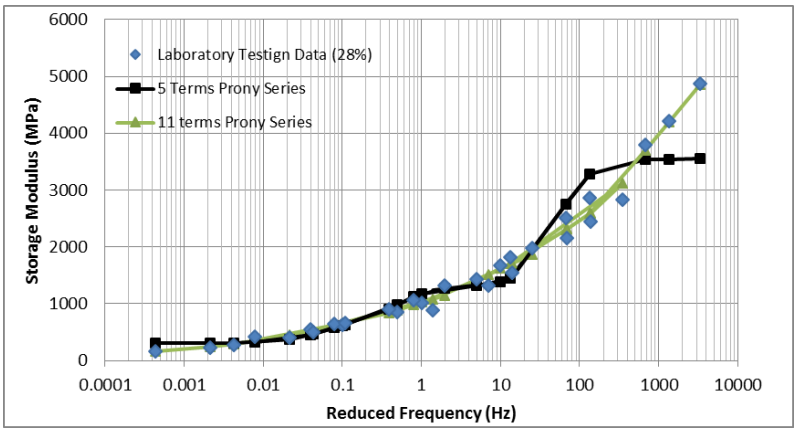

Figure 238. Comparison between 5-term and 11-term Prony series of ATPB-VA mixture of 28% air void content

PRONY SERIES OF OGBB-OK MIXTURES

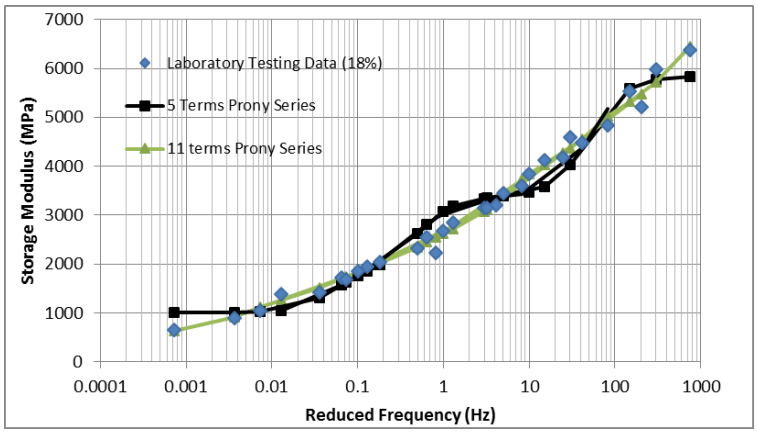

Figure 239. Comparison between 5-term and 11-term Prony series of OGBB-OK mixture of 18% air void content

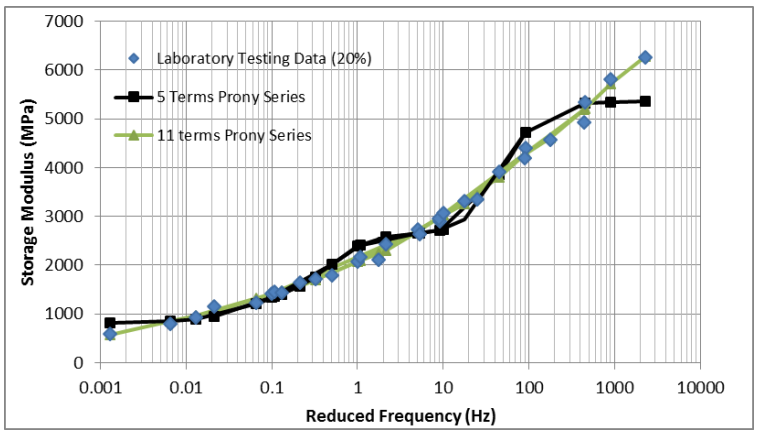

Figure 240. Comparison between 5-term and 11-term Prony series of OGBB-OK mixture of 20% air void content

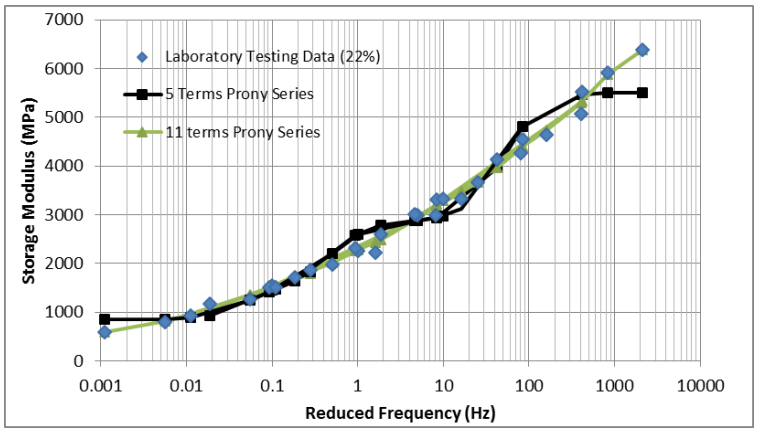

Figure 241. Comparison between 5-term and 11-term Prony series of OGBB-OK mixture of 22% air void content

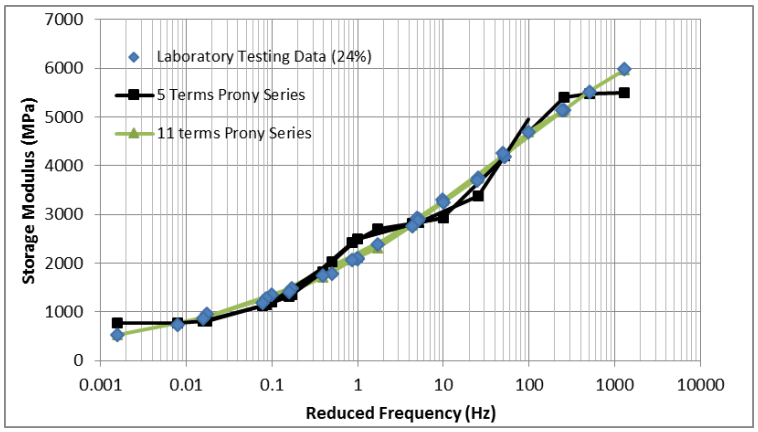

Figure 242. Comparison between 5-term and 11-term Prony series of OGBB-OK mixture of 24% air void content

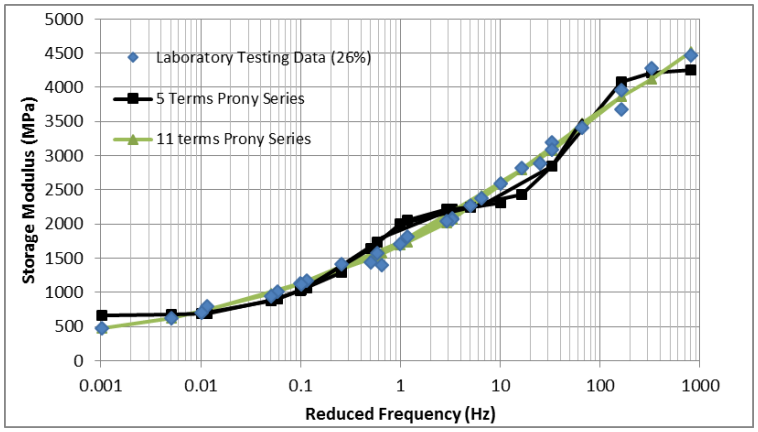

Figure 243. Comparison between 5-term and 11-term Prony series of OGBB-OK mixture of 26% air void content

Table 30. 11-terms Prony Series Parameters for OGBB-OK Mixture

18%				**20%**	
G_0	7604.807			G_0	8865.551
τ_1	0.00002	$\overline{g_1^P}$	0.086353	$\overline{g_1^P}$	0.088507
τ_2	0.0002	$\overline{g_2^P}$	1.31E-06	$\overline{g_2^P}$	0.236142
τ_3	0.002	$\overline{g_3^P}$	0.214042	$\overline{g_3^P}$	0.161483
τ_4	0.02	$\overline{g_4^P}$	0.164698	$\overline{g_4^P}$	0.155445
τ_5	0.2	$\overline{g_5^P}$	0.174489	$\overline{g_5^P}$	0.112449
τ_6	2	$\overline{g_6^P}$	0.105601	$\overline{g_6^P}$	0.077342
τ_7	20	$\overline{g_7^P}$	0.08291	$\overline{g_7^P}$	0.056829
τ_8	200	$\overline{g_8^P}$	0.080106	$\overline{g_8^P}$	0.045734
τ_9	2000	$\overline{g_9^P}$	0.029613	$\overline{g_9^P}$	0.025089
τ_{10}	20000	$\overline{g_{10}^P}$	0.036534	$\overline{g_{10}^P}$	0.021481
τ_{11}	200000	$\overline{g_{11}^P}$	0.007309	$\overline{g_{11}^P}$	0.010096

Table 30. (Continued)

22%		24%		26%	
G_0	8455.672	G_0	6890.931	G_0	5515.685
$\overline{g_1}^{\overline{P}}$	0.090539	$\overline{g_1}^{\overline{P}}$	0.108599	$\overline{g_1}^{\overline{P}}$	0.135636
$\overline{g_2}^{\overline{P}}$	0.165248	$\overline{g_2}^{\overline{P}}$	0.001568	$\overline{g_2}^{\overline{P}}$	1.81E-06
$\overline{g_3}^{\overline{P}}$	0.18266	$\overline{g_3}^{\overline{P}}$	0.17245	$\overline{g_3}^{\overline{P}}$	0.161823
$\overline{g_4}^{\overline{P}}$	0.142027	$\overline{g_4}^{\overline{P}}$	0.212505	$\overline{g_4}^{\overline{P}}$	0.200309
$\overline{g_5}^{\overline{P}}$	0.122231	$\overline{g_5}^{\overline{P}}$	0.178047	$\overline{g_5}^{\overline{P}}$	0.180075
$\overline{g_6}^{\overline{P}}$	0.090197	$\overline{g_6}^{\overline{P}}$	0.125827	$\overline{g_6}^{\overline{P}}$	0.105555
$\overline{g_7}^{\overline{P}}$	0.069205	$\overline{g_7}^{\overline{P}}$	0.075367	$\overline{g_7}^{\overline{P}}$	0.077109
$\overline{g_8}^{\overline{P}}$	0.053554	$\overline{g_8}^{\overline{P}}$	0.054572	$\overline{g_8}^{\overline{P}}$	0.053602
$\overline{g_9}^{\overline{P}}$	1.16E-06	$\overline{g_9}^{\overline{P}}$	0.00407	$\overline{g_9}^{\overline{P}}$	0.014166
$\overline{g_{10}}^{\overline{P}}$	0.029262	$\overline{g_{10}}^{\overline{P}}$	0.032156	$\overline{g_{10}}^{\overline{P}}$	0.035162
$\overline{g_{11}}^{\overline{P}}$	0.018662	$\overline{g_{11}}^{\overline{P}}$	0.019111	$\overline{g_{11}}^{\overline{P}}$	0.021895

PRONY SERIES OF ATPB-ID MIXTURES

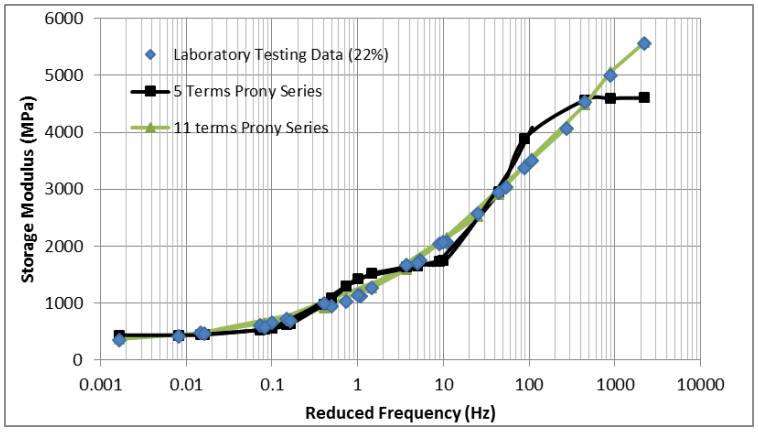

Figure 244. Comparison between 5-term and 11-term Prony series of ATPB-ID mixture of 22% air void content

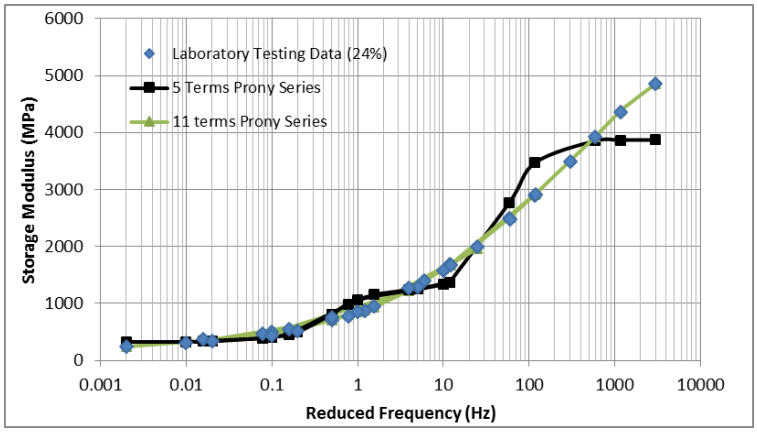

Figure 245. Comparison between 5-term and 11-term Prony series of ATPB-ID mixture of 24% air void content

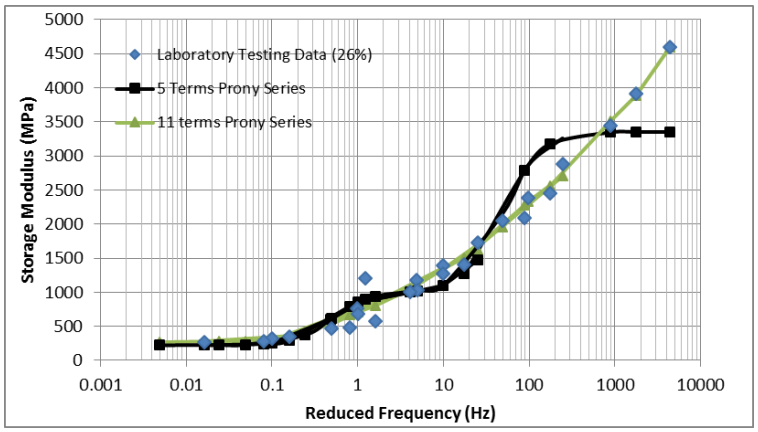

Figure 246. Comparison between 5-term and 11-term Prony series of ATPB-ID mixture of 26% air void content

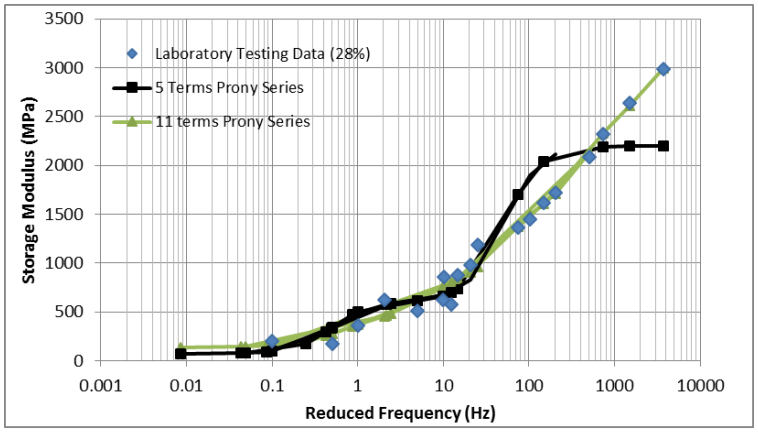

Figure 247. Comparison between 5-term and 11-term Prony series of ATPB-ID mixture of 28% air void content

Table 31. 11-terms Prony Series Parameters for ATPB-ID Mixture

22%				24%	
G_0	7407.62			G_0	6650.579
τ_1	0.00002	$\overline{g_1}^P$	0.090836	$\overline{g_1}^P$	0.114697
τ_2	0.0002	$\overline{g_2}^P$	0.174239	$\overline{g_2}^P$	0.201512
τ_3	0.002	$\overline{g_3}^P$	0.229881	$\overline{g_3}^P$	0.227692
τ_4	0.02	$\overline{g_4}^P$	0.199966	$\overline{g_4}^P$	0.197409
τ_5	0.2	$\overline{g_5}^P$	0.137965	$\overline{g_5}^P$	0.12292
τ_6	2	$\overline{g_6}^P$	0.072515	$\overline{g_6}^P$	0.061218
τ_7	20	$\overline{g_7}^P$	0.031353	$\overline{g_7}^P$	0.024017
τ_8	200	$\overline{g_8}^P$	0.013362	$\overline{g_8}^P$	0.016155
τ_9	2000	$\overline{g_9}^P$	0.014538	$\overline{g_9}^P$	1.5E-06
τ_{10}	20000	$\overline{g_{10}}^P$	0.026958	$\overline{g_{10}}^P$	0.021697
τ_{11}	200000	$\overline{g_{11}}^P$	1.35E-06	$\overline{g_{11}}^P$	0.000264

Table 31. (Continued)

26%		28%	
G_0	6449.903	G_0	4452.728
$\overline{g_1}^{\bar{P}}$	0.119936	$\overline{g_1}^{\bar{P}}$	0.167693
$\overline{g_2}^{\bar{P}}$	0.296355	$\overline{g_2}^{\bar{P}}$	0.243162
$\overline{g_3}^{\bar{P}}$	0.195816	$\overline{g_3}^{\bar{P}}$	0.229612
$\overline{g_4}^{\bar{P}}$	0.166835	$\overline{g_4}^{\bar{P}}$	0.176945
$\overline{g_5}^{\bar{P}}$	0.098669	$\overline{g_5}^{\bar{P}}$	0.090529
$\overline{g_6}^{\bar{P}}$	0.07937	$\overline{g_6}^{\bar{P}}$	0.06029
$\overline{g_7}^{\bar{P}}$	0.000211	$\overline{g_7}^{\bar{P}}$	2.25E-06
$\overline{g_8}^{\bar{P}}$	0.003156	$\overline{g_8}^{\bar{P}}$	0.007233
$\overline{g_9}^{\bar{P}}$	0.012193	$\overline{g_9}^{\bar{P}}$	0.007992
$\overline{g_{10}}^{\bar{P}}$	0.010156	$\overline{g_{10}}^{\bar{P}}$	0.007654
$\overline{g_{11}}^{\bar{P}}$	0.010172	$\overline{g_{11}}^{\bar{P}}$	0.006211

All the parameters shown in Figure 237 to Figure 247 were calculated by conducting the nonlinear optimization in Excel worksheet.

REFERENCES

1. Maupin, G. W. *Final Report. Design and Construction of a New Asphalt Drainage Layer*. Rep. VTRC 05-R11, VTRC, Charlottesville, VA, 2004.

2. Bejarano, M.O. and Harvey, J. Accelerated Pavement Testing of Drained and Undrained Pavements under Wet Base Conditions. In *Transportation Research Record 1816,* Transportation Research Board, Washington, D.C., 2002, pp. 137-147.

3. Harvey, J., Tsai, B., Long, F., and Hung, D. Asphalt-treated Permeable Base: Laboratory Testing, Performance, and Predictions. In *Transportation Research Record 1629,* Transportation Research Board, Washington, D.C., 1998, pp. 127-136.

4. Long, F., Harvey, J., Scheffy, C., and Monismith, C.L. Prediction of Pavement Fatigue for California Department of Transportation Accelerated Pavement Testing Program Drained and Undrained Test Sections. In *Transportation Research Record 1540,* Transportation Research Board, Washington, D.C., 1996, pp. 105-114.

5. Bejarano, M.O., Ali, A., Russo, M., Mahama, D., Hung, D., and Preedonant, P. *Performance of Drained and Undrained Flexible Pavement Structures under Wet Conditions Test Data from Accelerated Pavement Test Section 543-Drained*. Rep. UCD-ITS-RR-04-6. Pavement Research Center, Institute of Transportation Studies, University of California at Berkeley, 2004.

6. Harvey, J., Tsai, B., Long, F., and Hung, D. *CAL/APT Program—Asphalt Treated Permeable Base (ATPB)*. Rep. FHWA/CA/OR-99/09. California Department of Transportation, 1999.

7. Nokes, W.A., Harvey, J. T., du Plessis, L., Long, F., and Stolarski, P.J. Caltrans accelerated pavement testing (CAL/APT) program-test results: 1993-1996. In *8th International Conference on Asphalt Pavements*, Boston, MA, 1997, pp. 20.

8. Loulizi, A., Al-Qadi, Imad L. and Elseifi, M. Difference between in situ flexible pavement measured and calculated stresses and strains. *Journal of Transportation Engineering*, Vol.132, No.7, 2006, pp. 574-579.

9. Pologruto, M. Study of in situ pavement material properties determined from FWD testing. *Journal of Transportation Engineering*, Vol. 132, No. 9, 2006, pp. 742-750.

10. Federal Highway Administration, *Drainable Pavement Systems, Participant Notebook, Demonstration Project 87*. Rep. FHWA-SA-92-008, FHWA, Washington, D.C., 1992.

11. Fwa, T.F., Tan, S. A., and Guwe, Y. K. Rational Basis For Evaluation And Design of Pavement Drainage Layers. In *Transportation Research Record 1772*. Transportation Research Board, Washington, D.C., 2001, pp. 174–180.

12. Rokade, S., Agarwal, P.K., and Shrivastava, R. Drainage And Flexible Pavement Performance. *International Journal of Engineering Science and Technology*, Vol. 4, 2012, pp. 1308.

13. Federal Highway Administration, *Construction of Pavement Subsurface Drainage Systems (Reference Manual)*. Rep. FHWA/IF-01/014, FHWA, Washington, D.C., 2002.

14. Hunsucker, D.Q. and Meade, B.W. *Subsurface drainage of highway pavements*. Rep. KTC 97-8, University of Kentucky, Lexington, KY, 1997.

15. Mejias, M. and Rushing, J.F. Performance Evaluation of Military Airfield Pavement Drainage Layers. *Int. J. Pavement Res. Technol*, Vol.4, No.6, 2011, pp. 365-372.

16. Webb, D., Sholar, G., Musselman, J., Upshaw, P., and Page, G. *An Evaluation of Asphalt Treated Permeable Base*. Rep. FL/DOT/SMO/07-511, FDOT, FL, 2007.

17. Koroma, A.A. Evaluation of the performance and cost effectiveness of pavement sections containing open-graded base courses. Ph.D. dissertation, Department of Civil and Environmental Engineering, Michigan Technological University, Houghton, MI, 2011.

18. Mathis, D.M. Permeable Base Design and Construction. In *Proceedings of the Fourth International Conference on Concrete Pavement Design and Rehabilitation*, West Lafayette, IN, 1989, pp. 663-669.

19. Forsyth, R.A. *Asphalt Treated Permeable Material - Its Evolution and Application*. Rep. QIP 117, National Asphalt Pavement Association, Lanham, MD, 1991.

20. Zhou, H., Moore, L., Huddleston, J., and Gower, J. *Free Draining Base Materials Properties, Final Report*. Rep. FHWA-OR-RD-92-11, Oregon Department of Transportation, Salem, OR, 1992.

21. Ridgeway, H.H. *Pavement Subsurface Drainage Systems*. National Cooperative Highway Research Program, Synthesis of Highway Practice, 1982.

22. Hall, K.T. and Crovetti, J.A. *Effects of Subsurface Drainage on Pavement Performance Analysis of the SPS-1 and SPS-2 Field Sections*, Rep. TRB/NCHRP/REP-583, Aptek, Inc., Colorado Springs, CO. Texas Transportation Inst., College Station, TX, 2007.

23. Kozeliski, F.A. Permeable Bases Help Solve Pavement Drainage Problems. *Aberdeen's Concrete Construction*, Vol. 37, 1992, pp.660-662.

24. Al-Qadi, Imad L, Loulizi, A., Lahouar, S., Flintsch, G.W., and Freeman, T.E. Quantitative Field Evaluation and Effectiveness of Fine Mix under Hot-Mix Asphalt Base in Flexible Pavement. In *Transportation Research Record 1823*, Transportation Research Board, Washington, D.C., 2003, pp. 133–140.

25. Khoury, N.N., Zaman, M., Ghabchi, R., and Kazmee, H. *Stability and Permeability of Proposed Aggregate Bases in Oklahoma*, Rep. FHWA-OK-09-05, The University of Oklahoma, Norman, OK, 2010.

26. AASHTO T 342-11. Standard Method of Test for Determining Dynamic Modulus of Hot-Mix Asphalt Concrete Mixtures. American Association of State and Highway Transportation Officials, Washington, D.C., 2011.

27. Witczak, M. *Simple Performance Tests: Summary of Recommended Methods and Database*. Rep. NCHRP-547, Transportation Research Board, Washington, D.C., 2005.

28. Winkelman, T. J. *Open Graded Drainage Layer Performance in Illinois*. Rep. FHWA/IL/PRR 147, Illinois State Dept. of Transportation, Springfield, IL, 2004.

29. AASHTO T 312-12. Standard Method of Test for Preparing and Determining the Density of Hot-Mix Asphalt (HMA) Specimens by Means of the Superpave Gyratory Compactor. American Association of State and Highway Transportation Officials, Washington, D.C., 2012.

30. ASTM C192/C192M-12. Standard Practice for Making and Curing Concrete Test Specimens in the Laboratory. ASTM International, 2012.

31. AASHTO T 85-10. Standard Method of Test for Specific Gravity and Absorption of Coarse Aggregate. American Association of State and Highway Transportation Officials, Washington, D.C., 2010.

32. AASHTO T209-11. Theoretical Maximum Specific Gravity and Density of Hot-Mix Asphalt Paving Mixtures. American Association of State and Highway Transportation Officials, Washington, D.C., 2011.

33. Crouch, L.K., Copeland, A.R., Walker, C.T., Maxwell, R.A., Duncan, G.M., Goodwin, W.A., Badoe, D.A., and Leimer, H.W. Determining Air Void Content of Compacted Hot-Mix Asphalt Mixture. In *Transportation Research Record 1813*, Transportation Research Board, Washington, D.C., 2002, pp. 39-46.

34. Hall, K.D., Griffith, F.T., and Williams, S.G. Examination of Operator Variability for Selected Methods for Measuring Bulk Specific Gravity of Hot-Mix Asphalt Concrete. In *Transportation Research Record 1761*, Transportation Research Board, Washington, D.C., 2001, pp. 81-85.

35. Virginia Test Method – 84. Determining the Coefficient of Permeability of Open Graded Drainage Layer Material - (Physical Lab). 2000.

36. OHD L-44. Method of Test for Measurement of Water Permeability of Compacted Paving Mixtures. ODOT, 2004.

37. ASTM D 5084. Standard Test Methods for Measurement of Hydraulic Conductivity of Saturated Porous Materials Using a Flexible Wall Permeameter. ASTM International, 2010.

38. AASHTO T 283-07 (2011). Standard Method of Test for Resistance of Compacted Asphalt Mixtures to Moisture-Induced Damage. American Association of State and Highway Transportation Officials, Washington, D.C., 2007.

39. Tran, N.H. and Hall, K.D. An Examination of Strain Levels Used in the Dynamic Modulus Testing. *Journal of the Association of Asphalt Paving Technologists*, Vol. 75, 2006, pp 321-343.

40. Ongel A. and Harvey J. Analysis of 30 Years of Pavement Temperatures using the Enhanced Integrated Climate Model (EICM). Pavement Research Center, Institute of Transportation Studies, University of California, Berkeley, and University of California, Davis, 2004.

41. Diefenderfer, B.K. Moisture content determination and temperature profile modeling of flexible pavement structures. Ph.D. dissertation, Department of Civil and Environmental Engineering, Virginia Polytechnic Institute and State University, Blacksburg, VA, 2002.

42. Lund, J. R. *Asphalt Mix Characterization Using Dynamic Modulus and APA Testing*. Rep. FHWA-OR-RD-06-09, Oregon Dept. of Transportation, Salem, OR, 2005.

43. Xie, Hongbin and Watson, D.E. Determining Air Voids Content of Compacted Stone Matrix Asphalt Mixtures. In *Transportation Research Record 1891*, Transportation Research Board, Washington, D.C., 2004, pp. 203-211.

44. Witczak, M.W. and Bari, J. Development of A Master Curve (E*) Database for Lime Modified Asphaltic Mixtures. Department of Civil and Environmental Engineering, Arizona State University, Tempe, 2004.

45. Cross, S.A., Jakatimath, Y., and Sumesh KC. *Determination of Dynamic Modulus Master Curves for Oklahoma HMA Mixtures*. Rep. FHWA/OK 07 (05), Oklahoma Department of Transportation, Oklahoma City, OK, 2007.

46. Kim, Y.R., Momen, M., and King, M. *Typical Dynamic Moduli for North Carolina Asphalt Concrete Mixtures*. Rep. FHWA/NC/2005-03, North Carolina Department of Transportation, Raleigh, NC, 2005.

47. Timm, D.H., Turochy, R.E., and Davis, K.P. *Guidance for M-E Pavement Design Implementation*. ALDOT Project 930-685, Harbet Engineering Center, Auburn, AL, Project 930-685, 2010.

48. Guide for Mechanistic-Empirical Design of New and Rehabilitated Pavement Structures. Appendix EE-1: Input Data for the Calibration and Validation of the Design Guide for New Constructed Flexible Pavement Sections. ARA, Inc., ERES Division. 2003.

49. Paramount Asphalt, Inc. (2003). *Product Specification* [online]. Available: http://www.paramountasphalt.com/spec%20sheet/70-2213237.pdf.

50. Bari, J., and Witczak, M.W. Development of a New Revised Version of the Witczak E* Predictive Model for Hot Mix Asphalt Mixtures. *Journal of the Association of Asphalt Paving Technologists*, Vol. 75, 2006, pp. 381-423.

51. Kutay, M.E. and Jamrah A. *Preparation for Implementation of the Mechanistic-Empirical Pavement Design Guide in Michigan: Part 1-HMA Mixture Characterization*. Rep. RC-1593, Michigan State Univ., East Lansing, MI, 2013.

52. Hadi, M.N.S. and Bodhinayake, B.C. Non-linear Finite Element Analysis of Flexible Pavements. *Advances in Engineering Software*, Vol. 34, No. 11-12, 2003, pp. 657-662.

53. Al-Qadi, Imad L., Wang H., and Tutumluer, E. Dynamic Analysis of Thin Asphalt Pavements by Using Cross-anisotropic Stress-dependent Properties for Granular Layer. In *Transportation Research Record 2154*, Transportation Research Board, Washington, D.C., 2010, pp. 156-163.

54. Xiao, D.X., Hall, K.D., Wang, K.C.P. and Qiu, Yanjun. Long-term performance evaluation of permeable asphalt treated base in Arkansas. In *ICTE 2011 - Proceedings of the 3rd International Conference on Transportation Engineering*, Chengdu, China, 2011, pp. 2145-2150.

55. FHWA, (2009). TechBrief: Daylighted Permeable Bases [Online]. Available: http://www.fhwa.dot.gov/pavement/concrete/pubs/hif09009/

56. American Concrete Pavement Association. *Subgrades and Subbases for Concrete Pavements*. Rep. ISBN 978-0-9800251-0-1, Skokie, IL, 2007.

57. Schwartz, C.W. *Implementation of NCHRP 1-37A Design Guide, Final Report, Volume 1: Summary of Findings and Implementation Plan*. MDSHA Project No. SP0077B41, UMD FRS No. 430572, Department of Civil and Environmental Engineering, University of Maryland, Lutherville, MD, 2007.

58. National Cooperative Highway Research Program (NCHRP). Guide for Mechanistic-Empirical Design of New and Rehabilitated Pavement Structures. Final Report for Project 1-37A. Part 3. Chapter 3. Washington, D.C: NCHRP, Transportation Research Board, National Research Council. 2004.